Optimal Planning of Space Surveillance Network and Automatic Data Processing

Author:

Tommaso CARDONA

Supervisor:

Prof. Fabio SANTONI

Co-Advisor:

Prof. Fabrizio PIERGENTILI

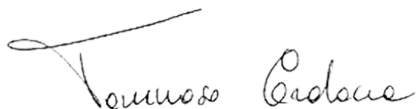*The Chair of the PhD Program:*

Prof. Mauro VALORANI

Declaration of Authorship

I, Tommaso CARDONA, declare that this thesis titled, *Optimal Planning of Space Surveillance Network and Automatic Data Processing* and the work presented in it are my own. I confirm that:

- This work was done wholly or mainly while in candidature for a research degree at this University.

- Where any part of this thesis has previously been submitted for a degree or any other qualification at this University or any other institution, this has been clearly stated.

- Where I have consulted the published work of others, this is always clearly attributed.

- Where I have quoted from the work of others, the source is always given. With the exception of such quotations, this thesis is entirely my own work.

- I have acknowledged all main sources of help.

- Where the thesis is based on work done by myself jointly with others, I have made clear exactly what was done by others and what I have contributed myself.

Signed:

Date: **January 8th, 2018**

The brick walls are there for a reason. The brick walls are not there to keep us out.

The brick walls are there to give us a chance to show how badly we want something.

Because the brick walls are there to stop the people who don't want it badly enough.

They're there to stop the other people

Randy Pausch

Ai miei genitori...

Acknowledgements

I am grateful to my thesis advisers Prof. Fabio SANTONI and Prof. Fabrizio PIERGENTILI for their guidance, support, patience and friendship. I will always be grateful for the opportunity they gave me to participate in so many research projects. I will always be thankful to Prof. Patrick SEITZER for his support during all these years. Thanks for teaching me how to be a scientist.

I take this opportunity to express my sincere thanks to Department of Mechanical and Aerospace Engineering of Sapienza University of Rome and Astronomy Department of University of Michigan for the possibility they gave me to improve my knowledge.

I wish to acknowledge the support received from the personnel of the Italian Space Agency and National Institute for Astrophysics, which made possible the realization of EQUO and NICO project. I also express, my sense of gratitude to all the staff and technicians of the Loiano Observatory for their invaluable help during the observing sessions.

This dissertation would not have been possible without the help of my friends that have continuously supported me for all these years.

To my family... All of this is dedicated to you.

Contents

List of Figures

Abstract

Nowadays, more than $17,000$ objects greater than $10\,cm$ in diameter are tracked and available in public catalog. Just nearly a thousand and a half are active spacecraft. In low Earth orbit (LEO), the increasing of Cube-Sat missions launched in last years is contributing to the growth of the space object population. Furthermore, large constellations to LEO are under development. Such constellations will lead to an unprecedented, step increase in the number of satellites in LEO. Consequently, to prevent the generation of debris in the short-term and the growth of the debris population over the longer-term is mandatory to avoid Kessler syndrome. Therefore, due to the continuous growth of number of operative satellites and the consequent risk of impact among them, an improvement in the observation is constantly demanding. The presented solution to provide a reliable and timely response in case of contingencies is the development of a worldwide sky-coverage network. In the framework of the Italian Space Agency (ASI) – Sapienza University of Rome Agreement (N.2013-078-C.O) for scientific cooperation at the Broglio Space Center (BSC) in Malindi (Kenya), S5Lab research team is developing a network of optical observatories. The presented thesis deals with the development of the network composed by an Italian observatory named MITO (Mid-latitude Italian Observatory), located near Rome and an equatorial observatory called EQUO (Equatorial Italian Observatory). The combinatorial explosion in the number of intervals to be scheduled has been caused by the increasing number of space debris to be observed with optical ground station. Therefore, new scheduling approach are needed to provide a solution to the new requests. In the framework of the Agreement between Italian Space Agency (ASI) and National Institute of Astrophysics (INAF) *Supporto alle attività IADC e validazione pre-operativa per SST* (N.2015-028-R.0) a scheduler has

been developed to manage the network. The presented thesis outlines the developed software called NICO (Networked Instrument Coordinator for space debris Observations) designed to allocate visibility windows to each optical sensor of the network by solving priority conflicts of the scheduling tasks. NICO goal is the harmonization of the different requests by taking care also of external limitations such as astronomical constraints and weather conditions. The development of a network of observatories and a scheduler to manage and organize the data acquisition routine has triggered the problem on how to manage the acquired data. Due to the increasing of the number of the observatory involved in data acquisition and the number of taken images per night, a new automated image processing tool for light-curves measurements was needed. This thesis presents the development and application of the automated software designed to process light curves acquisition. These are used to determine the dynamical state of the target in terms of attitude by processing the light reflected from the metallic surface of the object. Rapid changes in brightens of the response are investigated to reconstruct rapid changes in the attitude in the scale of a second or less. These data are extremely valuable to detect and investigate the attitude of an orbiting object and its evolution especially for future Active Debris Removal (ADR) missions.

Chapter 1

Introduction

The *Space Age* began with on October 4, 1957 with the launch of the first artificial satellite the *Sputnik I* by the Soviet Union [Warwick (1959)]. Since then, the interest in space and its possible commercial exploitation has continued to grow and the number of launches per year has increased year after year. Human space activities are mainly concentrated in specific regions: Low Earth Orbit (LEO), semi-synchronous orbit and Geostationary Earth Orbit (GEO). Each of these offers specific benefits. LEO (altitude range within $200 - 2,000\,km$) has the advantage of offering relative easy access to orbit and it is mainly used for high-resolution Earth observation satellite. Semi-synchronous orbits, ranging from $10,000$ to $20,000$ km, are crucial for navigation (such as GPS - Global Positioning System) and communication satellites. While GEO (about $36,000\,km$) is mainly used for telecommunications and meteorological satellites. In addition to operating satellites, the various orbital zones are populated by several objects classified as *space debris*. According to the definition of *Inter-Agency Space Debris Coordination Committee* (IADC), an inter-governmental forum whose aim is to co-ordinate space agency's efforts to deal with debris in orbit around the Earth, the term *space debris* identifies *all man-made objects including fragments and elements thereof, in Earth orbit or reentering the atmosphere, that are non-functional* [IADC (2002)].

These include satellites that are no longer operational, latest stages of launchers, but also debris produced from the fragmentation of large satellites due to high energy impacts or the liquid metal particles produced during propulsion. The orbital speeds that these objects can reach is up to $7.9\,km/s$, enough to severely damage a satellite or space vehicle even if the debris size is small. With the growth of the debris population, it increases the potential danger for all spacecraft, including the *International Space Station* (ISS) and other spacecraft with on-board humans. To keep track of all artificial object orbiting the Earth including space debris and to determine their trajectory, both the United States and Russia developed a network of radar and optical sensors to collect data. Orbital debris about $10\,cm$ or larger in LEO, and about $1\,m$ or larger in the geosynchronous orbit region are tracked by the *U.S. Space Surveillance Network* and maintained in the U.S. Satellite Catalog [Space Track (2017)]. The size of the population of objects smaller than $10\,cm$ in diameter is estimated on a statistical basis. To estimate the number of these small debris objects in LEO, scientists have inspected hardware that has been exposed to the LEO environment under known conditions and then returned to earth. Since the Space Shuttle stopped flying in 2011, very little hardware has returned from space in a condition suitable for counting orbital debris impacts. For orbital debris smaller than 1 millimeter in LEO, space-based in-situ measurements and the inspection of external hardware surfaces returned from space are the only options. An example of data from the sub-millimeter orbital debris population came from the inspection of the Hubble Space Telescope presented in Figure 1.1.

FIGURE 1.1: ESA built-solar cells retrieved from the Hubble
Space Telescope in 2002.

The risks of collision between a satellite and a debris are classified into three categories depending on the size of the involved debris. For objects larger than $10\,cm$, conjunction analysis evaluations and collision avoidance maneuvers for objects that can be maneuvered are the most effective strategies to reduce the risk of impact that would lead to the complete destruction of the satellite involved. Objects with a diameter less than $10\,cm$ are usually too small to be traced and too large for a satellite' shield to be effective in case of an impact that would lead to partial destruction or loss of a whole subsystem of the satellite. Protections such as debris shields are effective in enduring impact of particles of less than $1\,cm$ which would otherwise cause the loss of sensors or subsystems. Due to the increasing number of orbiting object and the presence of uncontrolled objects orbiting around the Earth a continuous monitoring system is required which main goal is to identify their positions, predict their trajectories and to perform conjunction analysis and collision avoidance maneuvers to avoid impact if needed. In 1978, Donald Kessler, NASA's Orbital Debris Program Officer, proposed a scenario [Kessler (1991)], which analyzes the number of satellite launches and the

trend with which these launches take place including the probability of collisions between satellites. If a collision occurs, it would produce fragments in orbit which would in turn increase the probability of further collisions. This chain reaction would lead to the formation of a *debris belt* around the Earth. This process, known as *Kessler's Syndrome*, is based on the theories regarding the growth of the asteroid belt, and for the first time exposed the issues of spatial debris and the need for new regulations for the launch of new satellites and measures to be implemented to reduce the risk of collisions between objects in orbit.

1.1   Space debris mitigation guidelines

IADC has promoted international guidelines [IADC (2002)] to regulate mission planning and the design and operation of spacecraft and orbital stages that will be injected into Earth orbit. The application is devoted to organizations for the identification of the standards to be applied during the establishing of mission requirements for planned spacecraft and orbital stages. Moreover, operators of existing spacecraft and orbital stages are encouraged to apply these guidelines to the greatest extent possible. The IADC guidelines identify specific protected regions characterized in which special procedure should be performed to ensure their future safe and sustainable use regarding the generation of space debris (Figure 1.2). Region A, Low Earth Orbit (or LEO) Region – spherical region that extends from the Earth's surface up to an altitude (Z) of $2,000\,km$ Region B, the Geosynchronous Region - a segment of the spherical shell defined by the following:

- Lower altitude = geostationary altitude minus $200\,km$.

- Upper altitude = geostationary altitude plus $200\,km$.

- $-15° \leq$ latitude $\leq +15°$.

- Geostationary altitude $Z_{GEO} = 35,786$ (the altitude of the geostationary Earth orbit).
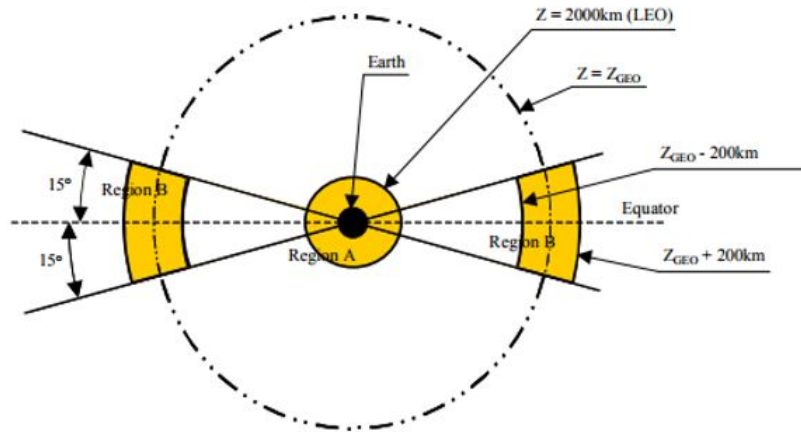
FIGURE 1.2: Protected region as specified in the IADC guidelines.

Great effort is needed not only during the operational phase of their missions but also during the design and testing phases to achieve the highest reliability for the post-mission disposal operations and the lowest residual lifetime. In fact, during an organization's planning for and operation of a spacecraft and/or orbital stage, it should take systematic actions to reduce adverse effects on the orbital environment by introducing space debris mitigation measures into the spacecraft or orbital stage's life-cycle, from the mission requirement analysis and definition phases. The mitigation measures include: limit debris released during normal operations, minimize the potential for on-orbit break-ups, minimize the potential for post mission break-ups resulting from stored energy, minimize the potential for break-ups during operational phases, avoidance of intentional destruction and other harmful activities. Furthermore, specific post mission disposal has been promoted. If the spacecraft that has terminated its mission is operating in GEO, it should

be maneuvered far enough away from GEO to not cause any interference with spacecraft or orbital stage still in geostationary orbit. The maneuver should place the spacecraft in an orbit that remains above the GEO protected region. This minimum increase in perigee altitude is identified by taking care of solar radiation pressure coefficient, the aspect area to dry mass ratio, the upper altitude of the GEO protected region ($200\,km$) and the maximum descent of a re-orbited spacecraft due to luni-solar geopotential perturbations ($35\,km$). Otherwise, if the spacecraft that is terminating its operational phases in orbits is in the LEO region, or that pass through and have the potential to interfere with the LEO region, should be de-orbited or where appropriate maneuver into an orbit with a reduced lifetime equal to 25 years [IADC (2002)]. Moreover, if a spacecraft or orbital stage is to be disposed of by re-entered into the atmosphere, debris that survives to reach the surface of the Earth should not pose an undue risk to people or property.

1.2 Current orbit population

Nowadays, more than $17,000$ objects greater than $10\,cm$ in diameter are tracked and available in public catalog [Space Track (2017)]. Just nearly a thousand and a half are active spacecraft (Table 1.1). Figure 1.3 to Figure 1.6 show the evolution of the population in different orbital regimes in the last years. It is possible to notice how the trend of new launches is increasing in the first six month of 2017 compared to the total launch of 2016 especially in LEO in sun-synchronous orbit (inclination greater than $90°$) and in MEO.

TABLE 1.1: Total number of operating satellites

Total number of operating satellites: 1,459			
(includes launches through 12/31/16)			
US: 593	Russia: 135	China: 192	Other: 539
LEO: 803	MEO: 96	HEO: 38	GEO: 522
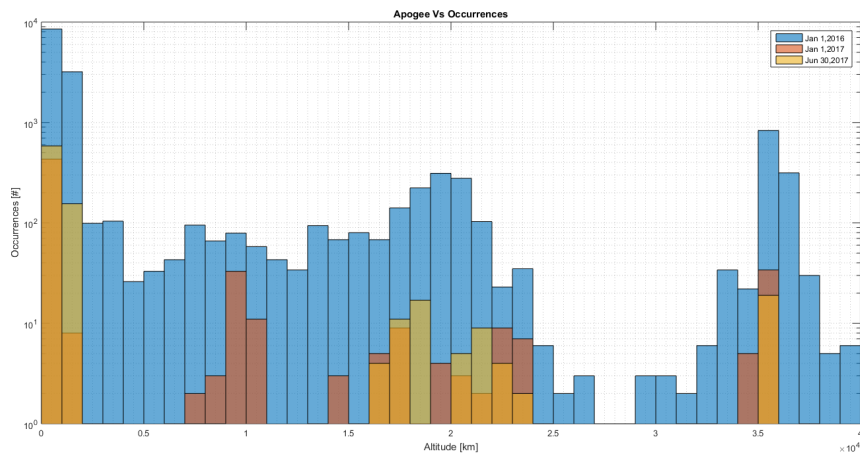
FIGURE 1.3: Apogee Vs Occurences.
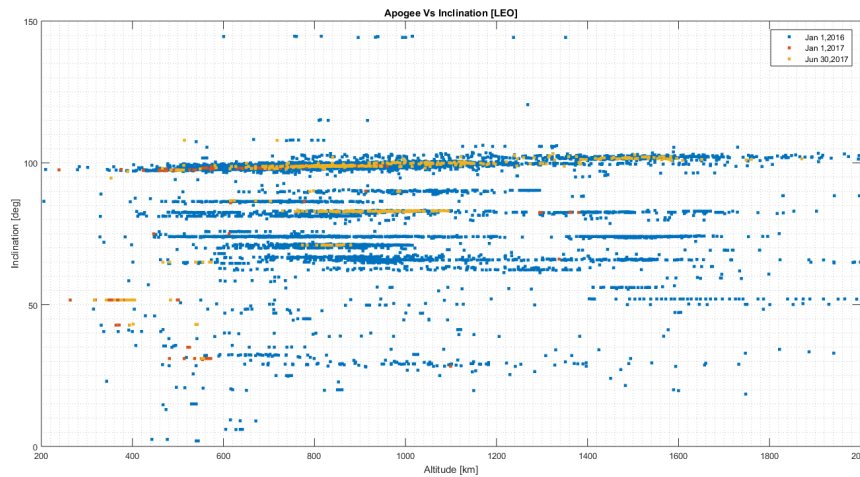
FIGURE 1.4: Apogee Vs Inclination.
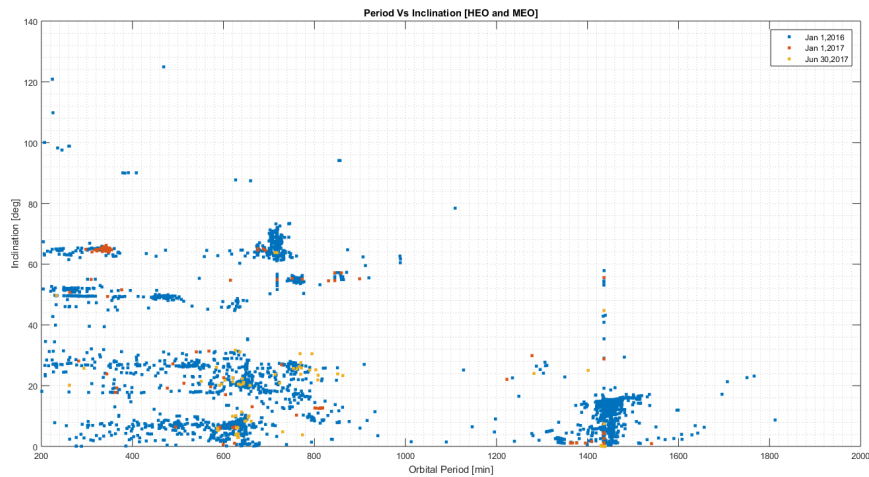
FIGURE 1.5: Period Vs Inclination.
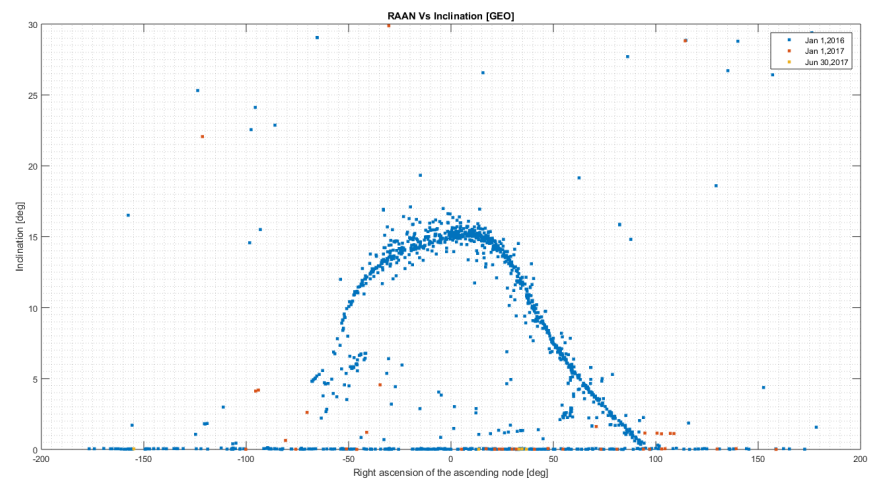
FIGURE 1.6: RAAN Vs Inclination.

In the geosynchronous region two main populations of objects are clearly distinguishable. The controlled satellites whose inclination is kept around zero by control maneuvers and whose right ascension of ascending node is nearly randomly distributed. The uncontrolled old satellites whose inclination oscillates, reaching a maximum value i_{max} 15° and then bouncing back

to $0°$, with a period of about 53 years under the influence of the perturbations due to the Sun, the Moon and the Earth oblateness. In recent years a peculiar population of objects having mean motion around 1 and high eccentricity (as high as 0.55) was detected by the ESA OGS telescope in Tenerife [Schildknecht et al. (2004)]. It was shown by that these are objects with very high area to mass ratio (ranging between $1\,m^2/kg$ up to $30\,m^2/kg$) whose dynamics is therefore strongly perturbed by the solar radiation pressure that significantly affects their eccentricity with small effects on the total energy of the orbit and, therefore, on the semi-major axis or mean motion. Most probably these objects are remnants of thermal blankets or multi-layer insulation (MLI) either detached from aging spacecraft or ejected by explosive fragmentation of old spacecraft, but their exact nature remains currently elusive due to lack of physical, spectroscopic studies. In lower orbit, the increasing of Cube-Sat missions launched in last years is contributing to the growth of the space object population. Furthermore, large constellations to LEO are under development to provide telecommunications and worldwide high-speed internet services. The launch of such constellations will lead to an unprecedented, step increase in the number of satellites in LEO (Table 1.2) [Ito (2017)]. Therefore, the effects that such missions may have on the sustainability of wider space activities must be considered and analyzed [Bastida Virgili et al. (2016)]. Consequently, to prevent the generation of debris in the short-term and the growth of the debris population over the longer-term is mandatory to avoid Kessler syndrome (Figure 1.7).

TABLE 1.2: Future mega constellation in LEO

Name	Apogee [km]	Perigee [km]	Constellation population
Boeing (Ph.1)	1200	1200	1396
Boeing (Ph.2)	1000	1000	1560
Iridium NEXT	780	780	72
Leosat	1430	1430	108
OneWeb	1200	1200	2600
Samsung	1400	1400	4600
SpaceX	1100	1100	4425
Total			14761
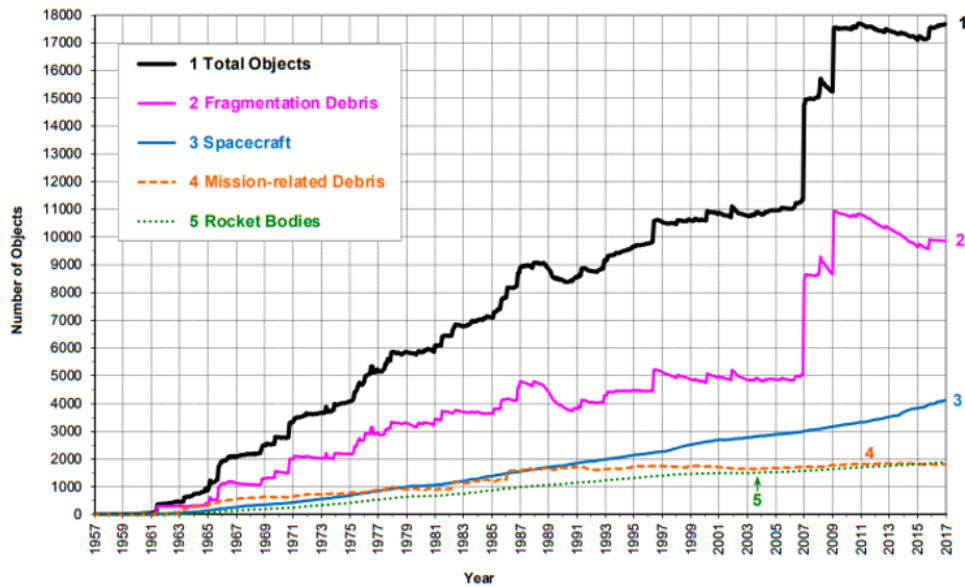
FIGURE 1.7: Montly number of object in Earth Orbit by Object type [NASA Orbital Debris Quarterly News (2017)].

1.3 Space debris issues

It is estimated that more than $700,000$ dangerous debris objects are in Earth orbit and they all travel at speeds up to $7.9\,km/s$, fast enough for a relatively

small piece of orbital debris to have the potential to damage or destroy operational satellites. The increment of space mission is consequently increasing of the total number of space debris. This rising population increases the potential danger to all space vehicles, but especially to the International Space Station and other spacecraft with humans aboard. Therefore, IADC's space agencies are pushing to increase their capabilities in terms of space surveillance of space debris. Some recent event has proved the importance of an improvement of the space surveillance capability in terms of sensors involved and quasi real-time data analysis. In particular in:

1.3.1 Space debris events in LEO

- **1996 Cerise impact**: on July 24, 1996, the first verified case of a collision between two objects occurred at an altitude of 685 km between the French military reconnaissance micro-satellite Cerise and a cataloged fragment object of an Ariane-1 H-10 upper stage which exploded on November 13, 1986. The collision ripped a portion of Cerise's gravity-gradient stabilization boom, which left the satellite severely damaged [Alby et al. (1997)].

- **2007 Chinese anti-satellite missile test**: on January 11, 2007, the Fengyun FY-1C polar orbit satellite while was orbiting at an altitude of $865\,km$ with a mass of 750 kg was destroyed by a kinetic kill vehicle traveling with a speed of 8 km/s in the opposite direction [Kelso (2007)]. This event was the largest recorded creation of space debris in history with more than $3,000$ pieces of trackable size ($>\ 10\,cm$) and an estimated $150,000$ debris particles. Nowadays more than $2,000$ cataloged debris are still in orbit [Space Track (2017)].

- **2009 satellite collision**: on February 10, 2009, Kosmos-2251 a deactivated Russian Strela military communications satellite with a mass of $950\,kg$ collided at an altitude of $789\,km$ with the active satellite communication satellite Iridium 33. The result was the complete destruction of both spacecraft and the creation of approximately $1,000$ pieces of debris larger than 10 centimeters [Kelso (2009)].

- **2012 Envisat loss of contact**: on April 8, 2012, ESA loss the contact with the Earth-observing satellite Envisat for a system failure [Gottwald (2012)]. The object is still orbiting in stable orbit at an altitude of $774\,km$ with a mass of $8,211\,kg$. The satellite is one of the candidate for future active debris removal mission [Saunders (2016)].

- **2017 Topex/Poseindon close encounters with Jason-2**: on June 20, 2017, the defunct satellite map ocean surface topography developed to map ocean surface topography and its successor Jason-2 had a close approach to within $400\,m$. Therefore, collision avoidance maneuvers have been disposed Jason-2 has been maneuvered starting on July 3, 2017 to lower the semimajor axis. Jason-2 has reached its new *Long-Repeat-Orbit* about $26\,km$ lower in semimajor axis than the original orbit. All orbit maneuvers executed without incident [Kucharski et al (2017)].

1.3.2   Space debris events in MEO

- **2016 IADC-WG1 IT 34.1**: The aim of the Internal Task proposed by IADC Working Group 1 (Measurements) at 34th IADC Meeting is to analysis and a list of options to statistically survey the population of objects in MEO and in particular Molniya orbit. This analysis will consider optical and radar instruments both to improve existing or to develop new observing techniques and strategies.

1.3.3   Space debris events in GEO

- **2004 High area-to-mass ratio debris population detection**: An un-expected orbital debris population has been detected in 2004 [Schild-knecht et al. (2004)] with the unique properties of a very high area-to-mass ratio. This population is thought to have origins in GEO re-gion. Many of these objects are uncharacterized with apparent area-to-mass ratios of up to 30 meters squared per kilogram. Their orbits are highly perturbed due to the combined effect of solar radiation pres-sure, anomalies of the Earth gravitational field, and third-body gravita-tional interactions induced by the Sun and the Moon ([Schildknecht et al. (2005)], [Schildknecht et al. (2008b)]).

- **2008 IADC-WG1 AI 23.4**: The aim of the Action Item proposed by IADC Working Group 1 (Measurements) at 23th IADC Meeting is to perform an International Optical Debris Campaign in Higher Earth Or-bit in the period between February and June 2008. Objectives of this campaign were to determine the extent and character of debris in HEO, specifically by obtaining distributions for the brightness, inclination, right ascension of ascending node, and mean motion for the debris.

- **2017 AMC-9**: On June 17, 2017, SES operator lost control of AMC-9, a large satellite in geostationary space. Shortly after, the AMC-9 satellite begins to fragment. At the current time, it is not clear if AMC-9 has been hit by a debris, or it could have been harmed by a space weather problem, sustained a failure due to manufacturing.

1.4 Space Situation Awareness

The United Nations Committee stressed the importance of International co-operation for the development of scientific and technological research to address the problem of spatial debris. Subsequently, the European Parliament set up a framework to start the Space Situational Awareness (SSA) Programme ([Bobrinsky and Del Monte (2009)], [ESA SSA Programme (2017)]). The aim of the program is to provide Europe with timely and precise information on space environment. The activities are mainly focusing on three macro areas:

- Space Weather (SWE): to monitor Sun and solar wind conditions including effects on Earth's magnetosphere, ionosphere and thermosphere to predict effects on satellite.

- Near-Earth Objects (NEO): to detect natural objects such as asteroids and comet that can potentially impact Earth.

- Space Surveillance and Tracking (SST): to track and provide prompt information regarding all orbiting objects including active and inactive satellites, discarded launch stages and fragmentation debris orbiting Earth.

1.4.1 Space Surveillance and Tracking segment

The European Parliament framework for Space Surveillance and Tracking (SST)

- Launch and early satellite operations, such as the confirmation of separation of satellite from launcher and to provide information on its initial orbit.

- Discrimination of each satellite in case of emission in orbit of multiple satellites at the same time or identification of new objects after separation or detection of in-orbit fragmentation.

- Contingencies, by tracking malfunctioning or passive satellites;

- Collision warnings, by performing conjunction analysis among satellites and other orbiting objects such as space debris or other operative satellites.

- Search for released or lost objects.

- Controlled and uncontrolled re-entry, by estimating trajectory, re-entry time and location, and risk evaluation to ground;

The main goals of the program are:

- To extract orbital data and to determine if they are referred to a new object or one already cataloged. If the object is one that has already been seen, then the observations are used to update the orbital parameter of the space debris. Otherwise, if the detected object is a new one, then follow-up observations from other sensors of the SST network are used to collect more data to refine its orbit. Then, the catalog is updated with orbital information of the new detected object.

- To support safe and secure operations of space assets, risk management and liability assessment, to characterize physical properties of space objects.

Orbital and attitude data of space objects are based on radar, laser ranging and optical measurements.

- Radars have a limited detection coverage of objects in the $1 \check{} 10\,cm$ size range and they are affected by several constraints connected to the maximum allowable slant range to the object in the order of 2,000 km [Mehrholz

et al. (2002)] .

- Laser ranging measurements is possible only for cooperative satellites that are equipped with specific retro-reflector. Ground-based laser ranging stations illuminate the target with a very short laser pulse that is reflected by the cube corner prism installed on-board. Then by measuring the round-trip time of the flight it is possible to determine the distance with a sub-centimeter accuracy [Kirchner et al (2012)].

- Optical data are useful to retrieve angular measurements for the observed target but are depended by illumination constraints. In fact, targets are visible only when directly illuminated by the Sun, while the ground-based observatory is in darkness. Moreover, local weather conditions tremendously affect the operation of the single ground station.

The SST support main activities can be batched as presented in Figure 1.8. The main block is *Observations* that represents the key of the SST program to characterize the population of man-made orbiting objects. The obtained data are processed for orbital determination analysis. Orbital elements are required to forecast the future path of the object, through the Orbit determination block. If the target is already present in the catalog, then its orbit is updated. Otherwise, if data are obtained from new target, its orbital parameters are added to the catalog. Measured data are use used to perform *Conjunction analysis* by merging data from different sources such as space weather database. If collision avoidance maneuvers are required to prevent the risk of an impact among an active satellite and a space debris, then support to external space operators is provided. This information is crucial in case of lower orbit which are highly influenced by perturbation such as atmospheric drag.
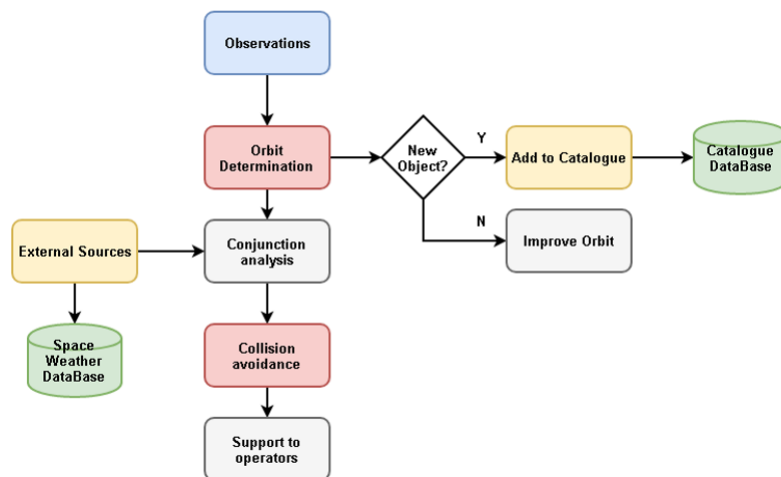
FIGURE 1.8: Space surveillance and tracking activities logical scheme.

1.4.2 The need for a network of sensors

The main idea of the SST program is to provide a reliable and timely response in case of contingencies. To afford such service a worldwide sky-coverage is mandatory. Observatories for space debris spreadly located worldwide greatly improve the capability to provide support to operative spacecraft both in different orbital regimes such as LEO and GEO for impact risk management and in orbital maneuver measurement. By operating a network, complementary observatories can be selected to perform simultaneous or sequential observations from multiple different sites. This will allow to enhance trajectory observability, in virtue of the different achievable geometrical configurations. For example, equatorial observatory would make it possible to track LEO or reentering high inclination objects over longer orbit arcs. Therefore, the same object could be tracked consecutively by observatories located at mid-latitude and equatorial latitude. Thus, the accuracy of achieved orbital parameters is increasing. Therefore, evaluation of the impact probability related to close approaches and the evaluation the impact points of reentering objects can be improved.

The sensors for space debris investigations are depending on the orbits:

- LEO objects are investigated mainly with radar for orbit determination and with optical for attitude determination.

- GEO and MEO regions are investigated mainly with optical telescopes.

- High Elliptical Orbit (HEO) uses both radar (at perigee) and optical (at apogee).

While radars for space surveillance purposes are used mainly by military, optical instruments are used by both military and civilian.

Network of optical observatories

The main goals of optical observations fully dedicated for space debris are:

- Maintaining the dynamical data base on space object orbits.

- Estimation of real population of artificial objects on high geocentric orbit.

- Determining of possible origin of the discovered objects;

- Verification of the space debris distribution and evolution models for high orbits.

- Estimation of the level of danger caused by space debris objects for operational spacecrafts on high orbits at present and in the future;

- Control of implementation of measures directed on decreasing the space debris population.

- Attitude estimation from light-curves measurements for future active debris removal mission.

These observatories must be highly robotic to handle observations without explicit human control. Therefore, the low-level behavior of the telescopes is automatic and computer controlled. The main advantages of robotic telescopes are:

- Speed: by removing the human from the controlling loop the response time is much faster; No human time is required to travel to the observatory and operate.

- Automating the routine: once the controlling software is operative, it can be implemented into each new developed observatory with the same architecture and communication protocol.

- Remote control: the observatory con be operated also in extreme or remote environments with the only constraints of the network bandwidth.

- Networking: whether fully robotic or operating in service mode, they can operate connected in a network. Therefore, the diurnal sampling problems that plague single-site observations of periodic variables can be avoided if an observer can acquire data from a second, geographically distant site. Another advantage of a robotic telescope network is the ability to make simultaneous observations, with both similar and different instruments (i.e. acquisition of photometric measurements in several filters).

Therefore, also to study and characterize orbital debris it is necessary to have an extended network of optical sensors to achieve data from sites under different meteorological conditions. An example of such network is ISON (International Scientific Optical Network) coordinated by the Keldysh Institute of Applied Mathematics (KIAM) of the Russian Academy of Sciences that includes more than 23 observation facilities of various affiliation in 11 countries

[Molotov (2011)]. The network is a dedicated to space surveillance for high orbits and its database collect about 7 million measurements of $3,300$ objects (35% more complete catalog than TLE public data).

1.4.3   Orchestrate the network

How to orchestrate a network is an important problem in operations for aerospace systems. It can be described as the allocation of tasks among a set of targets (i.e. active satellites or orbital debris) during visibility times. The three-main fields where orchestrating technique is applicable are:

- Communications task among satellites and ground stations, where the communication intervals are the temporal constrains.

- Earth observation satellite task, where the observations of spots on the Earth are binding.

- Sensor scheduling task, where the observations windows of satellites by ground sensors such as radar or telescope must be considered.

The progressive increase in the number of satellites and ground stations triggers to a combinatorial explosion in the number of these intervals to be managed and scheduled. In fact, the scheduling of these tasks has been posed as an optimization problem since its inception, and has been studied for decades.

State of the art

Each one of the small and large robotic telescopes in the world is controlled by its Telescope Control System (TCS) software to obtain as more scientific data as possible for the given instrument. There are numerous programs (open-source, proprietary, and custom-made) that can be used for telescope

operation such as pointing, tracking, image acquisition, as well as for planning observations. Examples of these are RTS2 [RTS2 (2017)], INDI [INDI (2017)] and ASCOM [ASCOM (2017)] that are open-source software that are commonly used for astronomical instrumentation for applications such as deep-sky and Solar system objects observations. Nevertheless, the SST program poses several significant constraints that are rarely needed in other types of observations such as the classical astronomical purpose. Most of the requirements are dictated by the relative proximity of objects to observer and thus their fast-apparent motion. Therefore, the accuracy of positional measurements for orbit determination is affected by timing dependencies. For higher orbit, the precision should be in the order of several tens of milliseconds, while for lower orbit in the order of fractions of millisecond. Moreover, for object following request, the system should support fast and variable-rate tracking according to the ephemeris. Furthermore, orbital debris observations require that the optical sensors can operate in different mode (i.e. survey, tracking, follow-up and specific sky region request) and each single request must be processed for the multipurpose coordination of the network. The state of the art of observatory network schedulers are:

- **SPIKE**: The Space Telescope Science Institute developed the Spike planning and scheduling software in support of the Hubble Space Telescope as a general toolkit for planning and scheduling. Nowadays Spike is used operationally by: Hubble Space Telescope (HST), Space Infrared Telescope Facility (SIRTF) and Advanced X-ray Astrophysics Facility (AXAF). The treats schedule construction as a constrained optimization problem uses a heuristic repair-based scheduling search technique called multi-start stochastic repair [Johnston et Miller (1994)]. The technique is composed by an initial trial assignment as an initial guess that generally have temporal or other constraint violations; then heuristic

repair techniques are applied to try to eliminate constraint violations; finally, conflicts are eliminated by removing any activities with constraint violations until a feasible schedule remains. Spike has long-, medium- and short-term ground based telescope scheduling capabilities, but the short-term scheduling operates within a week at a time, that is a time-step not reliable to offer an operative service for space debris observation purpose in case of contingencies in the SST framework.

- **RoboNet**: It was the first used a global network of fully robotic 2 m telescopes released in 2007. The networked operation allows imaging of only astronomical targets. The latest version called RoboNet-II consists in a set of web interacting program that can function as a single instrument, by optimizing and sharing the load of observations, or as individual instruments which perform the scheduled observations separately. The requests are sorted by the real-time scheduling algorithm which picks the next *best* observation to perform by optimizing against several selection/scoring criteria [Tsapras et al. (2009)]. The scheduler operates in a rapidly changing environment. Therefore, poor weather, changes in observing conditions, unexpected mechanical faults or software glitches does not allow to make any long-term scheduling decisions. The scheduler uses a simple dispatch mechanism which selects just a single group of observations to perform at each invocation. This has the disadvantage that global optimization criteria are not maximized.

- **MAJORDOME**: CNES developed the MAJORDOME scheduler for the TAROT network [Boer et al. (2017)]. It is designed to handle different user requests including constraints, priority and periodicity. The uses can set one or more constraints but does not know when the request

will be scheduled. The evolution of this scheduler is called MAJORDOME-II developed for the ARAGO (Advanced Robotic Agile Guest Observatory) and its main objective is to optimize the slot time for astronomical alerts such as Gamma-Ray Bursts. It is composed by two modules: the first is the daily module that develops during the day a plan scheme with different possible scenarios with alternatives. Then, the night module uses a reactive technique to observe the best slot from the list of the scheduled observations sets of the launched scheme.

- **FORTE**: ISON includes five groups of different size telescopes and three scheduling centers to better serve user's requests. The KIAM Space Debris Data Center is in charge for Daily scheduling of the ISON sensors for routine and special survey and tasking observations of GEO, HEO and MEO regions. The TCS software package that is used is called FORTE (Facility for Operating Robotic Telescope Equipment) and it is based on Python. The main components are: the scheduler; the Network Interface that is the common gateway for externally controlling and monitoring operation and uses XML (Extended Markup Language) based protocol for maximum portability; the Datalogger that automatic handles log message from all external modules that uses the same facility; the Ephemeris engine to provide the instantaneous target position and velocity for pointing and tracking; the imaging pipeline that includes a set of user-defined operation on image data [Molotov (2011)].

- **LCOGT**: Las Cumbres Observatory Global Telescope (LCOGT) is a worldwide network of fully robotic optical telescopes dedicated to astronomy. The network is controlled and operated from a central headquarters, through a distributed *hub and spoke* software architecture. The central hub tracks the status of observing requests are interrogated and updated by the network scheduler in response to changing conditions

and new observing requests, which are created by most users through the LCOGT Observatory Portal website. Requests that consist in a single target each are described with a list of celestial coordinates. These are not made for specific sites or telescopes but for class of telescopes. The LCOGT Global Adaptive Telescope Scheduler books each observation on the best telescope available, and re-books it on the next available telescope in the event of failure due to weather or technical problems [Brown et al. (2013), Saunders et al. (2006)]. When a new Request enters the system, the schedule is recomputed, and the new Request may be scheduled. Therefore, it is not possible to assign specific priority in case of a debris conjunction contingency.

Goal and outline of the thesis

In 2015, in the framework of the Agreement between Italian Space Agency (ASI) and National Institute of Astrophysics (INAF) *Supporto alle attività IADC e validazione pre-operativa per SST (N.2015-028-R.0)* a project started as a preliminary study to get national telescopes into operative mode within the SST program. The project is developed in cooperation in between IRA-INAF (Italian Institute of Radio Astronomy), Polytechnic of Milan, OAC-INAF (Astronomic Observatory of Cagliari), ISTI-CNR (Italian Institute for Science and Information Technology of National Research Center), Sapienza University of Rome, University of Padua, IFAC-CNR (Institute of Applied Physics of National Research Center), OATe-INAF (Astronomical Observatory of Teramo). The goal of the project is to:

- Perform optical and radar observation of orbital debris.

- Develop medium-long term evolutionary models of the debris population.

- Study the dynamics and consequences of explosions and/or catastrophic collisions in orbit.

- Evaluate possible measures to reduce or avoid the creation of orbital debris, or to reduce the risks associated with the debris.

- Develop techniques and algorithms to get both optical and radio national sensors into the SST program.

The goal of the presented research activity is to develop a network of observatory fully dedicated for space debris observations. The advantages of establishing a network of multipurpose fully robotic observatories is outlined in Section 2. In the framework of the ASI/INAF agreement for SST, a scheduler called **NICO** (Networked Instrument Coordinator for debris Observations) has been developed specifically designed for the harmonization of individual user requests by considering meteorological and astronomical constraints. Section 3 outlines the advantages of the developed custom solution based on modular architecture and presents NICO functionality. The conflict solver solution implements genetic algorithms with the possibility of optimizing a single telescope of the whole network while IADC observing strategies have been implemented as observing methods. Moreover, an automatic pipeline for the image data processing has been developed as external module of the scheduler to process the collected data is described in Section 4. The analysis tool has been designed to process light-curves measurements to extract the main frequencies of the observed objects in the scale of a second or less. This information is valuable for the dynamic state of the debris to evaluate evolutionary trend and for future active debris removal mission. Finally, Section 5 presents the conclusions.

Chapter 2

Network of observatories

Due to the increasing need to monitor the space environment, observation campaigns are continuously promoted by all the space agencies, especially to avoid possible collision among operative satellites and orbital debris ([Schildknecht et al. (2004)], [Piergentili et al. (2014)]). SPADE observatory was the first step of the *Italian Space Agency* (ASI) towards the establishment of an Italian space debris monitoring program and it has been designed and developed in 2006 by Sapienza - University of Rome. Currently, it is installed to the ASI Centre for Space Geodesy (CGS) in Matera and it is operated by ASI ([Porfilio et al. (2003)] [Porfilio et al. (2004)]). In 2009, Alma Mater Studiorum – University of Bologna conducted a study to design and realize a system for orbital object monitoring based on a mid-latitude and an equatorial observatory named ALMASCOPE. Compared to the use of a single telescope located at mid latitude, improvements in space debris detection and tracking were observed in surveying volume, object identification and orbital determination accuracy [Piergentili et al. (2014)]. Due to the constant growth of operative satellites and space debris in both GEO and LEO regions ([Bastida Virgili et al. (2016)], [Santoni et al. (2014)]), and to increase the space debris observation capabilities, the opportunity to establish a network of observatories outside Europe had been examined to significantly improve the Italian and European capability to provide support to operative spacecraft both in LEO

and GEO impact risk management and in orbital maneuvers measurement.

FIGURE 2.1: ALMASCOPE at Broglio Space Center in 2010.

In 2010, a dedicated optical campaign of the *ALMASCOPE* observatory was performed to demonstrate the increase the Italian monitoring capability in any orbital regime and inclination [Piergentili et al. (2014)]. The validation campaign was conducted in cooperation with ASI from the Italian Base Camp of Broglio Space Center (BSC) in Malindi (Kenya). The base is located on the coast of the Indian Ocean (40.19°E, 2.99°S) and it consists of two segments, the marine segment represented by the launch oceanic platform and the earth segment for the telecommunication center. Thanks to its equatorial location, the base is well suited for Earth based space surveillance activities. To verify the effectiveness of the Equatorial observatory, a three-week test campaign of BSC was carried out in September 2010, using the ALMASCOPE observatory. The observation campaign showed that the average measured seeing during the period around is about $3.5\ arcsecond$ (FWHM) was acceptable for space debris observations, moreover it should be noticed that it is extremely variable with the seasonal effect and close to sea level. Therefore, the test verified the complementary of the Malindi observatory to observatories located in Europe to improve the space surveillance capabilities. The first

improvement in observation capability provided by a network of two observatories located in Italy and in Kenya is the increase of the observed geostationary ring portion: orbit determination capability of GEO objects increases by permitting a more intensive coverage of this orbital regime in terms of surveying time over the arc of the geostationary ring which is visible from both sites by performing simultaneous or consecutive observations from two different sites. It allows to schedule more efficient strategies for different observing purposes. Secondly, by analyzing the visibility of the LEO objects for follow up observations of the same object it has been proven the Malindi site is less influenced by seasonal effect and no difference in frequency of observation opportunities between the equinoxes and the solstices is present. On the contrary the frequency of observation opportunities from the observatory in Italy depends on the combination of orbit shape and terminator groundtrack. Thus, lead ASI to increase the Italian space surveillance capability by considering the development of a network of optical observatories [Cardona et al. (2017b)].

2.1 MITO, the S5Lab Mid-latitude Observatory

In the presented context, Sapienza Space System and Space Surveillance Laboratory (S5Lab) research group of Sapienza - University of Rome, started the refurbishing of their mid latitude observatory fully dedicated to space surveillance located in Rome to improve the Italian capabilities to monitoring the near-earth orbital environment. In 2015, the observatory has been renamed *MITO* (Mid-latitude ITalian Observatory) and the telescope has been in operative phase since early 2016 (Figure 2.2).

FIGURE 2.2: MITO observatory.

- Telescope: 25.0 cm diameter f/3 in modified Cassegrain configuration has been chosen.

- Mount: The observatory is based on a commercial off-the-shelf (COTS) German equatorial mount.

- CCD sensor: it is based on a sensor, which has an array of 8176×6132 pixels, each pixel is 6 (sensor diagonal $61.3\,mm$). The total field of view is about $3.5° \times 2.5°$. The huge FOV is particularly indicated to statistically survey the GEO region and to perform light-curve measurements of bright LEO object.

- Observatory Control Software: The mount and the CCD sensor are directly controlled by the PC using an in-house *C* software to automatize the observation [Diprima et al. (2016)].

- Automatic Dome: the design of the dome has been developed by S5Lab research team and the main characteristic is that once the dome is open, the telescope can point with any azimuth angle without the need to

rotate the dome. Thus in order to reduce the moving parts needed for operations ans allows to track also fast LEO objects.

- External trigger: to have accurate tame tag in the header of the images a GPS receiver is connected to the computer. The GPS module is composed by the GPS receiver, the antenna and the cable. The main functions are:

  - Update computer's time.

  - Provide accurate trigger to the CCD shutter.

- Security cam: an IP infrared camera is used to monitor the status of the whole system during remote operations.

The functional scheme of the observatory is summarized in Figure 2.3.
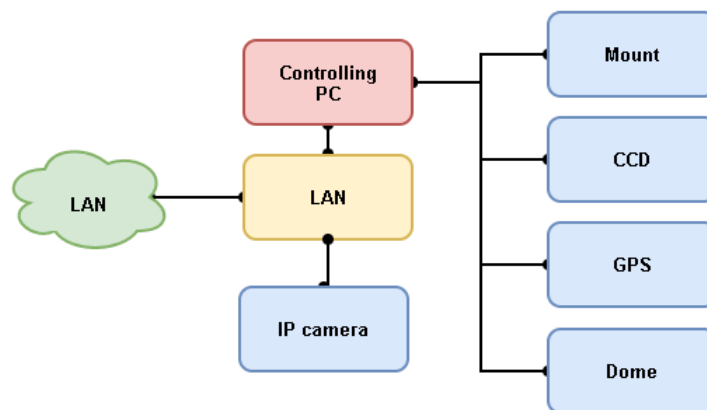
FIGURE 2.3: MITO architectural scheme.

2.2 EQUO, the S5Lab Equatorial Observatory

In 2015, a joint three-year project named *EQUO* (EQUatorial Italian Observatory) in cooperation between ASI and Sapienza has started in the framework

of the ASI-Sapienza Agreement (*N.2013-078-C.O*) ([Piergentili et al. (2015a)], [Piergentili et al. (2015b)], [Cardona et al. (2015a)] and [Cardona et al. (2016c)]). The goal is to develop a observatory composed by two telescopes to be installed at BSC in Malindi. The presented initiative concerns the cooperative development between ASI and Sapienza - University of Rome of an optical observatory at the BSC managed by the ASI for the study and the monitoring of orbiting object and re-entry campaigns. The activities involved concern the installation of an optical observatory equipped with a computing center with archiving equipment, local and remote point-of-view control over internet. The observatory consists in two optical telescopes located one at the base camp of BSC named *EQUO-OG* (EQUO-On Ground) while *EQUO-OS* (EQUO-Off Shore) on the Santa Rita 2 off-shore platform 6 km from the coast in the Indian Ocean. The main calculation center in located in Rome at S5Lab facility.

The main targets of the observations are active and non-operative satellites at different orbit, upper stages of launchers including LEO stages and objects in phase of return into the atmosphere. The performed observations will allow to perform statistical analysis both for scientific observation and investigation on the origin of the debris and for the planning of collision avoidance maneuvers. The scientific relapse of this project can be summarized as:

- Statistical survey of debris population in different orbit such as LEO / MEO / GEO / HEO for IADC international campaigns [IADC (2002)].

- Close approaches analysis for objects in LEO, using bistatic orbital determination with the observatories located in Italy and Malindi.

- Reconstruction of the attitude motion of orbiting objects from light curves.

- Photometric characterization of observed target.

- Optical tracking test of launchers (trajectory reconstruction, attitude, configuration, separation of the upper stages).

- Observations of re-entering objects as support of IADC international campaigns.

- Data fusion among optical and doppler data with the support of the ASI-Malindi telemetry receiver station.

EQUO has been designed to work on two systems, one telescope in a configuration with the widest field of view more suitable for the survey purpose while the other has been designed for the follow-up of observed objects and it is equipped with photometric and spectrometric sensors. Survey operations are preferentially carried out with EQUO OG that consist in a more flexible telescope located at the BSC. The peculiarity of the off-shore platform, which has an extremely dark sky background and therefore a very low noise from the sky background, make the observing site favorably suitable for high positioning analysis and spectro-photometric measurements. Nevertheless, both frames can perform the same types of IADC standard observation strategies.

2.2.1 EQUO-OG overview

The main components of the EQUO-OG observatory (Figure 2.4) are:

FIGURE 2.4: EQUO-OG installed at Broglio Space Center.

- Telescope: a Newtonian Reflector $20.0\,cm$ diameter telescope $f/4$ configuration has been chosen due to a field of view capable to support large size CCD. The main drawback of the Newtonian telescopes is its coma aberration, that has been reduced by using a commercial off-the-shelf (COTS) coma corrector.

- Mount: The mount has been selected with the following features:

    - Controlled by dedicated software.

– Capable to track objects with differential rate on two axes at HEO orbits.

– Suitable for LEO follow up observations.

– Suitable to be used at low latitude.

To satisfy these requirements it has been chosen to use a COTS Alt-Az mount that allow to easily track fast moving objects

- CCD sensor: for survey purpose, a sensor which has an array of 3056×3056 pixels, with a pixel size of 12 (sensor diagonal $51.9\,mm$).

- Controlling Computer: the environment in which the computer that controls the mount and the CCD sensor should operate is characterized by the presence of what can corrupt electrical circuits and mechanical parts. Moreover, it must resist to heavy rain due to the possibility of unexpected thunderstorms that are typical of rainy season in Malindi. These can be faster than the shutdown procedure of the observatory and the automatic closing system of the dome. Furthermore, the computer should hold up to very extreme operative condition due to the high temperature during summer (under the dome the temperature can exceed 40). For these reasons S5Lab research team decided to choose as controller computer a rugged pc, specifically designed to operate in harsh usage environments and conditions, such as strong vibrations, extreme temperatures and wet or dusty conditions.

- Observatory Control Software: the EQUO control software is a custom version designed by S5Lab of the software *Observatory Control* already used for MITO observatory.

- Weather station: it is a crucial component to complete the instrumentation of an astronomical observatory. Especially in the order to make EQUO a complete remotely controlled observatory. The main role of

a weather station is to evaluate the atmospheric condition to perform safely night observations. In fact, it should alert the system in case of clouds or rain and proceeds to the complete shutdown of the whole system (or not allow the user to start the observations). Moreover, a weather station allows evaluation the collected image quality. The weather station allows the S5lab research team to collect accurate weather data to create forecast and historic on temperature, rain and wind trends. The chosen station is a Davis VantagePro2 which main sensors are:

- – Pluviometer with rain collector.

- – Temperature and humidity sensors.

- – Anemometer.

- Automatic Dome: to perform fully automatic observation, a remote-controlled dome has been designed, realized and installed at BSC base camp on the roof of the basement of the MLD-2 antenna by S5Lab research team.

- External trigger: an analogous solution as MITO observatory has been installed to provide precise and accurate time tag and to control the shutter of the CCD.

- Security cam: as for MITO an IP infrared camera is used to monitor the status of the whole system during remote operations.

EQUO-OG installation at Broglio Space Center

The EQUO-OG installation campaign at BSC was conducted between March 11 and 20, 2016 ([Cardona et al. (2016c)]). The dome was developed and manufactured by the S5Lab research team (Figure 2.5). The dome manufacturing phases are presented from Figure 2.6 to Figure 2.10.
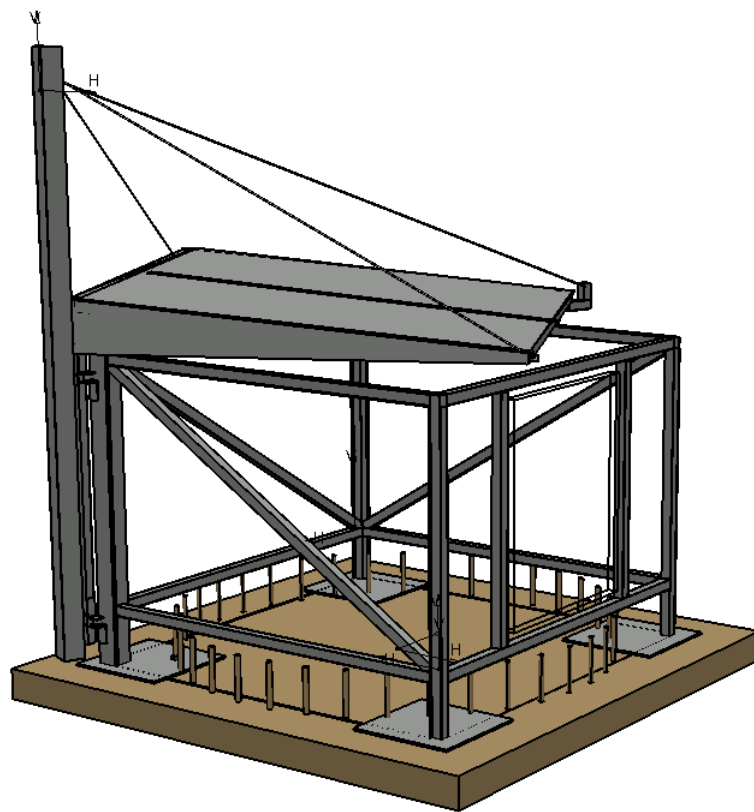
FIGURE 2.5: EQUO observatory.

FIGURE 2.6: EQUO observatory.

FIGURE 2.7: EQUO observatory.

FIGURE 2.8: EQUO observatory.

FIGURE 2.9: EQUO observatory.
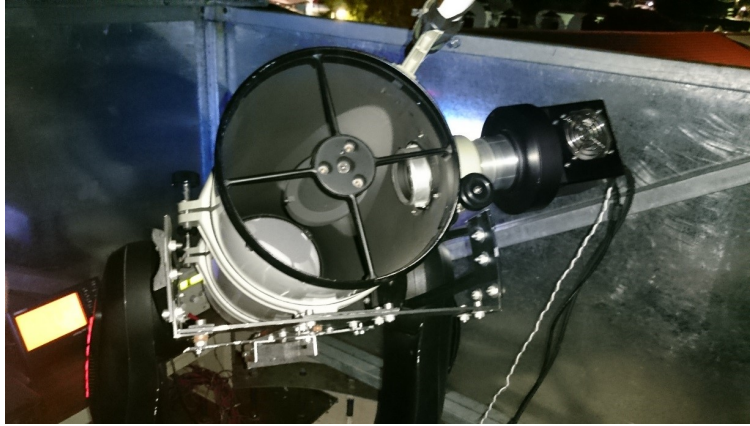
FIGURE 2.10: EQUO observatory.

During the ten-day installation campaign, more than $2,800$ images have been collected with EQUO-OG at different orbital regimes and different observing strategies as shown in (Figure 2.11) [Cardona et al. (2016c)].
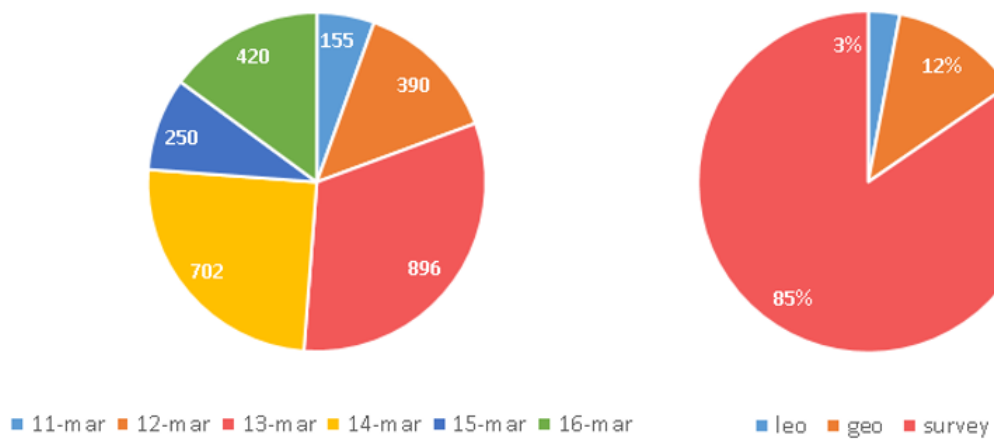
FIGURE 2.11: Collected images have been take for several orbital regimes.

2.2.2   EQUO-OS overview

EQUO observatory has been tested on both San Marco and Santa Rita 2 Off Shore platform to evaluate seeing condition for the installation of EQUO-OS [Santoni et al. (2017)]. The design of the off-shore observatory regards the system level analysis and the definition of different components to be assembled. The main components of the EQUO-OS observatory that have been identified are:

- Telescope: a $25.0\,cm$ diameter telescope $f/4$ configuration has been chosen. It doesn't need a coma corrector.

- Mount: The mount requirements for the off-shore observatory are the same of the ones for the on base solution. Therefore, a COTS Alt-Az mount has been selected to perform easily tracking of fast moving objects such as LEO targets and to perform beam-park observations (i.e. GEO survey).

- CCD sensor: The chosen CCD is an monochrome CCD back-illuminated camera with high quantum efficiency ($> 75\%$). The array is 1024×1024 pixels with a pixel size of 13 (sensor diagonal $18.8\,mm$). To perform color photometry, the CCD is equipped with a 1.25J filter wheel.

- Controlling Computer: the environment in which the computer is going to operate on the off-shore platform is even more challenging than the one on the base-camp. Therefore, similar rugged solution has been selected. Observatory Control Software: the EQUO control software is the same version designed by S5Lab of the software *Observatory Control* for EQUO-OG.

- Weather station: even if the off-shore platform is just 6 km far away from the BSC base camp, the weather conditions are extremely influenced by the see. Therefore, also the EQUO-OS observatory is equipped

with an autonomous Davis VantagePro2 weather station.

- External trigger: a GPS module will provide an update of the computer's time and the accurate trigger to the shutter of the CCD as for EQUO-OG.

- Automatic Dome: the design of the dome is analogues to the one of EQUO-OG.

- Security cam: an IP camera is used to control the status of the observatory during remote operations.

Evaluations on seeing and possible light pollution of the location have been performed during a two-night observing campaign on the off shore platform using the EQUO-OG telescope (from Figure 2.12 to Figure 2.14).
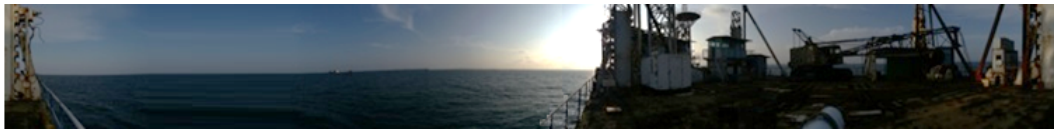
FIGURE 2.12: Full $360°$ azimuth range view from the location on the Santa Rita 2 Off-Shore Platform.

FIGURE 2.13: EQUO-OG tested at future EQUO-OS location site.

FIGURE 2.14: EQUO-OG tested at future EQUO-OS location site.

2.3 Partner observatories of the S5Lab network

Other observatories are partner of S5Lab network to conduct analysis on space debris. Mainly these instruments located worldwide are used for lightcurves data acquisition due to their large diameter and favorable seeing condition. Loiano observatory and Curtis-Schidmt observatory are used for GEO target, while Angell Hall observatory has been used for Monliya object and to test new observing strategy.

2.3.1 1.5-m Loiano Observatory

In 2011 a pilot program for the physical characterization of the space debris population in high Earth orbits through photometric measurements was started and has gone on since then at the *G.D. Cassini Observatory in Loiano*,

operated by *INAF Astronomical Observatory* of Bologna, Italy ([Rossi et al. (2011)], [Rossi et al. (2012)] and [Rossi et al. (2013)]). The telescope is a $152\,cm$ diameter in Ritchey-Chretien configuration system with $f/3$ at the primary focus and 8 at the secondary(Figure 2.15). The telescope system has been refurbished in 2015 and it can track with sidereal rate and non-sidereal rate mode. The system is equipped with a multipurpose instrument for imaging and spectroscopy, with an EEV CCD (array 1340×1300 pixels) with a field of view of $13' \times 13'$.

FIGURE 2.15: Loiano observatory.

S5lab research team is cooperating with INAF and ASI for characterization of

debris population using the Loiano Telescope ([Cardona et al. (2016a)], [Cardona et al. (2016b)] and [Parish (1994)]). The main application field are: analysis on the dynamic state of the object by analyzing the study the brightness variability as possible indication of variation in the attitude over timescales of a second and analysis on the possible origin of the debris by studying the materials to identifying the source. Therefore, the adopted strategies are:

- Long exposures with sidereal tracking with R filter [Gualandi et al. (2001)] are taken where the object image trails across the field of view to. To reduce the effect of star contamination on the streaks, multiple exposures of the same field will be acquired as mask subtraction of the background stars. The collected measurements contribute to create and maintain a catalog of the spin rate evolution of the object.

- Spectroscopy of GEO debris using the Blind Non-Sidereal Tracking strategy to keep the object inside the slit. The acquired spectra are then compared with laboratory spectral reflectance data on several typical common spacecraft materials including solar cells, circuit boards, various Kapton materials used for multi-layer insulation, and various paints ([Abercromby et al. (2013)], [Seitzer et al. (2013b)], [Cowardin et al. (2010b)], [Cowardin et al. (2009)], [Cowardin et al. (2010a)], [Seitzer et al. (2013a)]).

2.3.2 0.4-m Angell Hall Observatory at University of Michigan

The Angell Hall observatory (Figure 2.16) is run by the Astronomy Department of the University of Michigan (USA) and it is used for classes and public outreach. The telescope is a $0.4\,m$ Ritchey-Chretien reflector, equipped with a spectrograph and camera and its control system has been refurbished in 2016

with the new WinTCS (Windows Telescope Control Software) developed by DFM Engineering. Due to the executive protocol of the general agreement for scientific cooperation between Mechanical and Aerospace Department of Sapienza University of Rome and Astronomy Department of University of Michigan, specific. The telescope has been used to test the controlled streak algorithm presented in section 3.

FIGURE 2.16: Angell Hall observatory at University of Michigan.

2.3.3 0.6-m Curtis-Schmidt Observatory at Cerro Tololo

The Curtis-Schmidt telescope (Figure 2.17) is a 0.61 meter aperture $f/3.5$ Schmidt telescope and it is located at the Cerro Tololo Inter-American Observatory in Chile. Originally installed at University of Michigan Portage Lake Observatory in 1950, but then it was moved due to the light pollution of the location to the clearer skies of north central Chile in 1966. The telescope is fully dedicated to optical studies of space debris for NASA Orbital Debris Program Office at the Johnson Space Center. The acronym for the debris project is MODEST (Michigan Orbital DEbris Survey Telescope ([Seitzer et al. (2012b)] and [Seitzer et al. (2013b)]).
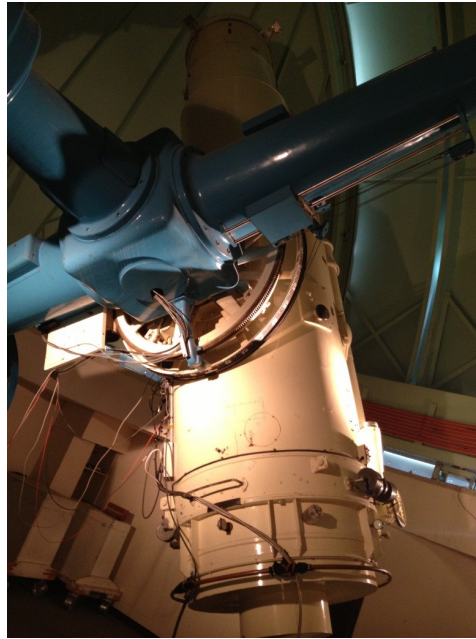
FIGURE 2.17: Curtis-Schmidt observatory at Cerro Tololo in Chile.

Chapter 3

Scheduling solution for space debris observations

3.1 Scheduling process

Scheduling can be considered as the allocation of resources over time to per-
form collection of tasks ([Burrowbridge (1999)]). The scheduling model of or-
bital debris can be considered as composed by a set of optical ground station
which move with the surface of the Earth, a set of space situation awareness
center which can be assumed connected to ground station, and orbital de-
bris travelling through different kind of orbit generating visibility windows
when the line of sight (LOS) to ground station exist ([Vazquez et al. (2015b)],
[Soma et al. (2004)]). The SSA operators aim to collect more information (i.e.
accurate orbit, attitude determination, spin rate evolution, etc.) about the de-
bris of interest but this can only be done through the ground station network.
The combinatorial explosion in the number of intervals to be scheduled has
been caused by the increasing number of space debris to be observed with
optical ground station. Therefore, new scheduling approach are needed to
provide a solution to the new requests ([Schalck (1993)], [Gooley (1993)] and
[Barbulescu et al. (2004)]). Based on the dynamic of the scenario and the

requirements of the mission, the ground station operators generate a set of requests characterized by constraints associated to these time windows [ESA SSA Programme (2017)]. The objective of the scheduler is to generate, from this set of requests, a schedule which is a subset of these requests selected for execution (Figure 3.1).
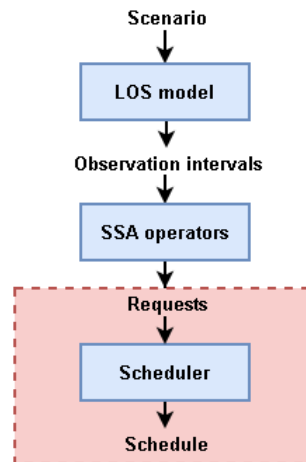
FIGURE 3.1: SSA scheme.

3.1.1   Scheduling horizon

The length of the visibility windows strongly depends on the geometry of the problem (orbit of the debris and geo-localization of the observatory). For example, an object in LEO might have a pass time over a station not longer than ten minutes. Given that relative small time, at least half of the whole visibility windows is required to acquire valuable data. On the contrary, for higher orbit, a visibility window might last longer than one hour (in GEO there might be continuous visibility). For this case, only a small section of the visibility windows might be needed depending on several observability constraints. Therefore, release time and due time should be detected to extract a section of the visibility windows in which the scheduler must operate

to identify the task. The finite time duration of the scheduler is normally defined as scheduling horizon in which all collected requests must be processed to obtain the schedule (Figure 3.2).
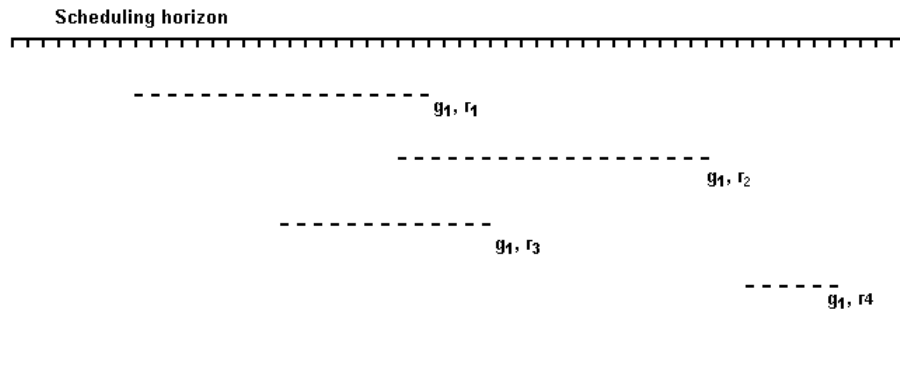
FIGURE 3.2: Scheduling horizon.

The problem of optical observations deals with allocating time on multiple instruments and the automatization of the procedures ([Johnston et al. (2006)], [Johnston et al. (2011)], [Damiani et al. (2006)], [Damiani et al. (2007)], [Johnston et al. (2012)], [Clement et al. (2005)] and [Dreihahn et al. (2007)]). The first crucial time-constraint in addition to the definition of the target variability windows is the observatory must operate in the darkness for the whole observation. Start and end are defined by the solar elevation angle. For astronomical purpose, the twilight definition is connected the geometric center of the Sun's disk that should stay between 12 and 18 degrees below the horizon. Therefore, night duration is not a constant during the year and it is shorter during summer and longer during winter. Managing a network worldwide distributed, is a solution to acquire data during the whole year by reducing the seasonality effect. It is important to consider that observatory operation during night can be disturbed by various factors. Those can be divided into predictable and unpredictable interruption. Predictable interruptions are usually caused by maintenance work, which must be performed at given time at the observatory. Unpredictable is weather,

which causes major observatory downtime, and technical issues with the instruments of the observatory, which causes some downtime. Depending on location, season and past years' experience, weather downtime can be statistically estimated, while technical downtime can be considered less than one percent. The time-related constraints on the requested are not the only ones [Wolfe et al. (2000)]. Astrometric data might be better to be acquired under certain astrometry condition (i.e. far from the moon to avoid light pollution or distant to Milky-Way to avoid background star contamination of the picture frame), or more critically, the SSA operators might to associate to the requests specific priorities to model these preferences. Additionally, the operators might plan to improve the orbit of a specific target therefore, multiple observation of the same target with multiple observatories or in successive night might be required [Vallado (2001)]. If time-overlaying requests associated either to the same satellite or ground station occurs, these are considered a conflict. For this case, a conflict solution approach must be applied. In fact, the scheduling problem requires to find a feasible schedule that maximize the sum of the priorities of the request included in the schedule, given the requests and the associated constraints ([Gooley et al. (1996)], [Pemberton (2000)], [Frank et al. (2001)]). In literature, the sum of these priorities is defined as metric of the schedule and represents the performance. The problem can be complicated even more by considering more debris to be observed by a network of optical observatories ([Warwick (1959)], [Schmidt (2011)]). A set of requests can be represented as in Figure 3.3 where the start and end times of the visibility windows are indicated along with their associated priorities based on user preferences. A feasible schedule is then shown where all conflicts have been solved.
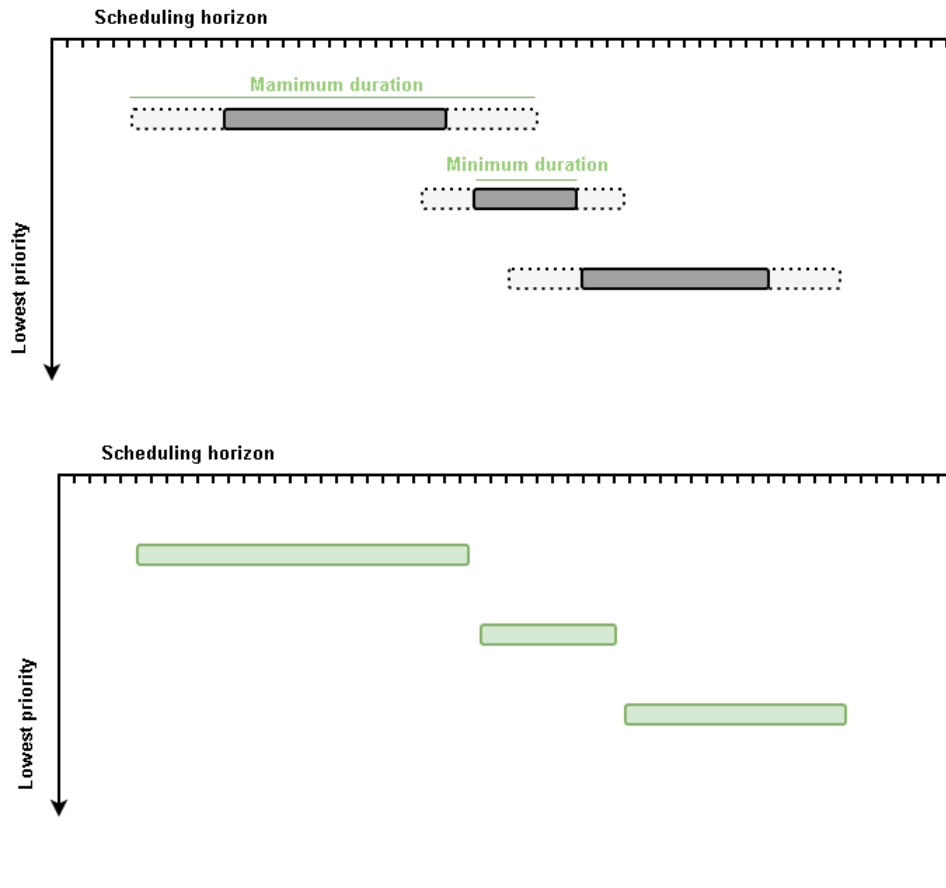
FIGURE 3.3: Scheduling horizon.

3.1.2 Scheduling characteristics

For general purpose, different kind of schedulers can be used to solve the problem, the choice depends on the additional constraints on the mission to be accomplished. In literature ([Vazquez et al. (2015a)], [Johnston et al. (2006)], [Vazquez et al. (2015c)]), the classification involves three parameters:

- Topology: the calculation of the schedule might be performed in a centralized way where a single schedule for the whole network is calculated based on the request given by the users and then transmitted to the whole ground station of the network, or a distribute method where the schedule for each ground station is computed independently without a coordinating entity.

- Uncertainty: the presented problem is deterministic if the entities are one-hundred percent reliable otherwise it is stochastic.

- Changes: the requests are static if they do not change from the start of the scheduling horizon to its end, otherwise the request are considered dynamic if they may change before the completion of the schedule.

3.1.3 Space debris scheduling problem

According to the presented distinction, it possible to describe the proposed scheduler fully dedicated for space debris observation as a centralized, almost deterministic and static. The schedules are for each observatory are computed in a centralized data-center and then transmitted to each observatory control computer to be executed; the entities are considered reliable for what concerns the tracking requests while the survey requests are calculated with a statistic approach; finally, due to the request are calculated to optimize the whole network the request are static. Therefore, the aim of the developed scheduler is to maximize the network performance, expressed in terms of metric of the schedule. In the framework of ASI/INAF agreement (*N.2015-028-R.0*), the S5Lab research group has developed algorithms for the reconstruction of dynamic state of orbiting objects from data obtained with the Italian optical observatories [Cardona et al. (2017b)]. One of the major task has been the development of a scheduler to coordinate the whole network. The developed scheduler is called NICO (Networked Instrument Coordinator for space debris Observations) and its main goal is the harmonization of the requests for optical observation from SSA entities by considering astronomical and weather conditions constraints.

3.2 NICO architecture overview

NICO architectural scheme is shown in Figure 3.4. Registered users can log in to NICO server via WAN (Wide Area Network) through their computers. They can query the login database for authentication and enter requests into the request database. The server then has the function to transmit collected requests to the NICO back end layer for processing. Request database management is multi-transaction and hashing password algorithms (`SHA256/HMAC`) are implemented [Fielding (2000)].
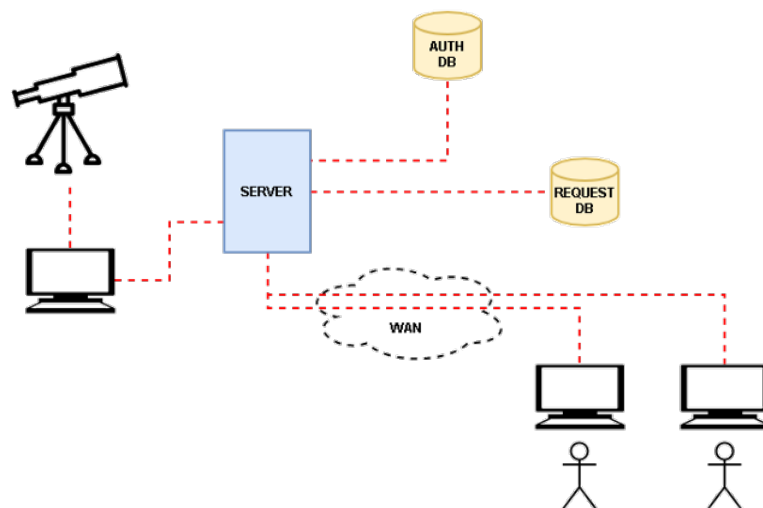
FIGURE 3.4: NICO network architecture.

3.3 NICO layers

NICO is composed by two main parts [Cardona et al. (2017b)]

- **Front-end layer** (FE) is designed to allow external registered users such as SSA entities to specify their observing requests according to their needs (Figure 3.5). The users can select different type of requests:

- Survey observation in Medium Earth Orbit (MEO), in GEO or in Molniya orbit. The scheduler will identify the most convenient celestial coordinates region in terms of statistical analysis of the population of the specified orbit to perform acquisitions;

- Light-curve observation [Cardona et al. (2016a)] by indicating the NORAD (North American Aerospace Defense Command) catalog identification code of the target;

- Follow-up observations.

- Specific celestial coordinates observation by indicating the right ascension (RA) and declination (DEC). This kind of request is not time-bounded and it has been designed to let the user acquire data on photometric calibration stars.

The users can select a specific priority for each of their request. Moreover, the user can set a preference for the observatory to be used for the specific request or let the system evaluate the one to schedule with. The front-end layer has been developed in *Node.js*. Through the FE interface, the login requests come through `http/POST` communication protocol to the *Back-End* (BE) layer. The BE queries the Login database and verifies the credentials to guarantee the access to the user. If the credentials are correct, an authorized FE side session is opened. Through this session, the user can access the BE layer through http/POST protocol to query the requests database and insert specific requests [Fielding (2000)]. The BE validates the requests and delivers the `OK/KO` result to the FE to be displayed (Figure 3.5).
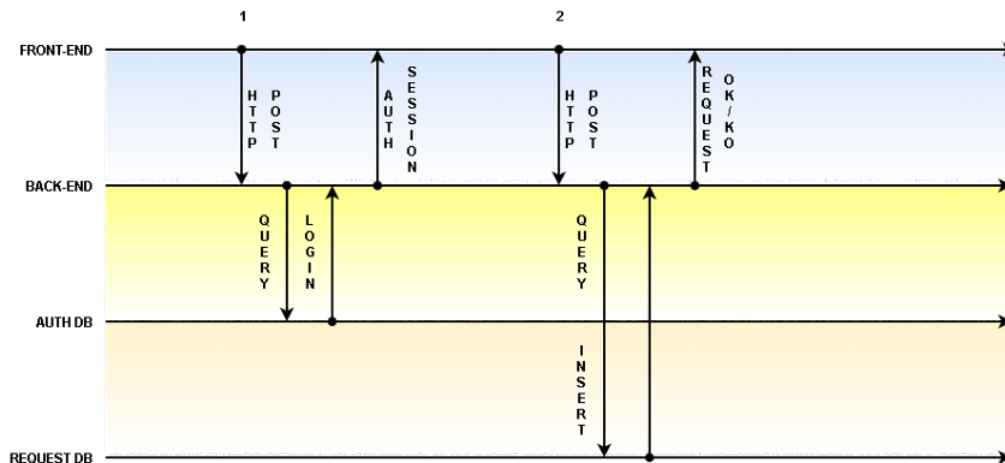
FIGURE 3.5: NICO front end layer architecture.

- **Back-end layer** (BE) is the core of the presented NICO scheduling software (Figure 3.6). Once all requests for the night have been collected into a database, the software automatically downloads and processes them to obtain the schedules for each observatory of the network. Data are downloaded from the requests database and pre-processed. Moreover, alert for maintenance status and weather condition for the night are collected from each observatory of the network to exclude specific observatory from the scheduling process for specific hours ore exclude them completely if not available for the whole night. The schedule is designed to resume observation from the previous day if it was not possible to include them in the final schedules due to conflict with another request or if are needed to be repeated (i.e. follow-up observations). One of the main tasks is the visibility window allocation process in which all requests are computed to allocate the time to be observed in the best conditions by taking care of several astronomical constraints ([Cardona et al. (2017b)]). Then, conflicts are solved using a developed implementation of genetic algorithms [Parish (1994)]. During this

phase, the duration of the requests is muted inside the parameters defined in the visibility windows and it is evolved toward better solutions. The goal of the optimization process is to maximize the metric of the schedules of the whole network [Barbulescu et al. (2006)]. Nevertheless, this setting can be modified in pre-launch phase by setting as target the optimization of a single observatory of the network. Finally, once the new temporal slots are defined for each accepted request, a specific schedule generator process is applied. This module implements the observing strategies defined in IADC meetings especially for survey [IADC (2002)]. Moreover, the implemented strategies are compliant to IADC-WG1 standard observing strategies adopted in Action Item such as AI23.4 and AI31.2. The implemented strategies consider the different characteristics of the sensors and mount (in terms of FOV, quantum efficiency, pixel scale, slew rate). The outputs are the schedule in a standard format to be transmitted to the observatories of the network. The whole process is monitored with a log to evaluate the performance of the software during the execution. Moreover, general and specific report for each observatory are generated and stored.
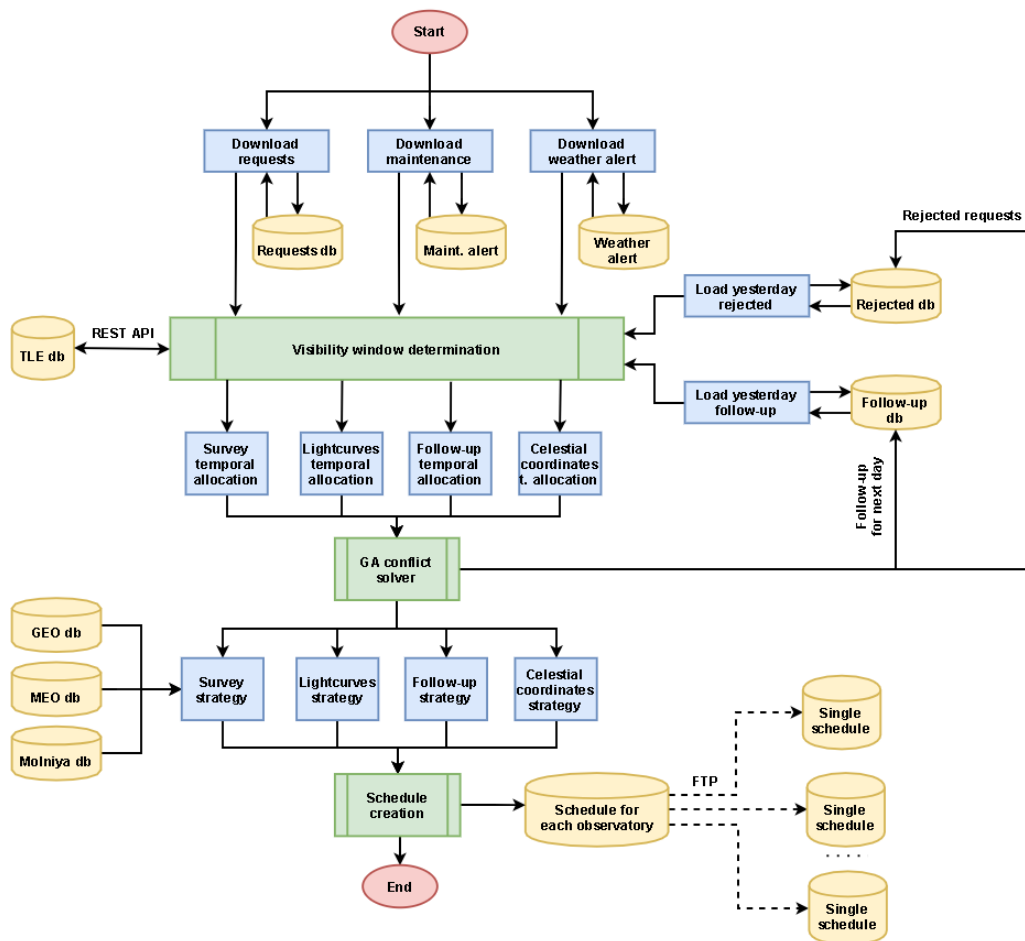
FIGURE 3.6: NICO back end layer architecture.

3.4 NICO front-end layer

The developed scheduler has been designed based on past S5Lab user experience in participating into international observing camping and incoming SSA requests. Therefore, the guidelines that driven the design and the implementation of the user requests have been evaluated based on past IADC international campaign.

3.4.1   Implemented operative modes

Four different operative modes have been implemented:

- **Survey**:

  In the last fifteen years several international campaigns have been promoted by IADC for the statistical evaluation of debris population in higher orbit. These observational surveys are carried out by delegations of all nations participating in IADC-WG1. The aim is to determine the extent and character of debris in HEO, specifically by obtaining distributions for the brightness, inclination, right ascension of ascending node, and mean motion for the debris. During these campaigns, it is crucial to calculate the complete sets of orbital parameters for example to discriminate GEO objects from ones in different orbits (i.e. GTO). These kinds of statistical studies are conducted by performing orbital analysis of uncatalogued (UCT) objects to avoid an overestimation of the number of GEO objects by eliminating repeated counts of the same object. The goal of these campaigns is to develop an understanding of the space debris situation in HEO [Molotov (2011)] through the following points:

  - Continue statistical monitoring orbital regimes.

  - Initiate small-object optimized observations of clusters in orbit pole distribution to provide information on evolution of GEO break-ups.

  - Facilitate opportunities for inter-facility co-operation by defining simple formats for exchange of data as appropriate.

  - Initiate collaborative observing of found objects with significant night-to-night motion, such as GTO and drifting GEO debris.

   – Extend observing techniques to enable estimation of eccentricity e to minimize contamination of surveys by $e > 0$ objects.

In the recent years, new international campaigns have been promoted, therefore NICO has been equipped with a specific module to perform survey scheduling. It allows request schedule for statistical survey of debris population in:

   – GEO ($0.95 \leq Mean\,Motion \leq 1.05$ and $e < 0.05$);

   – MEO ($600\,m \leq Period \leq 800\,m$ and $e < 0.25$);

   – Molniya orbit ($61° \leq Inclination \leq 65°$ and $1.90 \leq Mean\,Motion \leq 2.50$ and $e \leq 0.75$).

It is possible to notice that the Molniya request is compliant with the IADC-WG1 IT34.1 presented in Chapter 1. All surveys are based on a statistical analysis of the current population in the specific orbit. By processing the sky track of the celestial coordinates of each object for the selected night, a Region of Interest (ROI) is identified as the region with the highest density of object. Therefore, it can be considered as the region in which collision among object are more likely to happen. Different observing strategy have been implemented for each of the identified region depending on the orbital parameters of the object.

- **Light-curve**: Many satellites and space debris do not have a constant brightness [Somers (2011)]. They reflect flashes at typically regular times. This flashing behavior is caused by the rotation of the satellite around its rotation axis. The reflecting surfaces of the satellites or of the debris, such as metallic surfaces or solar panels, act as mirrors for the sun. Objects with a diffusely reflecting surface will also show varying brightness since the observer will see a changing amount of light reflecting area of the observed target as it tumbles in its orbit. Measuring

the period between two flashes or maxima/minima in the light curve can provide a good approximation for the satellite's rotation motion. However, the rotation period can be correlated to the flashes pattern through analysis of geometrical configuration and physical composition of the satellite if known. The attitude motion changes during space debris lifetime due to perturbations that act on the object, like the earth magnetic field, the solar radiation pressure or the atmospheric drag for LEO. Especially for HAMR object, solar radiation pressure is very important due to the intrinsically characteristic of high area to mass of the debris, therefore the interaction between the surface and the radiation pressure is very high. This interaction can change the attitude and these changings are observable even in short period on light curves. To investigate brightness changes, the object is let to trail across the FOV while the telescope is tracking at the sidereal rate. The exposure time is calculated to detect both streak ends of the observed object. Therefore, it strongly depends on the orbit of the observed object (lower the orbit shorter the exposure time will be) and the FOV dimension. Moreover, the exposure time is calculated to detect also the background stars whose position is available through star catalogs. Triangulation methods are used to assign the coordinates of specific points of the streak which are usually the midpoint and the endpoints and therefore reconstruct the orbit of the object. NICO has a light-curve method implemented to be able to schedule the collection of light-curves of the request target by taking care of several constraints to improve the image quality.

- **Follow-up**:

  Accuracy of an orbit determination depends on the number of observations, the length of the observed arc and the geometry of the system.

Therefore, to improve the orbit determination accuracy it is possible to optimize either one or all the just mentioned factors. When a piece of space debris is observed by optical telescopes, angular and angular-rate information can be precisely estimated from the track using basic kinematics. However, range and range-rate information is to a large extent undetermined, other than by a few weak physical constraints. The standard approach in performing an orbit determination between two separate tracks of data is the least squares approach. Batch least squares estimation is typically used as a post-processing estimation tool as all available data are batch processed to determine the epoch estimate. A reference spacecraft state is propagated from the epoch time throughout the measurement period and predicted observations of the spacecraft computed. The difference between predicted observations and experimental measurements are referred to as observation residuals; the least squares solution is the spacecraft state that minimizes the weighted sum of the squares of the observation residuals. This solution is used to update the reference state and the batch least squares is iterated until a defined convergence tolerance is met. NICO has a follow-up method implemented to be able to schedule the collection of astrometric of the request for at least two consecutive night giving to the request the highest scientific priority values. If one of the two nights is rejected, then the request is rescheduled again for a two-consecutive night observation.

- **Celestial coordinates**:

  Photometric calibration of CCD imaging data is a vital, yet time-consuming, requirement also for data processing of space debris measurements. The basic photometric toolbox must contain methods the following tasks: image centering, estimation of the background sky level, calculation of

the flux contained within the object of interest. In particular, the estimation of point source intensity is crucial to reconstruct the proprieties of the considered object. For space debris observation purpose, stars represent a source of background contamination when the flux distribution is studied over a streak. To solve these problems, it might be required to takes several exposures not time depending of specific field of view for mask subtraction techniques. These requests might also be for photometric-standard fields to perform photometry correction. Therefore, NICO has been developed with the possibility to request specific celestial coordinates with no time-specification. These requests can be applied with no precession (*JActual*) or in classic *J2000* precession.

3.5   NICO back-end layer

The goal of the scheduler is to allocate telescope resources to collect data to assure the optimal operability of the observatory according to the request genereted during the input phase as presented in Section 3.4. The main advantage of the NICO back-end layer is its the modular architecture as presented in Figure 3.6 and it adaptability to a possible evolution of the network which must manage and coordinate. In fact, all specific settings of the network including number of observatories involved, their location, the sensors they are equipped with and their parameters are automatically loaded from external files. In this way, it is possible to adapt the presented solution to new operative environments. Moreover, each operative phase is surrounded by a logging phase that is crucial to evaluate not only the statistics of the NICO in terms of metrics of the scheduler, but mostly the correct behavior of the code and allows the operators to estimate an optimization level for

the different task. The back-end layer is designed to process not only the request generated during the input phase in the last 24-hour. At specific Time of Day (TOD), the scheduler is designed to automatic download the new request from the database and it is also intended to search for the previous day requests that need to be rescheduled. In fact, requests can be denied if there is no valid pass over the ground stations of the network or can be rejected due to a conflict with other request with higher priority. Nevertheless, these are not discharged but are stored into a separate database ready to be rescheduled the next day with the highest user priority value. Moreover, as previously mentioned, follow-up requests need to be successfully scheduled for at least two consecutive nights for orbit improvement. Therefore, these are appended to NICO data-set for scheduling evaluation.

3.5.1 Scheduling problem

The first step of the process is the visibility windows generation. This is obtained by propagating the current population of orbital objects by using TLEs. A `API-REST` is used to download current TLE population available in external public catalog. Starting from this database, three subsets are also generated for the specific survey population (GEO, MEO, Molniya) basing on the mean motion, inclination and eccentricity values as defined in Section 3.4.

As presented in literature ([Vazquez et al. (2015a)], [Vazquez et al. (2015b)]), let t_0 be a time instant and T a time windows (scheduling horizon) such that $t_0 \in [t_0, t_0 + T]$. Let $S = \{s_h\}$ be a set of space objects and $G = \{G_i\}$ a set of ground station. Whereas ground stations can be moving with the surface of the Earth, satellites travel through different kinds of orbits. These two different motion dynamics generate visibility time windows when LOS between satellites and ground stations exist. The interactions in terms of observations, are limited to occur within these visibility windows.

3.5.2   Model of the observing request

As described in Section 3.4, a set of requests for the interactions among the target and the ground stations are defined, which are constrained to occur inside the visibility windows described in Section 3.5.1. Let r_j and d_j the release and due times of a request associated to a visibility window $o_j = (\tau_{sj}\,;\,\tau_{ej})$ then $\tau_{sj} \leq r_j < d_j \leq \tau_{ej}$.

A the minimum time need over each request is defined as $\underline{\rho_j}$, while a maximum time is defined as $\overline{\rho_j}$ inside the interval $[r_j\,;\,d_j]$. Each request has an associated priority to the interaction depending on several constraints.

3.5.3   Problem constrains

As mentioned in Section 3.5, the visibility windows allocation is evaluated individually for each observatories and different requirements are applied depending of the kind of the request. These constraints can be classified according to their origin.

Maintenance constranits

One of the main information needed from the scheduler to evaluate the operability of an observatory of the network are the maintenance constraints. If ordinary or extra-ordinary maintenance procedure are scheduled at a specific observatory, it has to flagged as non-operative for the whole night or out of service only for specific hours. Therefore visibility target allocation has to be redirected to other operative observatories of the network.

Weather constrains

An analogous process to the one described in Section 3.5.3 it has been implemented for the weather constraints. S5Lab network is designed to be equipped with standalone weather station. Specific weather forecasts are available for each observatory. If the sky is forecasted to be fully cloudy or if the seeing will be over a certain value (greater $5\,arcsecond$ due to humidity level) NICO is designed to not schedule observations at all at for the specific observatory and all the observations will be scheduled on the other observatories of the network.

Target constrains

The visibility window for each target starts when the object to be observed exceeds a minimum elevation. This limit is needed to avoid any ground based obstacles that can disturb the observations and to avoid any possible light pollution caused by ground illumination systems installed nearby the observatory. The implemented value has been obtained by performing a full 360-degree azimuth range analysis at each observatory of the network. Space debris scheduling problem means to schedule a multitude of request per day between a network of telescopes and the number of possible targets is increasing. The scheduling of the observations must take place in a time windows because the target is visible from the observatory only for limited time during its orbit (when the elevation is greater than the defined limit for the specific observatory). This visibility windows are shorter for low-altitude satellites than for medium or high-altitude satellites. The longer time window of the higher-altitude satellites makes scheduling them less difficult than scheduling the low-altitude satellites. As shown in Figure 3.7, the

minimum duration required for LEO object to collect valuable data is defined as half the maximum visibility windows.
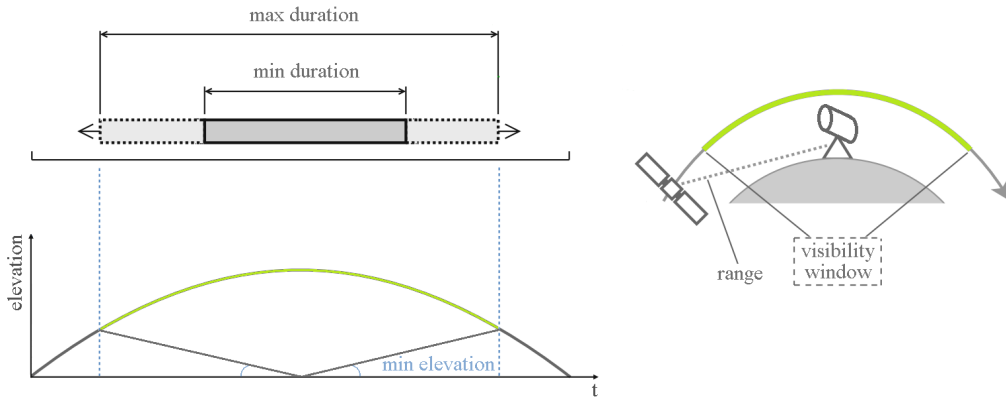
FIGURE 3.7: Time window limit definition.

Astronomical constrains

For better data acquisition and to avoid rejection during the data processing phase, several astronomical constraints need to be implemented.

- Maximum elevation of the sun: the maximum elevation angle of the sun to be considered is $-18°$ (limit of the *astronomical twilight*). To avoid limitation in detection of early LEO passages, the selected limit is $-12°$ (*nautical twilight*).

- Maximum Solar Phase Angle: Solar Phase Angle (SPA) is defined as the angle between the direction to the Sun and the direction to the observer, as seen at the object being observed. SPA disregards important illumination geometry, which has a dramatic effect on the irradiance measurements. By considering a body reference coordinate system centered in the orbiting object (Figure 3.8 and Figure 3.9) it is possible to define the two angles needed to describe the position of the sun and the two angles for the position of the observer.
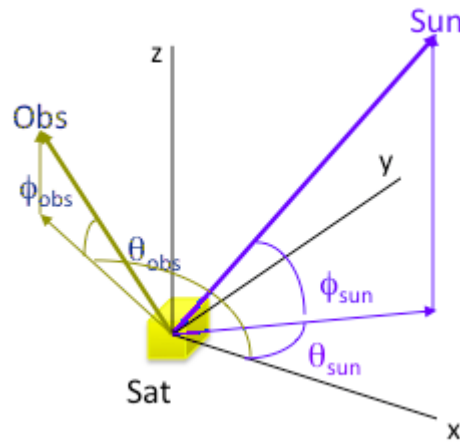
FIGURE 3.8: Body reference coordinate system for the Solar Phase Angle definition.

Therefore:

$$\widehat{n}_{sun} = [\cos\theta_{Sun}(t)\cos\phi_{sun}(t)]\,\widehat{x} + [\sin\theta_{Sun}(t)\cos\phi_{sun}(t)]\,\widehat{y} + [\sin\phi_{Sun}(t)]\,\widehat{z}$$

$$\widehat{n}_{obs} = [\cos\theta_{obs}(t)\cos\phi_{obs}(t)]\,\widehat{x} + [\sin\theta_{obs}(t)cos\phi_{obs}(t)]\,\widehat{y} + [\sin\phi_{obs}(t)]\,\widehat{z}$$

$$SPA(t) = \arccos\left[\widehat{n}_{sun}(t)\cdot\widehat{n}_{obs}(t)\right]$$

$$(3.1)$$
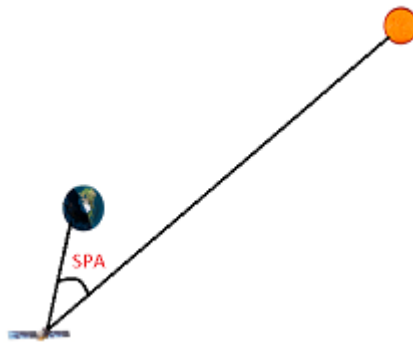
FIGURE 3.9: Solar Phase Angle definition.

- Minimum angular distance to the Moon: during night time, moon is the

greatest source of non-artificial light pollution. The main effect on image quality consists into a sensible reduction of the signal to noise ratio (SNR) of the observed target on the sensor caused by a higher median value of the background sky. The consequence is that the maximum detectable magnitude can drop down significantly. Depending on Moon phases, a minimum distance is required to collect valuable data. Based on user experience with the S5lab network, the defined limits are:

  – Moon phase percentage $\leq 5\%$ the defined limit is $5°$

  – Moon phase percentage $\in\ ]5:10]\%$ the defined limit is $5°$.

  – Moon phase percentage $\in\ ]10:25]\%$ the defined limit is $10°$.

  – Moon phase percentage $\in\ ]25:50]\%$ the defined limit is $20°$.

  – Moon phase percentage $> 50\%$ the defined limit is $30°$

• Minimum angular distance to *Milky-Way Galaxy*: for light-curves analysis star contamination represents a huge problem. The attitude of the observed target can be reconstructed by processing the variation of the reflected light from the metallic surface over a certain period. Different strategies can be applied: if the telescope is equipped with a fast read out sensors such as a *CMOS*, the telescope can track the satellite at non-sidereal rate to keep the target as a dot inside the field of view and then process the total flux on each collected image per time to reconstruct the light curve. Another strategy applied with CCD sensors is to let the target trails across the FOV by taking long exposure at sidereal rates. In the way, the object appears as a streak. The evaluation of the light curves is performed by analyzing the variation of the flux in the along-track direction. If the observations are taken close the Milky-Way star contamination of the field is highly possible to occurs. In specific, if a star trails over the target (non-sidereal rate strategy) or if the target

cross over a star (sidereal-rate strategy) the total count for the specific pixels are affected by an error connected with the background of the image. This comports in processing phase of the image of the implementation of algorithm to reduce the error caused by the star (i.e. mask subtraction of the sky field). Therefore, to reduce the impact of this phenomena the best solution is to avoid light-curve data acquisition while the target's celestial coordinates are close to the Milky Way.

3.5.4 Priority

As mentioned in Section 3.2, users can set a specific user weight w_{u_k} depending on the associated priority that the single user confers to the spceific requests. The global priority value w_k is defined as:

$$w_k = \prod^{k} w_{u_k} w_{s_k} \tag{3.2}$$

Where w_{s_k} is a specific scientific value of the request computed by the system depending on the contingency of the user's request

3.5.5 Schedule metrics

The scheduling problem for a network requires to find a feasible schedule that maximizes the operative phase of the network itself. In order to characterize the quality of the schedules it is necessary to introduce a metric, which allows to dene the scheduling problem ([Vazquez et al. (2015a)], [Vazquez et al. (2015b)]).

Given a schedule P_{sub}, let the metric $\|\cdot\|_{\sum w}$ be:

$$\|P_{sub}\|_{\sum w} \sum_k w_k \cdot \delta_k \, \forall P_k \in P_{sub} \tag{3.3}$$

Where δ_k is the allocated time for the specific request and $\delta_k \in [\underline{\rho_j} \, ; \, \overline{\rho_j}]$ where $\underline{\rho_j}$ and $\overline{\rho_j}$ have been defined in Section 3.5.2

Finally, the scheduling problem can be defined as finding the optimal schedule ([Vazquez et al. (2015a)], [Vazquez et al. (2015b)]). Given an initial set of passes P, and the set of all the feasible schedules $\{P^f\}$, the *scheduling problem* can be stated as finding the optimal schedule P^*:

$$P^* = arg\max(\|P_{sub}\|_{\sum w}) \, \forall P_{sub} \in \{P^f\} \tag{3.4}$$

When two or more requests are in conflict, a conflict solver approach is needed to accept the requests with the higher value of metrics and rejects the ones with the lower. For the space debris scheduling problem, it is important to compensate the difference that non-homogeneous request might have in terms of temporal allocation: for example, a request such as a survey in GEO is much more time-consuming than a follow-up of a LEO object. By setting different scientific priority weight to the four-different kind of request it is possible to avoid situation in which short time demanding requests are systematically rejected due to a conflict with a much more time-consuming type of request.

The implemented NICO scheduler is intended to define length and the required time windows for each observation relies on the goal of the observations itself, as well as which observatory can serve the requests if the user does not specify which observatory prefers to take observations. Due to the need to maximize the metric of the schedule, the time windows may need to be restricted than the physical visibility limit. In this way two request

that presents an overlapping in the allocation of a specific observatory may be scheduled consequently by reducing the observing intervals inside their visibility windows. It is mandatory to assure that each telescope performs observations of only on target at a time. The schedulers must also allow for a required turn-around time between observations to allow the mount to be reoriented (Figure 3.10). Therefore, the results are the night-schedule.
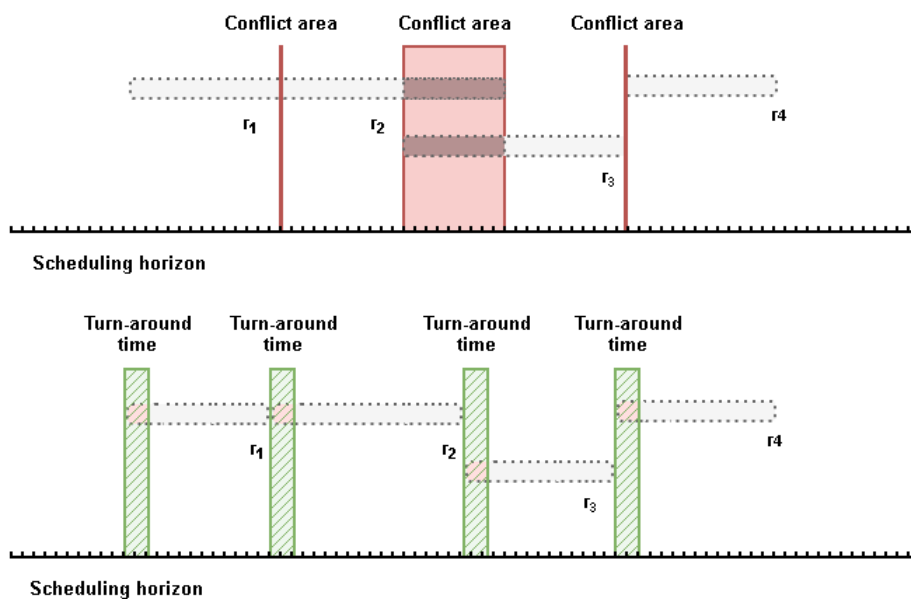
FIGURE 3.10: Conflict area solving procedure must consider turn-around time.

3.6 Solving the scheduling problem

Many standard scheduling problems can be formulated as mixed-integer programming problem where some decision variables take on integer value while other variables, such as time, have continues value. While a mathematical programming formulation generally guarantees an optimal, or best possible, solution, the computation times requires to find exact optimal solutions may be prohibitive for practical-sized problems. This because many scheduling problems belongs to the class of *NP-complete problems* ([Garey et

al. (1979)], [Parish (1994)]). In such NP-complete problems, the solution time my increase exponentially with the number of variables. For example, a problem with 10 times number the variables as an original problem might take an order of 210 times longer to solve. Because of these possible long solution times, heuristic techniques are often used to find good solutions in a reasonable amount of time. Heuristic are procedures which do not guarantee optimal solutions. They usually, but not always, provide feasible solution, often require human ingenuity in their development, and are often quire problem specific. Heuristic methods for solving scheduling problems that are less dependent on the specific problems could be useful in solving problem of managing SSA requests. This would be especially true when the constrains of the problem are difficult to put in mathematical form. One such method for finding good solution to scheduling and other optimization problems is called genetic algorithms.

3.6.1 Genetic Algorithms

GA are artificial intelligence search methods base on the idea of natural selection and evolution and applications include problems in optimization and machine learning ([Parish (1994)], [Soma et al. (2004)]). Although initially applied to function optimization problem, genetic algorithms have also been applied to scheduling and combinatorial optimization problems. The main strength of genetic algorithms is their ability to quickly explore a large space of possible solutions for good, if not optima, solutions. They differ from many traditional algorithms as their search is based only on the overall evaluation of a set of parameters. As such, they do not need to rely on derivative information to proceed. GAs are also able to find solution where multiple optimal solutions exist.

The goal of the GAs is to maximize the metric of the schedule as described in Section 3.5.5), that is the temporal allocation of as many observations as possible during the night while satisfying the constraints of time windows, turnaround time and possible maintenance down-time. If a conflict among two observations cannot be solved by rescheduling the durations inside the visibility windows, the one with the lower metric will not be scheduled.

Implementation of GAs

GAs are used to simulate biological evolution to difficult problems to find a good solution. They simulate how artificial adaptive systems can evolve or change in response to their environment to solve problems. Therefore, the implementation is divided into steps. The first step is the choosing of a proper coding to map the problem solution space into genetic strings, called chromosomes, and to randomly create an initial population of individuals with varying strings. It possible to summarize this coding in a sequence of binary code. The second step is the evaluation metrics. The chromosomes are evaluated for their fitness by entering their parameters into an evaluation function. The best chromosomes reproduce by mating with each other to produce offspring for the next generation of the population. Each chromosome has a probability of reproduction in proportion to the ratio of its fitness and the total fitness of the population. The chromosomes whose proportion are greatest should on average be selected more often than the less-fit strings. During mating, a crossover operation takes places: two chromosomes swap part of their genes consequently, the child-chromosome have parts of each of his parents. The child-chromosomes which fitness ratio is above the average are more likely to survive, while the others tend to extinguish. As happens

in nature, mutation can randomly occur and change a gene of the chromosome. Each of the phases (evaluation, selection crossover mutations) are repeated for each generation until terminator conditions occurs (generally, the reach of the total number of generations that is set). The result is a solution in which the population converges: all chromosomes evaluate to the same fitness. Nevertheless, GAs may converge to local-optimum solution. Generally, the best way to avoid such problem is to increase the population size. A smaller population might converge quickly but usually to a sub-optimum solution, larger population converges more slowly, and generally finds a better final answer.

Application to scheduling problem

The approach followed to solve scheduling problem of space debris observations with genetic algorithm is the direct chromosome representation with multi-objective. In a direct problem representation, the production of the schedule itself is used as a chromosome. The main advantage is that the genetic algorithm can search the entire solution space, not just ordering the request. Therefore, no decoding procedure is necessary. It requires the construction of domain-specific recombination operators and it is problem-specific. Managing a single observatory means to create a schedule with the objective to maximize the metric of the received requests. GA approach can be used to solve the problems and solve the conflict. When the observatory is part of a network, each schedule to be created has an individual objective to be satisfied. Moreover, these objectives under consideration can conflict with each other, and optimizing a solution for an observatory with respect to a single objective can result in unacceptable results with respect to the other objectives. A reasonable solution to a multi-objective problem is to investigate a set of solutions, each of which satisfies the objectives at an acceptable level

without being dominated by any other solution. Therefore, a multi-objective approach is needed. The pre-processed requests for each observatory are evaluated. The main information for each request are the starting time of the request, indicated with X, the total duration of the visibility windows, indicated with L and the weight associated W. These data are used to generate the first population of the chromosomes. Several constrains are applied to chromosome population. The starting time X can mutate from the beginning of the temporal windows to the half of the temporal windows.

$$
\begin{aligned}
\min(X) &= t_0 \\
\max(X) &= \Delta t/2 = \tfrac{t_1 - t_0}{2}
\end{aligned}
\tag{3.5}
$$

Consequently, the total duration L is limited from $\Delta t/2$ to Δt to never exceed the visibility windows. It is important to notice that for data acquisition operation it is mandatory to keep the turn-around time to allows the movements of the mount and the mount to follow the initial position to acquire the target. Figure 3.11 represents an example of the generation of a chromosome. The start time for the allocation is inside the first half of the visibility window. A turn-around phase is considered, then data can be taken for the whole duration of the slot. The orange line represents the readiness for operativity service of the single telescope over the single request. It goes from zero to one, with a transactional phased during the turn-around time. This can go to one minutes to several minutes depending on the observatories. S5Lab network observatories are designed with an open dome, therefore no time is needed for its movement except for the opening phase at the beginning of the observing night. The moving-rates of the telescopes are up to $5°/sec$.
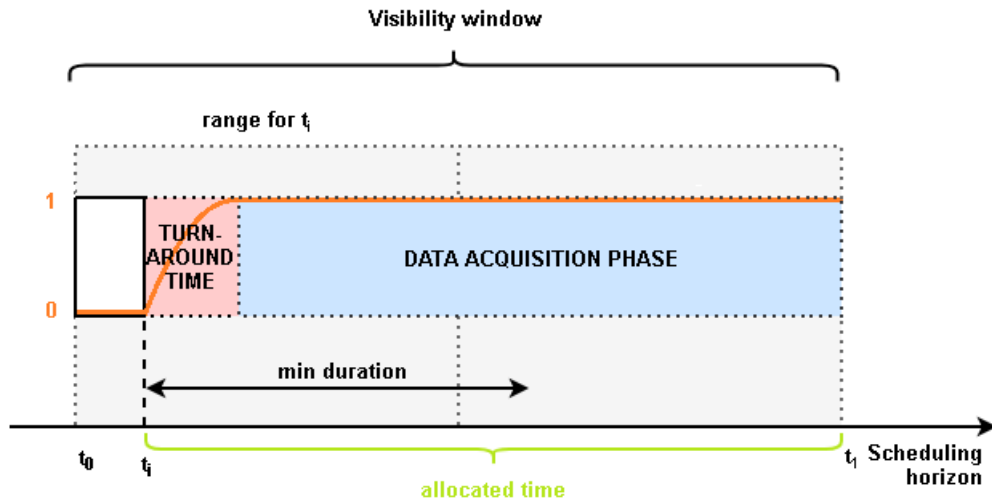
FIGURE 3.11: Allocation time constraints.

Consequently, the fitness-function described in Equation 3.4 is implemented to calculate the metric of the schedule. The fitness is the metric of the schedule. The goal of the GA is to generate a population that maximize the metric within a certain amount of generations. The fitness function is defined to work on each observatory of the network simultaneously as the core of the multi-objective approach of the scheduling problem. Conflict are solved as follows:

- If two consecutive requests $R1$ and $R2$ are not in conflict (each point of $[X2; X2 + L2] \notin [X1; X1 + L1]$), the $W1$ and $W2$ are evaluated to calculate the metric $Y = L1 \cdot W1 + L2 \cdot W2 = Y1 + Y2$.

- On the contrary, if two requests are in conflict, a preliminary individual metric figure $Y1$ and $Y2$ are computed as previous described. If $Y1 > Y2$, then $W2$ is set equal to zero (request is rejected). Therefore, the total metric is evaluated as $Y = Y1 + 0$.

The GA set options are:

- Population size: indicating the number of individuals. As previously mentioned, with a large population size, the GA searches the solution space more thoroughly, thereby reducing the chance that the algorithm returns a local minimum that is not a global minimum [typical value for the analysis: 200].

- Generations: indicating the maximum number of generations allowed [typical value for the analysis: 200].

- Crossover fraction: indicating the fraction of genes swapped between individuals [typical value for the analysis: 0.8].

- Migration direction: represent the direction that fittest individuals from the various sub-populations may migrate to other sub-populations [both directions. Therefore, the nth sub-population migrates into both the (n–1)th and the (n+1)th subpopulation].

- Migration interval: specifies how many generation pass between migrations [typical value for the analysis: 5].

- Migration fraction: specifies how many individuals move between subpopulations [typical value for the analysis: 0.2].

3.7 Generation of the scripted operation for the automated observatories: observing strategies

After NICO-GA's run, the new schedules are created. For each observatory, it is composed by a starting time, expressed in Julian Date rounded to closest starting minute, and duration time expressed in minute. Each observation is separated in time to allows the turn-around time for mount (and eventually dome) rotation for pointing. Then, a routine to implement the different

observing strategy is needed according to the specific requirements of the requests.

- Light-curves acquisition and Follow-Up observations require the same observing strategies: for these two operative modes, the telescope need to track at sidereal rate ($\sim 15arcsec/sec$ in RA) to let the desired object to trails across the field of view while the starts appear as dots. Consequently, astrometry is performed by solving the stellar field and the endpoints of the streaks are calculated by taking care of the distance in pixels for from the solved stars by knowing the pixel-scale of the frame specific for each observatory. To allow this kind of acquisition the observation follows the scheme:

  - Slew the telescope to the first detectable position (elevation greater than limit).

  - Set the exposure time depending on the orbit and the FOV dimension, example large FOV such as MITO can contain both endpoints of a six-second trail of a LEO object.

  - Wait for the object to enter inside the FOV and then start the exposition at t-Texp/2 to have the target in the middle of the field at half the exposition.

  - Wait for the read-out time of the sensor (depending on the camera, typically 10 seconds) and then move to the next position and repeat the acquisition routine.

  Each round has a total duration of about one minute, therefore a ten-minute LEO pass is composed by ten acquired images.

- Survey: the statistical analysis of the debris population in different orbital regimes (MEO, GEO, Molniya objects) is based on the definition of several *Region of Interest* (ROI) specific for each orbital regime and

depending on the location and the characteristics of each observatory. The aim is to identify for each observatory involved in the routine, the target region in which probability to have passages of objects from the selected orbital regime is the highest. All population is propagated and the celestial coordinates for pointing of the object are evaluated for the whole observing night. The ROI (identified in terms of range of right ascension (RA) and declination (DEC) for GEO and MEO and in terms of azimuth (Az) and elevation (El)) is defined as the region that contains the highest number of catalogued objects therefore it the region in which the possibility of a close approaches is higher. By monitoring these regions, it might be more likely to detect a new debris. Observatories equipped with the highest FOV can guarantee and higher coverage of the selected region. The ROI are evaluated by taking care of:

– Current population available in TLEs public catalog for the selected orbital regime.

– Different observing sites in terms of latitude and longitude;

– A-priori constraints (nautical twilight; angular distance with sun greater than $45°$; moon distance function of the moon phase, angular distance from galactic plane greater than $20°$, *hour angle HA* (defined as $HA = LST - RA$ where LST is the *Local Sidereal Time*) less than $5\,hr$, minimum satellite elevation depending on the observatory ($20°$ typically).

The dimension of the ROI depends on the orbital regimes and the implemented values (from Figure 3.12 to Figure 3.14) are compliant with IADC observing campaign such as IADC-AI31.2.
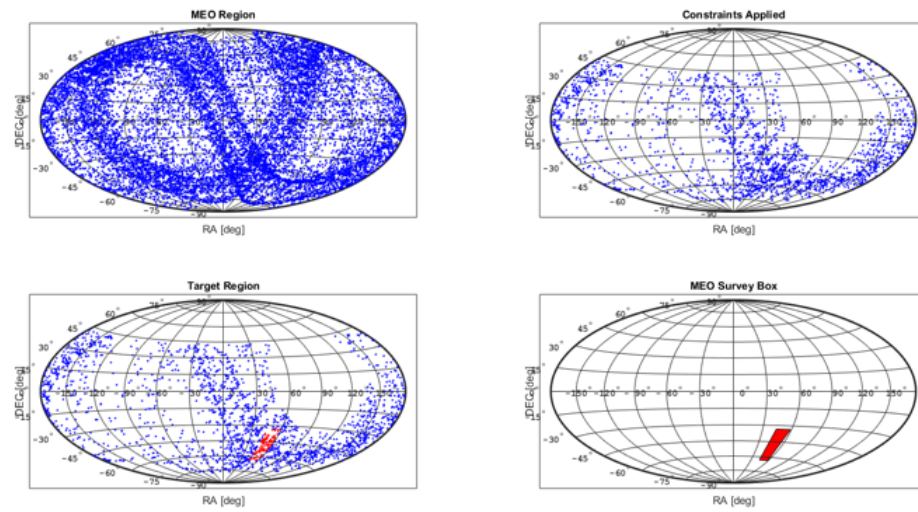
FIGURE 3.12: Definition of ROI_{MEO} survey as observed from EQUO-OG.
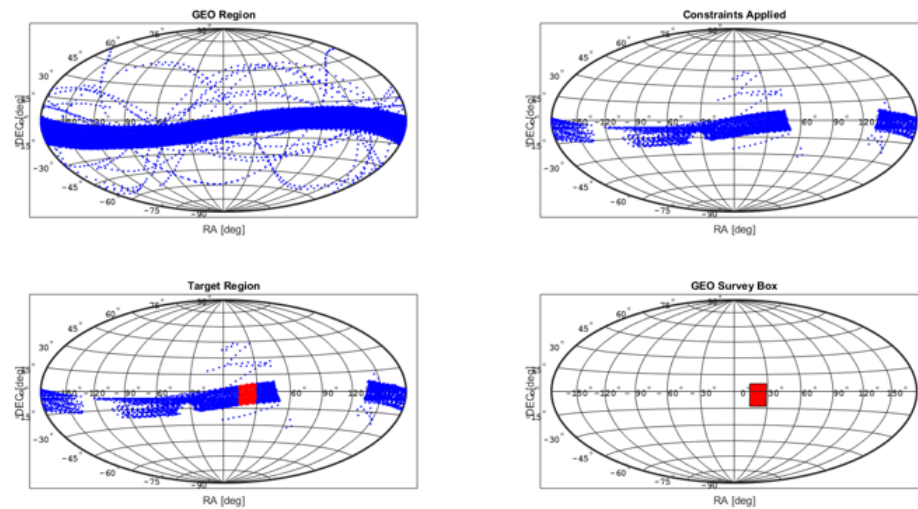
FIGURE 3.13: Definition of ROI_{GEO} survey as observed from MITO.
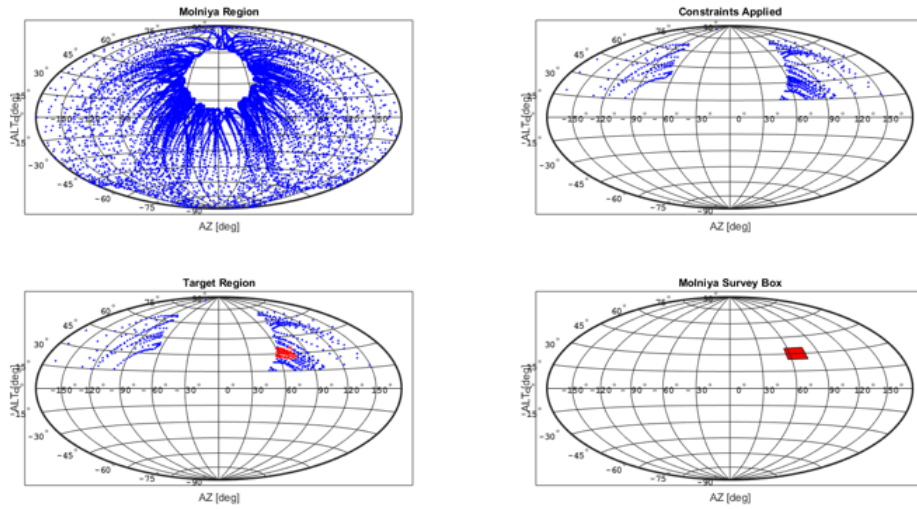
FIGURE 3.14: Definition of $ROI_{Molniya}$ survey as observed
from MITO.

Once the ROI are selected, different observing strategies are imple-
mented. Molniya and MEO strategies consist in a complete full cov-
erage of the selected ROI. It is important to maintain an overlapping
region between two consecutive images to assure the coverage of the
region. This overlapping region is identified as a third of the FOV.

For GEO, the implemented observing strategy is IADC compliant. The
region is divided into two segments (East and West) separated by half-
one hour in RA ($7.5°$). fist image is taken at the RA coordinate desired.
Then, the FOV is shifted west and east of an angular distance equal to
half the camera FOV. Then the declination is reduced by a step equal to
$1°$ and the process starts again. Thus, to span the whole region. Each
segment scan lasts thirty minutes. Then the telescope moves the FOV
to the west segment. After this time, the telescope moves the field to
the original position and the process starts over again in order to scan
all crossing GEO target. With this observing strategy it is expected to

observe the same target every half an hour. Therefore, analysis on the stability of the orbit can be conducted.

- Celestial coordinates: If your science goal requires a calibrated measurement of a flux or surface brightness, then it is mandatory to observe photometric standard stars. The celestial coordinates request type is used for this purpose. Photometric measurements often require dithering techniques. A dither is defined as an offset in either spatial usually the purpose of recovering resolution with sub-pixel offsets, or ameliorating background irregularities with multi-pixel offsets. The celestial coordinates type can be used to perform mask subtraction of already observed region. Therefore, the implemented observing strategy is to acquire a series of multiple exposure of the identified field and then moving the FOV (vertically, horizontally and diagonally at $45°$) to cover more area. Images can then be processed and combined for the multiple purposes.

3.7.1   Schedule generation in a standard data format

To manage a network means not only to organize the observations, but also to define standards to be adopted for the communication between the data center and the single data acquisition center. These criteria can be referred to the definition of the interface, the selection of the software to run the observatory, the format of the output as image data, the standardization of the data processing tool and also the definition of the schedule format. The S5Lab network of observatories has been designed to be *ASCOM* compliant [AS-COM (2017)]. ASCOM is a standard interface for astronomy purpose that runs in a Microsoft Windows environment. It acts as an abstraction layer between the client and hardware thus removing any hardware dependency

in the client, and making the client automatically compatible with all devices that supports the minimum required properties and methods. Therefore, the observatory controller software designed by S5Lab research group is designed to operate with standard input files generally used with commercial scripting and automation software. Observatory Control is compliant with *Orchestrate^{TM}* software by *Software Bisque* that is commercially used for automating multiple astronomy devices, allowing fully automatic operation and data acquisition. NICO has Orchestrate-compliant data output. The Orchestrate scripting language consists of a sequence of commands. These result in some sort of action when executed. Typically used commands are:

- `WaitUntil` allows to set a delay prior than executing the consecutive commands. It is possible to set the time of day and date when execute the next action.

- `SlewToRaDec` instructs the telescope to move to a specific equatorial coordinate. The equatorial coordinates are the arguments associated with the command. Most commands require at least one argument.

- `TakeImage` commands the CCD camera to acquire an image using the preset settings for binning. The exposure time is expressed in seconds. Using a combination of these three main commands, it is possible to implements the presented observing strategies.

3.8 Monte Carlo simulation

To validate the code, several *Monte Carlo* (MC) simulation runs have been applied ([Buxey (1979)], [Spangelo (2013)]). MC simulation is a technique used to study how a model responds to randomly generated inputs. It typically involves a three-step process:

1. Randomly generate N inputs called scenarios.

2. Run a simulation for each of the N scenarios. Simulations are run on a computerized model of the system being analyzed.

3. Aggregate and assess the outputs from the simulations.

NICO performance has been evaluated using MC prior than the operative phases to evaluate its performance in terms of merit, number of rejected request, computation time [Cardona et al. (2017b)].

3.8.1   Results

Five-hundred Monte-Carlo simulations have been run referred to a specific date. Each scenario was composed by a set of thirty single requests for each one of the four-different observatory involved in the simulation (MITO, EQUO-OG, EQUO-OS, SPADE). The set of requests was initialized as follows:

- 15 Light-curves requests.

- 5 First night follow-up requests.

- 5 Second night follow-up requests.

- 2 Survey requests.

- 3 Celestial coordinates requests.

Each request has been generated randomly using random probability for the user assignment and priority value. The SSN number for the light-curve and follow-up request have been selected randomly from a list of two-hundred LEO and MEO object already observed in past S5Lab observing campaigns. The coordinates for celestial coordinates pointing have been selected using

coordinates of standard field visible from the different observatory locations. Measurements are generated in terms of

- Number of selected request to be processed.

- Number of requested scheduled using GA approach for conflict solving.

- Merit of global schedule.

- Maximum weight assigned to the single request.

- Computational time.

For the analysis an *Intel i*5-5200 2.20 *GHz* with 8*GB* of RAM has been used.

The computational time histogram for the whole NICO run is shown in Figure 3.15 to present the occurrences during the MC simulation. The median computation time value is 270 *s*.
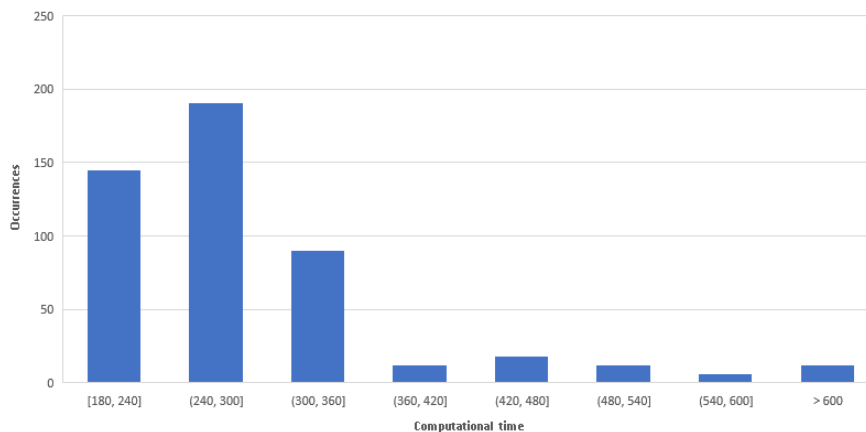
FIGURE 3.15: Computational time occurrences.

For each scenario the value the ratio between the number of processed request versus the scheduled one is obtained. Then the global network merit is divided for the maximum weight of the single request. Finally, it is normalized to the maximum merit from all scenarios. The results are shown in

Figure 3.16. The mean value for the schedule percentage of request is 80% with a normalized merit above 70%.
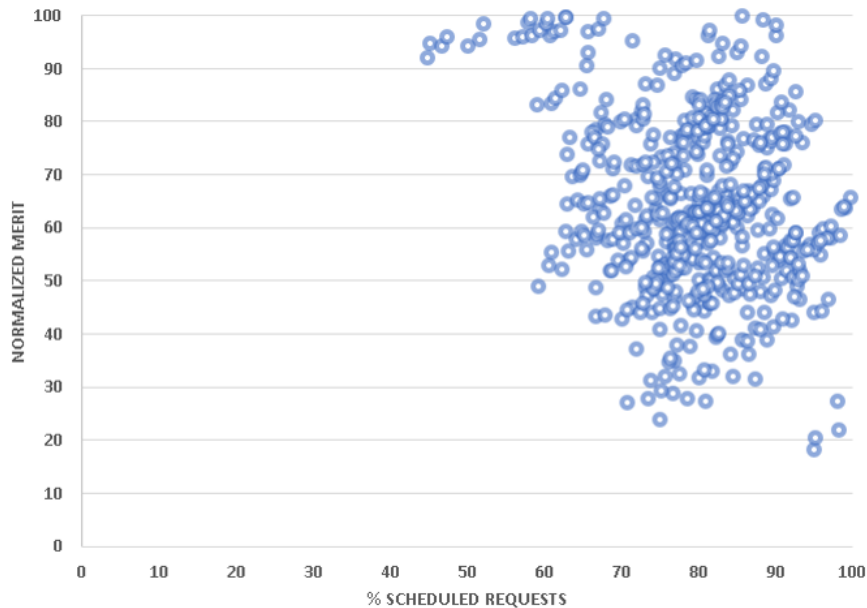
FIGURE 3.16: Monte Carlo simulations.

3.9   Validation campaign for IADC-WG1 AI31.2

NICO has been successfully used for the IADC international observing campaign for target scheduling process. In particular it has been used for the IADC-AI31.2 *Reflected signal variations measurements of massive LEO objects*. The objectives of the Action Item were to:

- Individuate promising techniques to characterize LEO debris attitude motion.

- Compare data collected over a common collection period.

- Compare data collected using different means (optical/ radar).

Italian delegation has participated with MITO observatory to the data acquisition. In March 2017 a one-month observing campaign has been conducted

to collect light-curves of a selected list of LEO debris (Figure 3.17). The list of observed objects includes target with *clear periodic event* in which the spin period is evident and does not changes with time, *ambiguous event* character-ized by a certain periodicity depending on the time of the observation. A to-tal number of three-hundred light-curves have been collected and processed (Figure 3.18). Most of the clear periodical and ambiguous events showed the evidences a few times out of many light-curves of their own. This may be caused by the viewing angle effects.
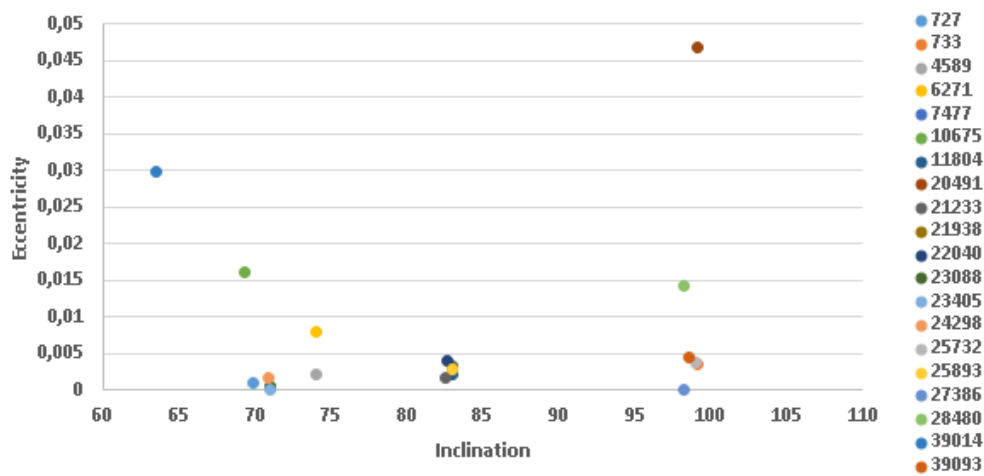
FIGURE 3.17: LEO observed target (Inclination versus Eccen-tricity).
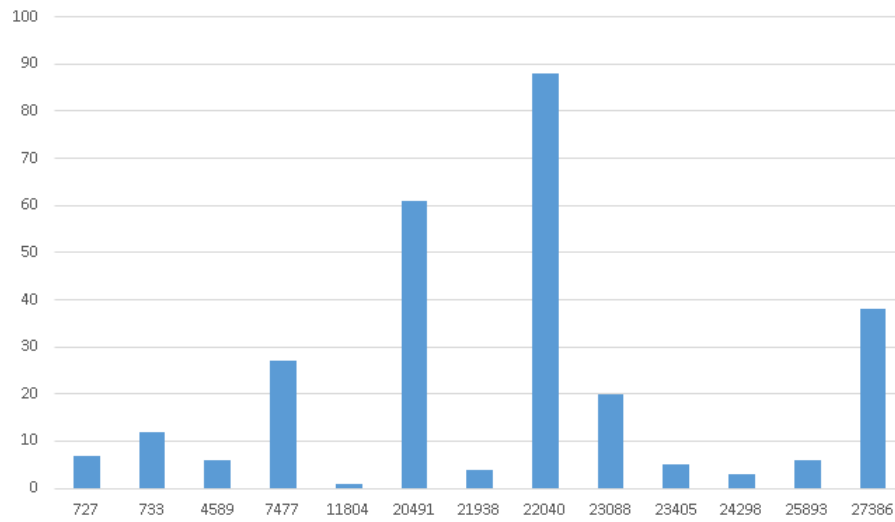
FIGURE 3.18: Number of collected light-curves for each LEO observed target.

Chapter 4

Automatic image processing tool

The development of a network of observatories and a scheduler to manage and organize the data acquisition routine has triggered the problem on how to manage the acquired data. A single observatory can collect more than five-hundred images per night depending on the requested observing strategies. Surveys are more time consuming and can contain images without a target while light-curves and follow-up observations need to be processed individually for multiple information extraction. Surveys observations are performed to determine the statistical population of the observed orbital regimes and their classification ([Schildknecht et al.(2007)], [Seitzer et al. (2012a)], [Herzog et al. (2013)], [Payne et al.(2002)]). Preliminary Orbit Determination (POD) is performed by processing collected images to identify the orbital parameters of the acquired target. This task is fundamental to discriminate target and avoid contamination of the statistical analysis from object with different orbital regimes rather than the one under investigation. The result of the analysis is a representation of the current population of the orbit with a distinction on the cataloged (CT) and un-cataloged (UCT) object [Seitzer et al. (2004)]. Follow-up observations are used to reconstruct the orbit of the object by performing multiple acquisition of the target and reconstruct the celestial coordinates of the observed object with the respect of the background star field. Light-curves acquisition are used to determine

the dynamical state of the target in terms of attitude by processing the light reflected from the metallic surface of the object ([Yanagisawa et al. (2012)], [Schildknecht et al. (2015)], [Schildknecht et al. (2008a)], [Fruh et al. (2010)]). Rapid changes in brightens of the response are investigated to reconstruct rapid changes in the attitude in the scale of a second or less [Kaasalainen et al. (2001)]. In fact, orbital objects do not have a constant brightness because they reflect light from the sun and give off flashes at typically regular times. This flashing behavior is caused by the tumbling motion of the object. By measuring the period between two flashes or maxima/minima in the light curve can give a good approximation for the satellite's rotation motion ([Cardona et al. (2017b)], [Parish (1994)], [Kucharki et al. (2014)], [Earl et al. (2014)]). S5Lab research team has developed in the past tool for automatic data processing for survey analysis and follow-up observations to improve the orbit [Piattoni et al. (2014)]. Due to the increasing of the number of the observatory involved in data acquisition and the number of taken images per night, a new automated image processing tool for light-curves measurements was needed.

4.1   Data reduction and plate solving

All collected images are raw data and need to be pre-processed to be analyzed to collect valuable data. These procedures are called data reduction and plate solving. The first one is to remove imperfection within the image, while the second is used to reconstruct the background field of the image. To reduce data and to solve the plate, automatic tools are available both commercial (*MaximDL^{TM}*, *TheSkyX^{TM}*) and open source (*Astrometry.net*). S5Lab research team has developed custom software for preliminary analysis: a custom routine based on `IRAF` and a plate solver based on a triangulation

approach. To recognize the triangle created using the reference stars in the images, a triangle database of the whole sky is used based on a star catalog [Piattoni et al. (2014)].

4.1.1 Bias, Dark and Flat field

CCD image reduction is a standard procedure used for astrometry, photometry and spectroscopy defined to calibrate the acquired image [Massey et al. (1992)]. The procedure relates to specific parameters of the sensors [Gullixson (1992)].

Bias

The first parameter is the value for the zero of the zero collected photo-electrons translated after readout and A/D conversion [Adams et al. (1980)]. If no corrections are applied, the mean value has a small distribution around zero. Nevertheless, if negative numbers would have represented in a `16-bit` images, the first `bit` must to be set to represent the sign. Generally, a value equal to `1` is used for positive and `0` for negative value. By scarifying this bit for the sign, only `15-bit` would have left to represent the data, consequently the overall dynamic range is reduced. To avoid negative number in the output, CCD are set to provide a positive offset value for each accumulated image. This offset value is called bias. To evaluate the bias and the zero-noise level associated, specific bias frames can be collected. Bias frames are observations without exposure to light (the shutter stay closed) for a total integration time of zero second. The result image is a simple read-out of the unexposed CCD pixels through the on-chip electronics through the A/D converted and then to the acquiring computer producing a 2-D zero image.

Generally, multiple exposures are taken to be combined into a master bias-frame. The distribution of median bias is a Gaussian distribution with mean level offset of the CCD (Figure 4.1). The width of the Gaussian bell is connected to the read-noise of the CCD and the device gain using the expression:

$$\sigma_{ADU} = \frac{Read\ noise}{Gain} \tag{4.1}$$

Where σ represent the FWHM of the distribution.
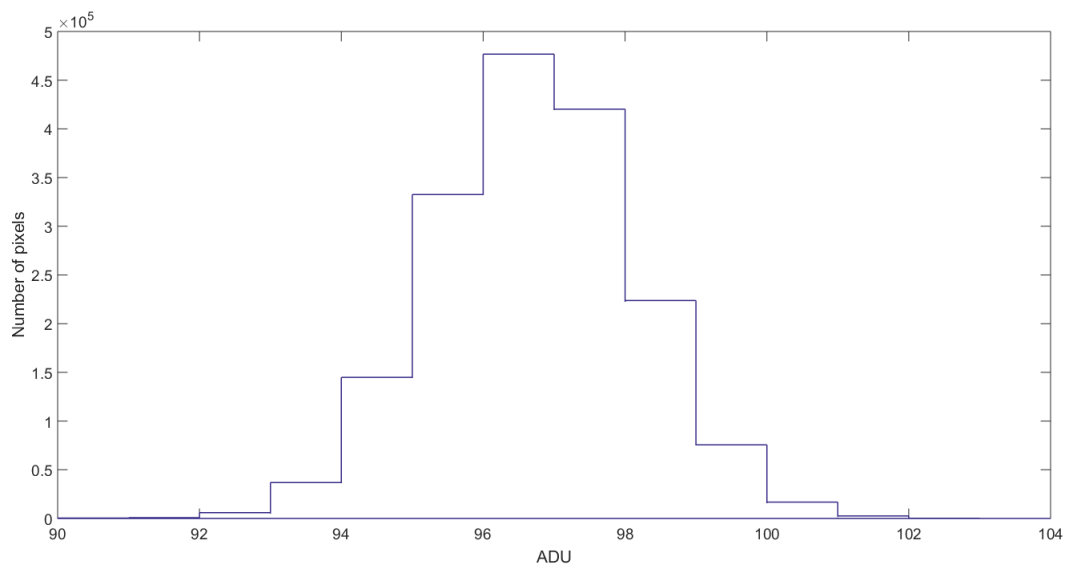
FIGURE 4.1: Bias gain.

Flat field

The gain of a CCD that is set by the output electronics. It represents how the amount of charge collected in each pixel will be assigned to a digital number in the output image. Gain values are usually given in terms of the number of electrons needed to produce one ADU (*Analog Digital Unit*) step within the A/D converters [e^-/ADU]. Within the CCD, each pixel has a slight different gain or *quantum efficiency* (QE) value when compared with its neighbors. To flatten the relative response for each pixel to the incoming radiation, a flat

field image is needed. Ideally, a flat field image is a uniform illumination of every pixel by a light source of identical spectral response of that of the observed objects. Generally, these images are produced by illuminating the inside of the telescope dome with a source light, point the telescope to the bright spot and then acquire short exposures to not saturate the sensor. If multi-filter observations are performed, multi-filter flat field images need to be acquired due to the response of the sensors to different color light [Zhao et al. (2016)]. Similar analysis as the one for biases can be conducted for flat field. The result of the histogram plot of the median value of the collected flat of the desired filter produce a Gaussian distribution with a width related to the read noise and the gain of the detector. Therefore, the second main parameter, the mean lever of the flats $\overline{F}$, can be calculated and used to evaluate the width σ_{ADU} given by

$$\sigma_{ADU} = \frac{\sqrt{\overline{F} \cdot Gain}}{Gain} \tag{4.2}$$

By combining bias frames and flat fields, the read noise and sigma can be determined. By indicating two bias frames and two flat field frame images it is possible to evaluate the median values $\overline{B}_1$, $\overline{B}_2$, $\overline{F}_1$ and $\overline{F}_2$. It is possible to subtract the two images to create $B_1 - B_2$ and $F_1 - F_2$ and to measure the standard deviation $\sigma_{B_1 - B_2}$ and $\sigma_{F_1 - F_2}$. Then, the gain and the read noise can be calculated as

$$Gain = \frac{(\overline{F}_1 + \overline{F}_2) + (\overline{B}_1 + \overline{B}_2)}{\sigma^2_{F_1 - F_2} - \sigma^2_{B_1 - B_2}}$$

$$\tag{4.3}$$

$$Read\ noise = \frac{Gain \cdot \sigma_{B_1 - B_2}}{\sqrt{2}}$$

The signal-to-noise ratio (SNR) can be extracted as:

$$SNR = \frac{N_*}{\sqrt{N_* + n_{pix} \cdot (N_S + N_D + N_R^2)}} \tag{4.4}$$

Dark

Where N_* is the total number of photons collected from the object of interest, n_{pix} represents the number of pixel of the region of interest, N_S is the contribution per pixel of the background sky noise, N_R^2 represents the total number per pixels resulting from the read noise, while N_D the terms for the dark current per pixel that represents the thermal noise. In fact, CCD images are in influenced by the temperature of the sensor. Therefore, dark frames are images taken with the shutter closed but for some time-period, usually equal to that of your object frames. Other than information on dark current, they also can give you information about bad or *hot* pixels that exist as well as provide an estimate of the rate of cosmic ray strikes at your observing sites. By cooling down the sensors (N_2 or Peltier cooler system) the dark current effects can be significantly reduced. For bright objects the denominator of the equations is $o(\sqrt{N_*})$ therefore it possible to approximate the equation as,

$$SNR \sim \frac{N_*}{\sqrt{N_*}} = \sqrt{N_*} \tag{4.5}$$

For space debris observations, which are characterized by low value of SNR (caused by high background sky noise level or faint sources) it is standard procedure to compute the SNR as [Massey et al. (1992)]

$$SNR = \frac{N_*}{\sqrt{N_* + n_{pix}(1 + \frac{n_{pix}}{n_B})(N_S + N_D + N_R^2 + G^2\sigma_f^2)}} \tag{4.6}$$

Where $n_{pix}(1 + \frac{n_{pix}}{n_B})$ correct any errors introduced by the higher value of the background sky noise and n_B is the total number of pixels considered to estimate the value; G is the Gain of the CCD expressed in e^-/ADU and σ_f depends on the internal A/D and typically has value ~ 0.289. σ standard deviation of the measurements $(S/N = 1/\sigma)$ is then

$$\sigma_{magnitude} = \frac{1.0857\sqrt{N_* + p}}{N_*} \tag{4.7}$$

Where $p = n_{pix}(1 + \frac{n_{pix}}{n_B})(N_S + N_D + N_R^2 + G^2\sigma_f^2)$ and 1.0857 is the correction error term between error expressed in flux (e^-) and in magnitudes. If the exposure time t is considered, then the equations became

$$SNR = \frac{Nt}{\sqrt{Nt + n_{pix} \cdot (N_S t + N_D t + N_R^2)}} \tag{4.8}$$

Where N is the count rate of photons per second and t the exposure time of the sensor. Therefore, the it is possible to notice that $SNR \propto \sqrt{t}$ The equation can be solved for t to describe the expected magnitude as function of the exposure time:

$$t = \frac{(SNR)^2(N + n_{pix}(N_S + N_D)))}{2N^2} +$$

$$\frac{\sqrt{(SNR)^4(N + n_{pix}(N_S + N_D))^2 + n_{pix}(2 \cdot SNR \cdot N N_R)^2}}{2N^2} \tag{4.9}$$

Therefore, to reduce the acquired data the procedure is to first subtract the bias frame and dark frame (if needed) from the object frame. Then, the result image is divided by a bias subtracted mean flat frame in the same filter as the raw data. The image is then corrected for bias level, dark current, and non-uniformity of each pixel. During the analysis, the background sky

contribution to the noise can be reduced by performing mask subtractions techniques.

4.1.2 Plate solving

The problem of plate solving relies to spherical coordinates (RA or α and DEC or δ) to be projected onto a flat image plane with linear measurement in that plane (Figure 4.2) [Adams et al. (1980)]. It is possible to define Standard Coordinates (X, Y) an orthogonal coordinate system in the image plane of the telescope with its origin at the intersection of the optical axis with the image plane and axes running East(E)-West(W) and North(N)-South(S). This system coordinates (X, Y) are measured in units of the focal length.
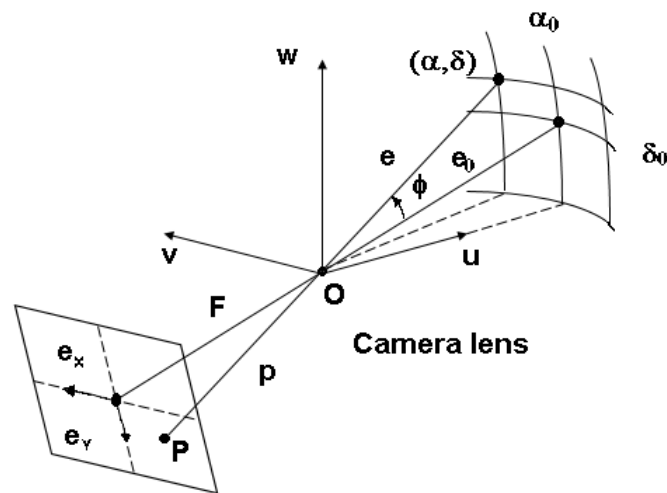
FIGURE 4.2: Plate solving.

Let be (α, δ) sky coordinates of an object at point P and (α_0, δ_0) the projected coordinates of optical axis (field center). It is possible to evaluate the relationships:

$$\alpha = \alpha_0 + \arctan\left(\frac{-X}{\cos(\delta_0) - Y \sin(\delta_0)}\right)$$

(4.10)

$$\delta = \arcsin\left(\frac{\sin(\delta_0) + Y \cos(\delta_0)}{\sqrt{1 + X^2 + Y^2}}\right)$$

Similarly:

$$X = -\frac{\cos(\delta)\sin(\alpha - \alpha_0)}{\cos(\delta_0)\cos(\delta)\cos(\alpha - \alpha_0) + \sin(\delta_0)\sin(\delta)}$$

(4.11)

$$Y = -\frac{\sin(\delta_0)\cos(\delta)\cos(\alpha - \alpha_0) - \cos(\delta_0)\sin(\delta)}{\cos(\delta_0)\cos(\delta)\cos(\alpha - \alpha_0) + \sin(\delta_0)\sin(\delta)}$$

Therefore, it is possible to compute the standard coordinates for objects whose RA and DEC are known (reference stars), and compute the RA and DEC of an object if its standard coordinates are known. To convert image position measured in pixel into standard coordinates it is important to consider instrumental errors:

- Displacement of the origin O: yields constant difference between measured and true coordinates.

- Error of orientation: the x and y axes of the measurements will be rotated by some θ angle from true $N - S$, $E - W$.

- Non-perpendicularity of axes: the axes of measurements will not be strictly orthogonal.

- Scale error: the standard coordinates (X, Y) are expressed in terms of focal length, which will not be constant and may differ in x and y.

To consider all the presented error, the solution will be in the form:

$$X = ax + by + c$$

$$(4.12)$$

$$Y = dx + ey + f$$

Where (X, Y) are the standard coordinates and (x, y) are the measured coordinates in any convenient units. The constant (a, b, c, d, e, f) are called *plate constant*. The goal of the plate solution is to determine the plate constant. This is solved by measuring the position of the reference stars, whose standard coordinates are possible to be computed. Since six-constants must be determined, at least three reference stars should be measured because each star yields a pair (x, y) of measurements. Other non-linear errors, such as:

- Plate tilt: error due to non-perpendicularity of image surface to the optical axis.

- Sphericity of the focal surface and coma.

are not accounted in six-constant solution. To consider these, the equations became (twelve-constant):

$$X = ax + by + cxy + dx^2 + ey^2 + f$$

$$(4.13)$$

$$Y = gx + hy + ixy + jx^2 + ky^2 + l$$

Therefore, six-reference stars are required. The non-linear error can be considered very small for CCDs, so the three stars solution gives already valuable results. The solution of the plate field is performed by comparing the reference stars with star catalog. Older ones might have different source of errors:

- Random error: random errors in catalog positions are likely to be small and are averaged out by least square method.

- Systematic: catalog position can have systematic error that vary from the center to the edge of the original plates, and from field to field and can affect the final accuracy (order of $3\,arcsec$).

- Proper motions: older catalogs do not include proper motion.

Therefore, new catalogs have been released that have greatly reduced systematic error and include proper motion. For example, star catalog *USNO B1.0* has more than one-billion entries. Position, magnitudes (in filters B, R, I) and proper motions are indicated and it is available online (solution require web access). The accuracy for photometry is at best 0.1 magnitude. Once the image has been processed for data reduction and plate solving, it is ready for data analysis.

4.2 Automatic light-curve data analysis

Observations of orbiting objects such as operative satellites or space debris obtained while the telescope is tracking at the sidereal rate, and the object is trailed across the FOV might show flash due to specular reflection of sunlight. These flash periods are normally the apparent flash periods as seen by the observer. Analysis on the intensity changes along the trail reveals the primary frequencies of the object's brightness variations on time scales of a second or less. This can be used to evaluate the spin period of the observed objects. Moreover, light-curve data analysis can be used to evaluate the spin axis of the satellites. By considering the varying geometry of the observer-satellite-sun angle during the observations caused by the movements of the observer and the satellite due to earth rotation and orbital motion (known as *synodic effect*) it is possible to notice that this difference between the apparent flash rate and the rotation or tumble rate of the satellite is not constant but typically varies with time as a function of the changing geometry. The

magnitude of this variation for a given changing geometry is a function of the orientation of the spin axis of the spinning satellite with respect to the observer-satellite-sun geometry. This varying synodic period can be used to provide an estimate of the orientation of the spin axis of the satellite. These data are extremely valuable to detect and investigate the attitude of an orbiting object and its evolution especially for future *Active Debris Removal* (ADR) missions [Liou (2011)]. Although the architecture of ADR system can vary a lot depending on the de-orbit method, the number of the debris to capture and the orbits, the typical ADR mission scenario to remove a debris is usually like the one shown in Figure 4.3.
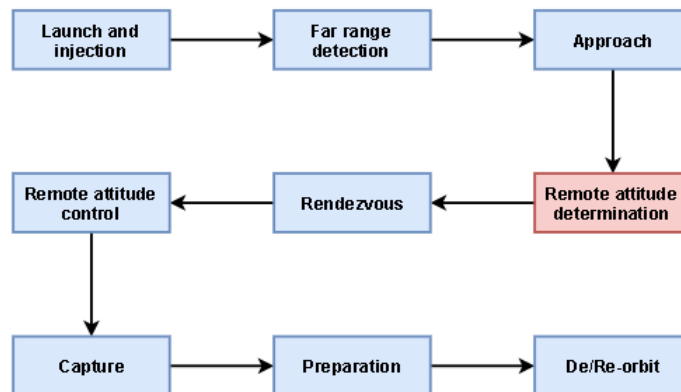
FIGURE 4.3: Typical ADR architecture mission.

Therefore, a tool is needed to perform analysis for the *Remote attitude determination* block to provide reliable data. To process the collected data an automatic software has been developed to process the detected target within the frame. The pre-processed images, results of the `IRAF` and plate tool routine, are loaded and specific settings depending on the observatories used are loaded. These settings take care of the different FOV, plate scale, maximum detectable magnitude and geo-location and are defined for each observatory of the network.

(Figure 4.4).
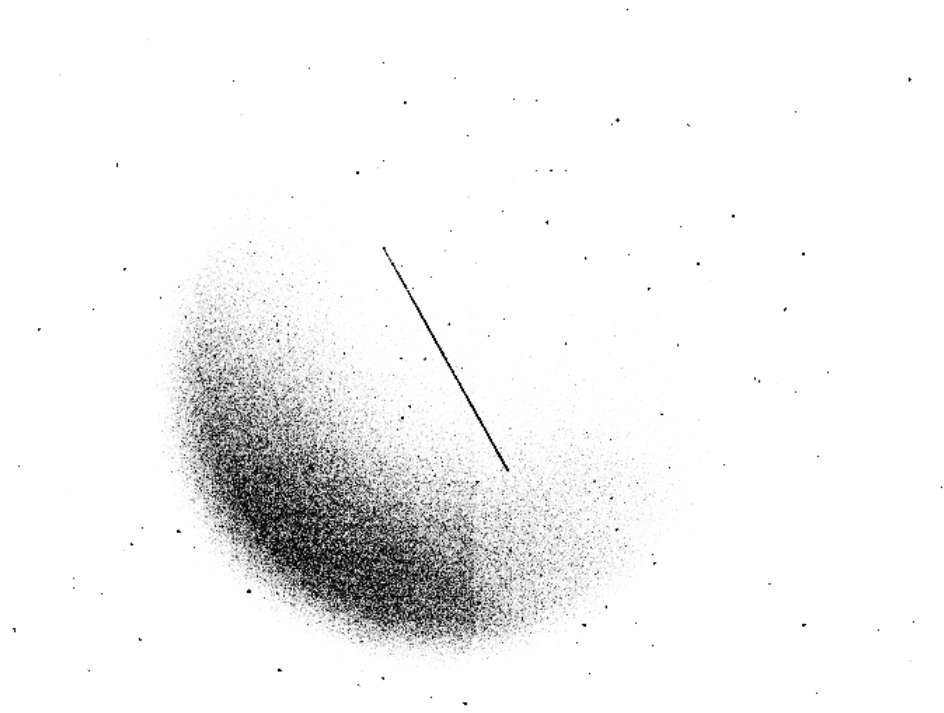
FIGURE 4.4: Collected trailed object.

Images are processed by considering the solved field (in terms of RA and DEC in $J2000$ precession) and the FOV dimension to detect each possible satellite that can have been collected in the acquired images at the specific times [Larsson et al. (1996)]. These data are loaded from the processed header of the image. TLEs are automatically downloaded using API-REST protocol and then are propagated using SGP4 [Vallado (2001)] to evaluate possible candidates within each frame. If a cataloged orbiting object is identified as possible candidate its SSN catalog number is stored into a database together with the image name, the exposing date and the FOV coordinates. For each candidate of the collections all available TLEs are downloading staring from ten-day prior than the observation to ten-day after. Thus, to evaluate the stability of the evaluated orbit. The main core of the tool (Figure 4.5) is the

automatic image processing phase. Its consist in four main blocks:

- Streak detection routine: the image is processed to identify the end-point of the streaks, then the original image is rotated horizontally and a sub-frame containing the streak is extracted.

- Streak data extraction: the horizontal streak is processed on both across track (for PSF - Point Spread Function analysis).

- Frequency analysis: the extracted data are processed using different techniques to identify the main frequencies.

- Report creation: the results are stored into a report.
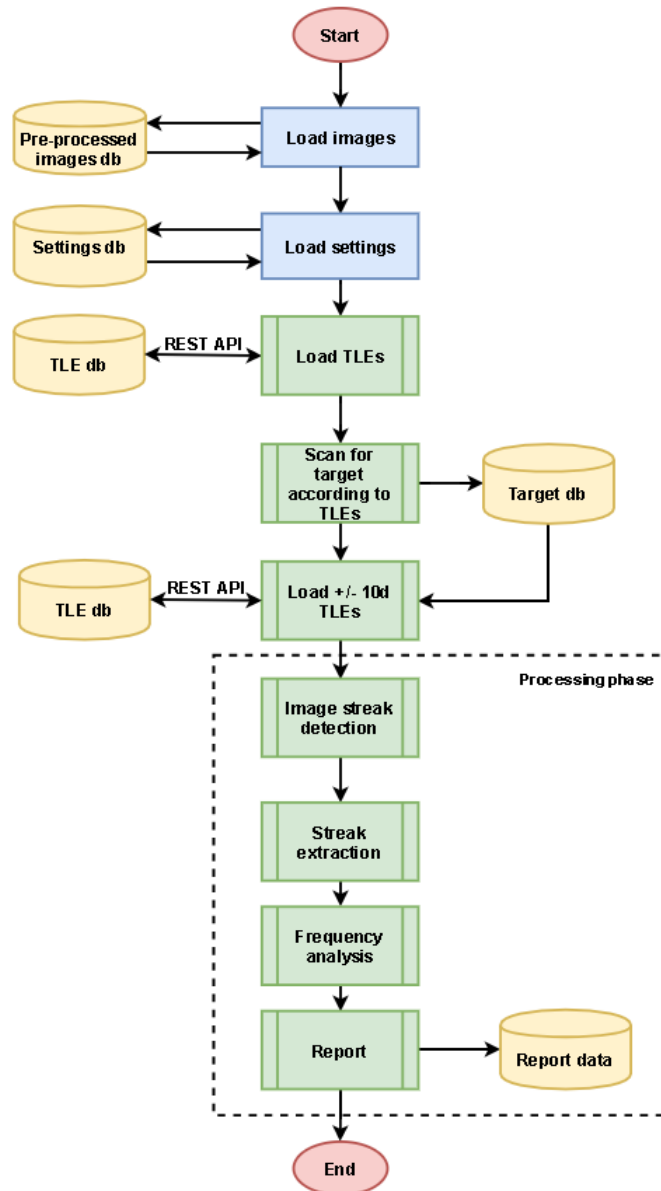
FIGURE 4.5: Image processing tool scheme.

4.2.1 Detection procedure

The reduced image is processed using the information given by the plate solving ([Gonzalez et al. (1992)], [Soille (1999)]). The evaluated rotation angle of the image θ is used to correct the orientation error of the frame (Figure 4.6).
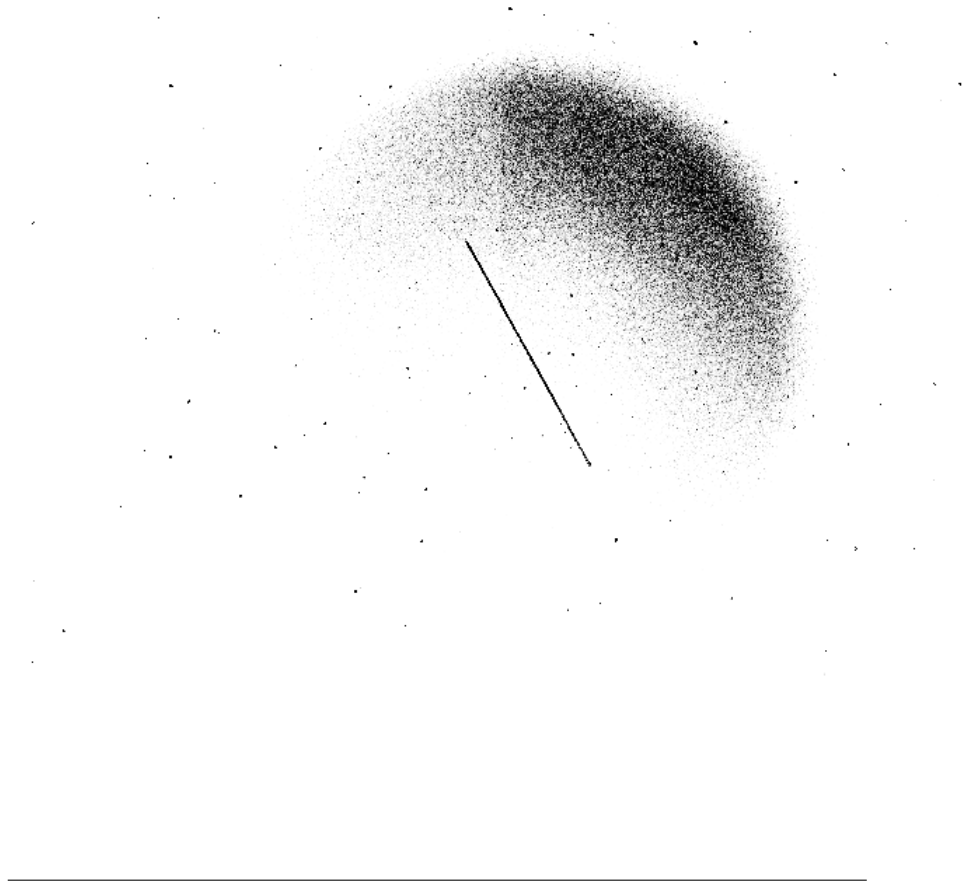
FIGURE 4.6: First rotation.

In this way, the image is oriented with true N-S, E-W. Then, the plate scale of the collected images that is evaluated as

$$P = \frac{206265 \cdot pixel\ size\ [\mu m]}{1000 \cdot f\ [mm]} \quad [arcesec/pixel] \tag{4.14}$$

Where f is the focal ratio of the telescope given by:

$$f/ = \frac{focal\ lenght\ of\ primary\ mirror}{primary\ mirror\ diameter} \tag{4.15}$$

is used to detect the target within the FOV. The propagated TLEs are used to detect the coordinates in terms of RA and DEC of the endpoints of the streaks (observed at instant t_0 and $t_0 + t_{exp}$).The difference from their position

and the center of the FOV expressed in arcsecond is then converted in pixels using the plate scale. These coordinates in the frame reference systems are used to extract an initial sub-frame (SF1) of the image containing the streaks. Due to several possible error sources such as:

- Poor alignment of the telescope.

- Error in the TLEs.

- Error in the data acquisition systems.

- Bad *seeing* conditions.

A safety factor equals to 5% of the maximum length of the sub-frame is applied to extract SF1 (Figure 4.7). The tool allows user manual intervention in case of error in the detection of SF1 to give to possibility to refine its dimension.

FIGURE 4.7: First subframe SF1.

Once the streak is extracted from the main frame, specific edge detection tools are applied to identify the target within SF1. For the edges identification process, Canny edge detection algorithm is used [Canny et al. (1986)].

Edge detection and filling algorithm

The Canny edge detection algorithm is composed by a seven-step procedure:

1. The first step is to convert the image into a binary frame to be processed. The conversion is performed using a two thresholds algorithm: the pixels which values are under the first threshold are considered black ($= 0$)

to eliminate part of the background noise. The pixels which values are above the second threshold are considered white (= 1). The values of the two thresholds are computed from the histogram of SF1.

2. To reduce noise effects on edge detection process, a Gaussian filter is applied to prevent false detection caused by noise. The equation for a Gaussian filter kernel of size $(2k + 1) \times (2k + 1)$ is given by:

$$H_{ij} = \frac{1}{2\pi\sigma^2} \exp\left(-\frac{(i - (k+1))^2 + (j - (k+1))^2}{2\sigma^2}\right) \qquad (4.16)$$

For faint debris detection purpose, σ can be set equals to 2.0 and the mask has 15×15 dimension.

3. An edge can point in a variety of directions (horizontal, vertical and diagonal), therefore the algorithm uses four different filters for edges detection. By indicating the first derivative in the horizontal direction as G_x and the one in the vertical direction as G_y, then the gradient G and the direction angle Θ are evaluated as

$$G, = \sqrt{G_x^2 + G_y^2}$$

$$(4.17)$$

$$\Theta = \arctan2(G_x, G_y)$$

Then Sobel masks are applied to the 3×3 neighborhood of the $a_{i,j}$ pixel in both x and y directions [Piattoni et al. (2014)].

4. An edge thinning technique defined as non-maximum suppression is applied because the edge extracted from the gradient value might be unclear. Non-maximum suppression is used to suppress all the gradient values to 0 except the local maximal, which indicates location with the sharpest change of intensity value.

5. Next, hysteresis threshold is applied. Large intensity gradients are more likely to correspond to edges than small intensity gradients. Two thresholds are used: *high* and *low*. The high threshold identifies that the pixel is surely on an edge, while the low one shows that the pixel is certainly no part of an edge. For values in between the two thresholds, assumptions might be posed. If $a_{i,j}$ pixel is indicated as part of a vertical edge but its gradient value is not higher than the high threshold, the pixel above and below are checked to verify if they are also part of a vertical edge. This is performed in all directions.

6. Then connected-component labeling (*blob analysis*) procedure is applied to detected edges and to performs morphological closing on the binary image, returning the closed image. The morphological close operation is a dilation followed by an erosion, using the same structuring element (generally disk with small aperture to reduce computational time) for both operation.

7. The obtained image can contain holes (set of background pixels that cannot be reached by filling in the background from the edge of the image) caused by the blob analysis. Therefore, a flood-fill operation on these background pixels is performed (Figure 4.8).
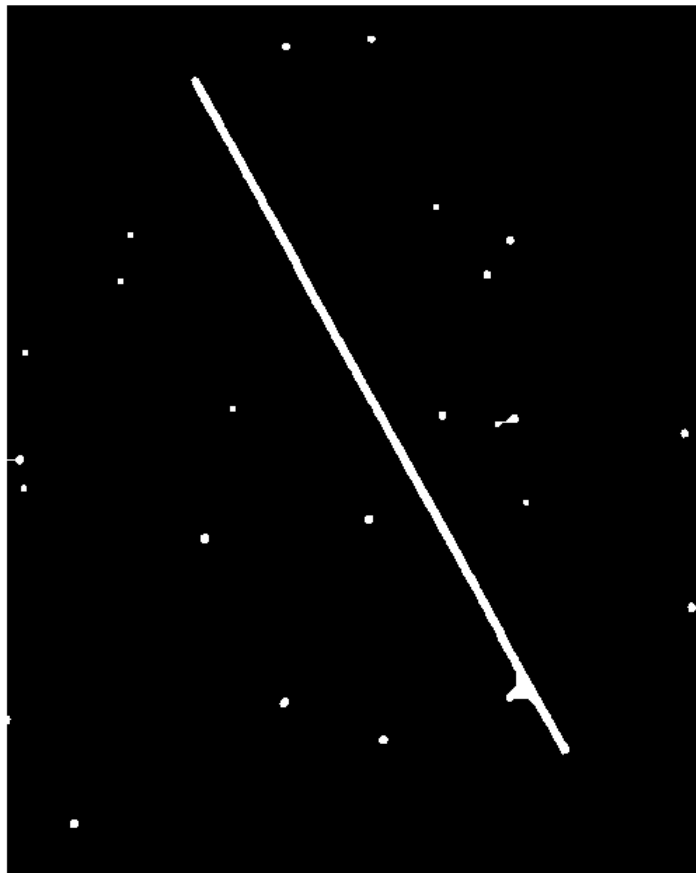
FIGURE 4.8: Binary subframe.

Target streak discernment

The result of the edge detection and filling procedure is a binary image in which target trails and background stars have been identified. To automatically distinguish its streak from the stars an analysis based on the inertia theory of sections is performed on each connected object recognized in the binary image [Piattoni et al. (2014)]. For each connected objects, by indicating with n_p the number of pixels which compose the object, X_i and Y_i with $i \in [1, np]$ the width and height in pixels of the object, it is possible to calculate:

Centroid (X_{GC}, Y_{GC}): the coordinates of the center of mass evaluated as:

$$X_{GC} = \frac{\sum_{i=1}^{n_p} X_i}{n_p}$$

$$Y_{GC} = \frac{\sum_{i=1}^{n_p} Y_i}{n_p}$$

(4.18)

Major Axis Length and Minor Axis Length: it specifies the length (in pixels) of the major/minor axis of the ellipse that has the same normalized second central moments as the region. To evaluate them, inertia axes I_{XX}, I_{YY} and I_{XY} are computed:

$$I_{XX} = \sum_{i=1}^{n_p} (Y_i - Y_{CG})^2$$

$$I_{YY} = \sum_{i=1}^{n_p} (X_i - X_{CG})^2$$

(4.19)

$$I_{XY} = \sum_{i=1}^{n_p} (X_i - X_{CG})(Y_i - Y_{CG})$$

Then, the major and minor axis length are calculated as:

$$I_{max} = \tfrac{1}{2} \cdot \left(I_{XX} + I_{YY} + \sqrt{(I_{XX} - I_{YY})^2 + 4(I_{XY})^2} \right)$$

$$I_{min} = \tfrac{1}{2} \cdot \left(I_{XX} + I_{YY} - \sqrt{(I_{XX} - I_{YY})^2 + 4(I_{XY})^2} \right)$$

(4.20)

Orientation angle θ is the angle between the x-axis and the major axis of the ellipse that has the same second-moments as the region. The value is in degrees, ranging from -90 to 90 degrees and it is computed as:

$$\theta = -\frac{1}{2} \cdot \left(\frac{I_{XY}}{\frac{1}{2} \cdot (I_{XX} - I_{YY})} \right)$$

(4.21)

Due to the observing strategy of tracking at sidereal rates, stars appear as dots in the sky while the target is moving at different rates depending on the orbit and appears as a streak in the frame (Figure 4.10). Therefore, connected objects relative to stars should have a ratio $I_{max}/I_{min} \sim 1$ while detected object trails should have a ratio $I_{max}/I_{min} \gg 1$. To avoid misleading in the identification process caused by the false detection of an object cause for example by cosmic rays or galaxies, the discernment ratio is defined as

$$\frac{I_{max}}{I_{min}} > \epsilon \tag{4.22}$$

Where

$$\epsilon = \frac{rate_{trail} \cdot t_{exp}}{plane_{scale}} \cdot s_f \tag{4.23}$$

function of the orbit of the satellites, the exposure time of the image, the plate scale and an empirical safety margin s_f generally ~ 0.5.
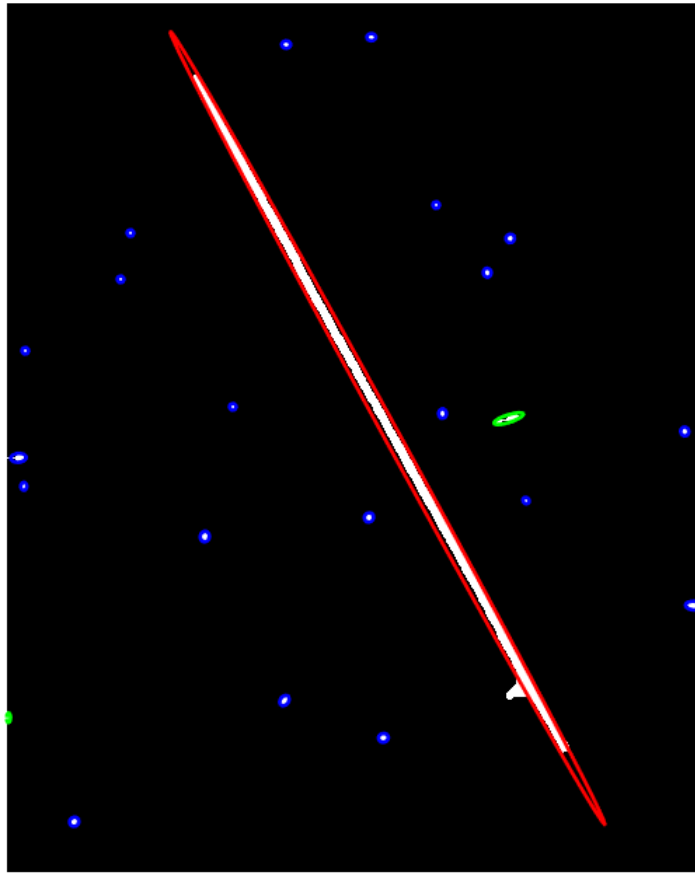
FIGURE 4.9: During the binary identification process, the streak is identified and marked in re, the stars in blue and cosmic rays or galaxies in green.

The developed tool can detect satellites also with different observing strategies (non-sidereal rate) where the stars appears as trails with fixed length depending on the rates during the exposure. Figure 4.10 shows an example of the presented technique applied for plate solving. The stars appear as trails, but only the ones with both ends contained in the picture frame are recognized as stars and processed to evaluate the centroid. The position of the centroid can be assumed reached at half of the exposure time. The result is then computed to solve the field and the triangulation are compared to an observation taken at sidereal rates to verify the results.
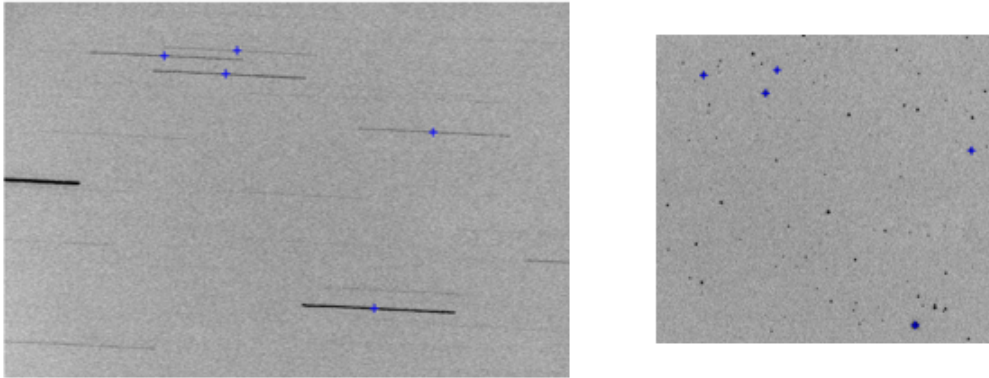
FIGURE 4.10: Star position reconstructed from images obtained with non-sidereal tracking strategy.

Once the target is identified, its orientation angle θ is used to rotate the original frame by the same angle to obtain the streak horizontally (Figure 4.11). Thus, the along track dimension is disposed along the X-axis, while the cross-track dimension is in Y-axis of the rotated frame. A second subframe SF2 is then extracted containing the horizontal streak (Figure 4.12). The endpoints position evaluated at the previous step is rotated according to θ.
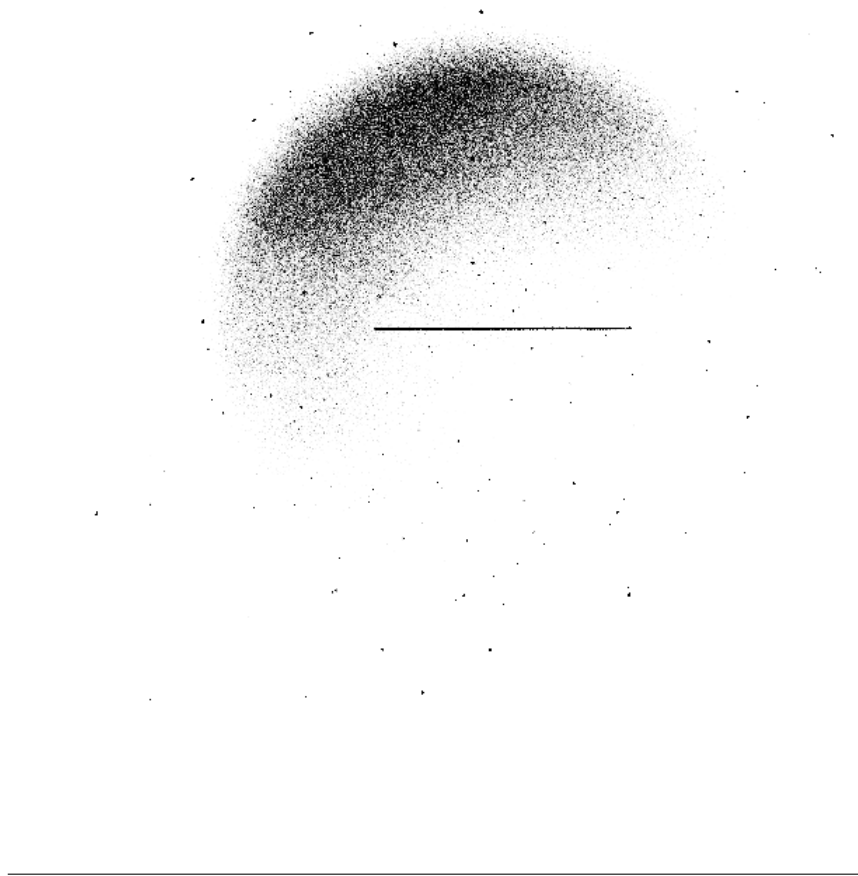
FIGURE 4.11: Horizontal streak.
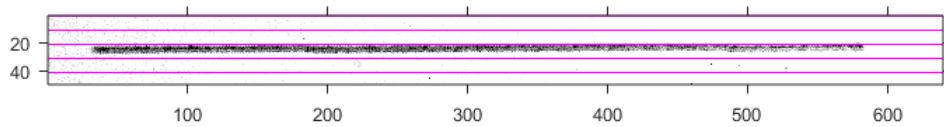
FIGURE 4.12: Horizontal subframe.

SF2 contains the streak oriented horizontally, but the real endpoints position is still unknown. Therefore, a second Canny loop has implemented to accurate determine the streak position within SF2. The threshold values are evaluated again due to different `min`, `max` and standard deviation of pixel values of SF2 compared to SF1. The sub-frame is then evaluated in cross-track direction to identify the Y coordinate of the streak. The proposed solution is to

process SF1 in the Y-direction and evaluate the count Gaussian distribution for the whole X-axis. SF2 is constructed to contain the streak with a safety margin. Therefore, also stars can be included in the frame. If an average analysis on the Y-peak distribution on the X-axes is performed, stars that are much brighter than the streak can affect the results considerably. Therefore, a median analysis is performed. Due to the count distribution connected with the presence the streak is dominant in the X-axes (along- track direction) the identified Y-peak position is detected. As mentioned in Section 4.1.1, the importance of properly estimating the background level of a CCD resides in the fact that the same pixels that collected photons of interest reflected from the target also collect photons from background sky which are no interest. If non-properly reduced, the background includes also read noise, thermally generated dark current and other noise sources. All the unwanted additional photons need to be estimated and removed from the image before a final analysis of the flux is made. For stars, a common technique is to consider an annulus around the source of interest and then use statistical approach to estimate its mean level on a per pixel basis. The sky annulus is defined by an inner and outer radius. The background level is then estimated by extracting the values within the annulus and divide by the total number of pixel within the annulus. This provides an average value per pixel for the background level of the CCD image. For a good statistical determination of the value, the total number of pixels contained within the annulus should be relatively large. For streak analysis, a similar approach has been implemented in the Y-axis. The Gaussian distribution of the counts in the across-track is evaluated using *Point Spread Function* (PSF).

- Streak vertical margin: comparable to the star aperture in the sky annulus techniques, it is defined as the limit of the area of the PSF that contains the counts reflected from the orbiting target.

- Sky inner margin: like the sky annulus inner radius, it is greater than the streak vertical margin and it defines the start of the sky region.

- Sky outer margin: like the sky annulus outer radius, it is defined as the sky inner margin plus a width.

The streak vertical margin is evaluated by a study of the histogram of the streak in the cross-track direction: the Gaussian distribution is processed to identify the median intensity value S_M, then a 3σ distribution cutoff technique is applied. Therefore, the whole cross direction of the streak is identified as $S_M \pm 3\sigma$ (Figure 4.13). When applying the filter and the cutoff, the remain annulus pixels are used to construct the background histogram computed with a bin resolution of 1 ADU. The histogram is centered in the S_M value and contains values outside the 3σ region. Then a statistical approach is used to identify the mean value for the background $\overline{B}$ and the inner and outer margin are identified. Therefore, two different sky regions are identified: one above the streak (sky upper region) and one below the streak (sky lower region). The median value of the sky per pixel in the extracted by computing the two regions.
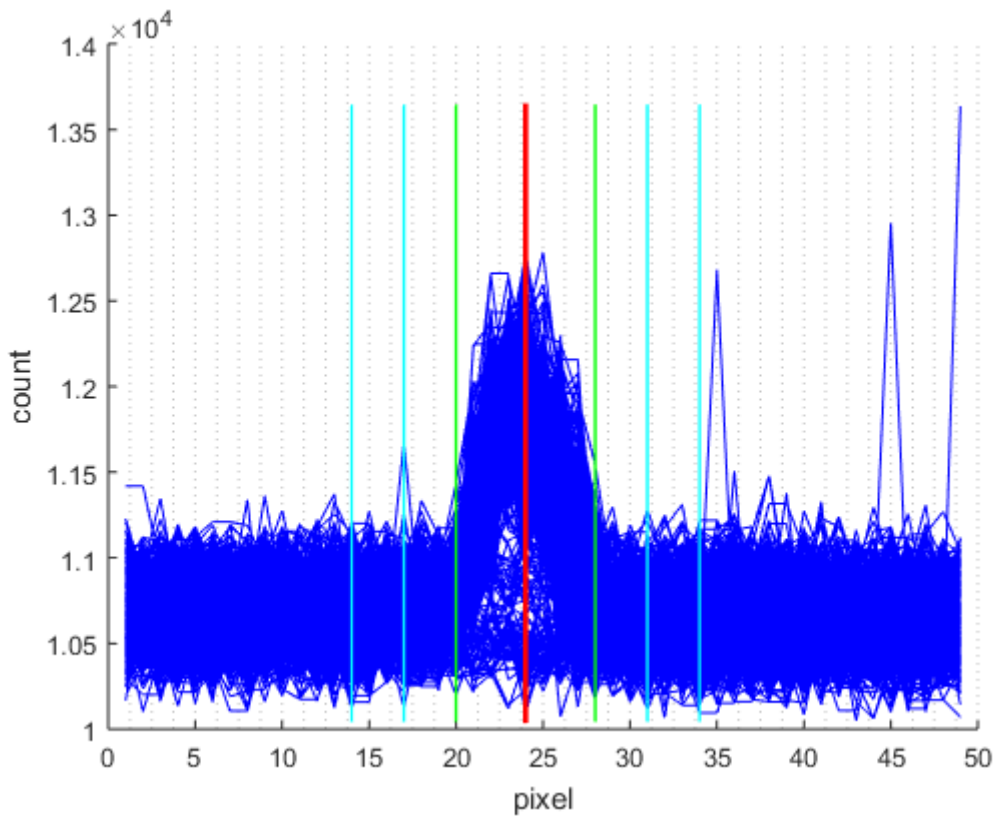
FIGURE 4.13: Along-track Vs cross-track analysis for Y-coordinate identification.

Endpoints analysis

Once the Y-coordinate of the horizontal trails is detected and the streak dimension and the sky value are evaluated, crucial point is to estimate the streak endpoints position. The discernment of the ends is fundamental for orbit attitude reconstruction analysis. During the exposure time, the object trails across the FOV. If the total length of the streak is affected by an error or if the endpoints position is false, the analysis on the rates of the satellites is compromised. The analysis in the along-track direction is performed in a similar way to the cross-track analysis. Once the result of the media sky value is computed, a windowing of the SF2 is performed by selecting a section with the same width of the streak and with the X-dimension of the total SF2. The

counts are summed in the cross-track direction for the whole length of the windows. The profile distribution for the whole X-dimension is processed to evaluate when the count levels exceed the sky background. Therefore, the two endpoints of the streak are computed. During this phase, it is important to take care about any possible source of contamination. If a star is close to the ends of the streak it can create a false positive end identification. Therefore, analysis on the total length of the counts profile above sky level is done to reject stars or cosmic rays. The success in the determination of the main frequencies of target depends mostly on the accuracy of the measurements of the flash peak times that relies on to the precise identification of the streak ends [Somers (2011)]. Optical signatures of faint debris might appear as a series of disconnected flashes in a CCD image due to the diffuse reflections that are often dimmer than the sky background (Figure 4.14). These flashes also tend to overcome and obscure the background diffuse reflection. When the flash occurs near the start or end of the time exposure, the location of one of the ends of the streaks is obscured. Thus, it is difficult to accurately assign a precise time scale to the streak. By considering this and the fact that the diffuse reflection may be less than the detection limit, it might be difficult or even impossible to determine the end of the streak.
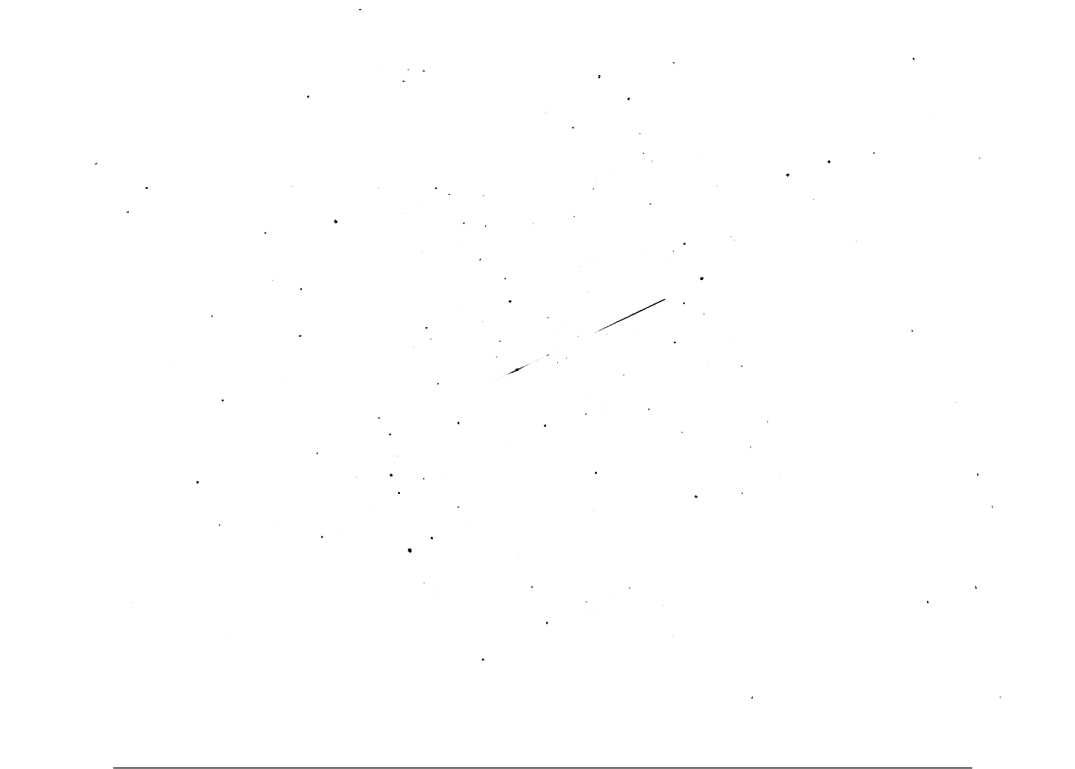
FIGURE 4.14: Topex/Poseidon LEO debris, its collected streak presents parts in which the collected signal is dimmer than the background sky.

This causes an uncertainty in the determination of the time of the flash. In fact, the relative uncertainty of the flash peak times compared to the flash period, and the number of flashes that can be observed and measured, depends on the time span over which the measurements are made, and whether these measurements occurred at opportune times when the variation of the peak times is changing significantly from the rotation times [Parish (1994)]. Precise time measurement for start and ends of exposure time is mandatory to avoid systematic error in frequency analysis. To reduce the effect of uncertainty of the observed streak endpoints, a different approach has been followed and implemented in the tool. TLEs of the observed targets are used to determine theoretical length of the streaks by computing the rates. An analysis on the variability of main orbit parameters allows the tool to evaluate the effectiveness of the TLEs analysis at the observing period. Once the TLEs are verified,

the predicted length of the streak is evaluated by considering the rate in the along-track direction derived from the TLEs position (RA rate and DEC rate are assumed constant during the exposure time t_{exp}).

$$rate_{a.t} = \sqrt{(RA_{rate})^2 + (DEC_{rate})^{2)}} \quad (4.24)$$

where:

$$RA_{rate} = \frac{RA_{end} - RA_{start}}{t_{exp}}$$

$$(4.25)$$

$$DEC_{rate} = \frac{DEC_{end} - DEC_{start}}{t_{exp}}$$

This analysis is performed for all the TLEs downloaded over the span time $\pm 10\, d$ from the acquisition day and the median value is extracted. By considering the t_{exp} and the plate scale, the total theoretical length in pixel of the streak is computed. The length obtained from the TLEs analysis l_{TLE} is the compared with the one reconstructed from the image l_{fits}. Three-different situations can occur:

- $l_{fits} = l_{TLE}$: the two measurements in pixels correspond.

- $l_{fits} > l_{TLE}$: the length of the streaks calculated from the image analysis is greater than the one calculated from TLEs data. This might be caused by several factors: error in the TLEs, rates not constant during the exposure, star contamination of the streak therefore it appears longer, coma effect, etc...

- $l_{fits} < l_{TLE}$: the length of the streaks calculated from the image analysis is smaller than the one calculated from TLEs data. This might be caused by difficulties in the identification of the endpoints caused by brightness variability of the streaks close to the ends that make them

dimmer than the background stars or error in the TLEs and rates as the previous point.

To process the image the following approach has been implemented: the length evaluated from the TLEs is assumed as true, therefore the evaluated difference $l_{TLE} - l_{fits}$ is added (or subtracted) for the l_{fits} to make the two with the same size. The difference expressed in pixels need to be added (or removed) at the ends, but the results are depending on where the modification is implemented. In fact, the error in the ends detection could be in both extremes or just in one of the two. To process this, an end-shifting routine has been implemented. As shown in Figure 4.15, if the original length is shorter (on the top of Figure 4.15 or longer on the bottom) than the one computed from the rates of the TLE by n pixels, all combinations (n_p of difference +1) are calculated with a shifting end routine of about one pixel at the time to have all the same lengths as the on obtained from the TLE.

(Figure 4.15).
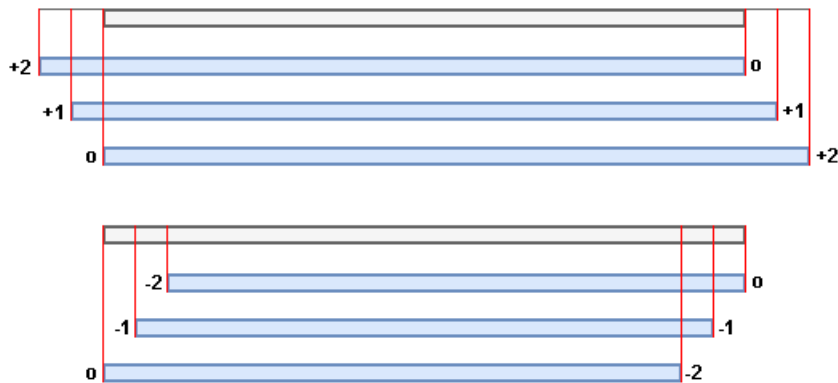
FIGURE 4.15: Shift endpoints procedure: on the top if the case in which the length reconstructed from the image is shorter than the one computed from TLEs and assumed as true; while on the bottom the vice versa case.

The consequence of the routine is a multitude of streaks to be processed with

different endpoints location. All streaks are processed individually to identify the main frequencies. Then the results are combined to obtain the frequencies profile of the light-curves.

4.2.2   Frequencies analysis

All obtained streaks are processed with a Savitzky–Golay filter ([Savitzky et al. (1964)], [Broumba (1981)]). The implemented low-pass filter is based on local least-squares polynomial approximation of the fourth order at the purpose to smooth noisy data at high frequency. Therefore, the instantaneous magnitude in the along-track direction evaluated. Using the aperture identified in Section 4.2.1, it is possible to extract the values from all pixels within the area of the streak (delimited by the endpoints in the along-track direction and by the streak vertical margin in the cross-track direction) and sum them to form the quantity S, the total integrated photometric source signal. The sum S contains contribution from the reflected light of the orbiting object but also underlying background sources within the evaluated area. To remove the contribution of the background it is possible to use the median sky background $\overline{B}$ evaluated in Section 4.2.1. Therefore, the collected source intensity I can be calculated as

$$I = S - n_{pix}\overline{B} \qquad (4.26)$$

Where n_{pix} is the total number of pixels contained in the streak area. The source magnitude can be calculated as:

$$Magnitude = -2.5log_{10}(I) + C \qquad (4.27)$$

Where I is the source intensity per unit time, that is the flux per second, and C is a constant ($\sim 23.5 - 26$) determined in such manner so that the calculated source magnitude is placed on a standard magnitude scale (i.e. Johnson system [Johnson et al. (1953)]). The streak can be intended as a sequence of image at any given time of the brightness of the objects. Therefore, it is possible to compute the instantaneous magnitude profile by sum in the cross-track direction the pixels within the streak area and then proceed as previously described. The result is a signal profile over time than can be processed to identify the main frequencies. In literature ([Yanagisawa et al. (2012)], [Schildknecht et al. (2015)], [Schildknecht et al. (2008a)], [Fruh et al. (2010)]), several approaches on how to extract frequencies from light curves are used. The most common is the Fourier analysis. The implemented tool computes the discrete Fourier transform (DFT) of the light curves using a *fast Fourier transform* (FFT) algorithm [Welch (1967)]. Another method is the *Periodogram* analysis used in literature ([Schildknecht et al. (2013)], [Papushev et al. (2009)]) to investigate the *Power Spectral Density* (PSD). This method often used to cross-check results from FFT. Both these methods, required to have equally space data. However, due to the problem of a flash peach that might be dimmer than the background sky, different approach has been implemented. A reliable method able to deal with unevenly spaced measurements in time series is the *Lomb-Scargle periodogram*. The methods return the Lomb-Scargle power spectral density estimated. The algorithm is set to identify the first six main frequencies with the highest power spectrum (expressed in dB). Then all the identified peaks for the three methods are compared with a statistical tool to evaluate the occurrences. The frequencies with the highest number of occurrences can be considered proper of the satellites as less affected by ends determination error effects.

4.2.3   Simulations

To validate the code, a simulation environment has been created. The main goal is to create from user defined profile of light-curves a simulated light-curve with known main period. Using the presented code, the main frequencies are extracted and then compared to real data from the user defined profile. Starting from real data, a sky-mask is created. It is the combination of a median stack process of real observations taken with MITO and then processed using a $2D$ Gaussian filter with standard deviation of 2 to smooth the profile. The pixel values are then randomly distributed in the frame to simulate a non-uniform background without any star (Figure 2.2).
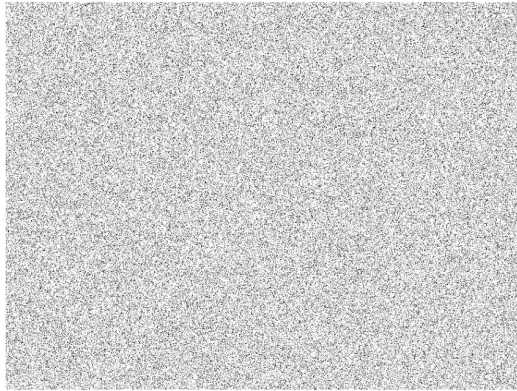
FIGURE 4.16: Median Sky.

Best case

Then, the light Curves is generated a combination of two sine waves. As presented in Figure 4.17 the equation of the two waves are:

$$w_1 = sin(16\pi x_{pxl})$$

$$(4.28)$$

$$w_2 = \frac{\pi}{3} \cdot sin(8\pi x_{pxl})$$

The light-curve wave is the result of $w_{tot} = w_1 + w_2 + G$, where G is the gain used to change the dimmer effect of the light-curve.
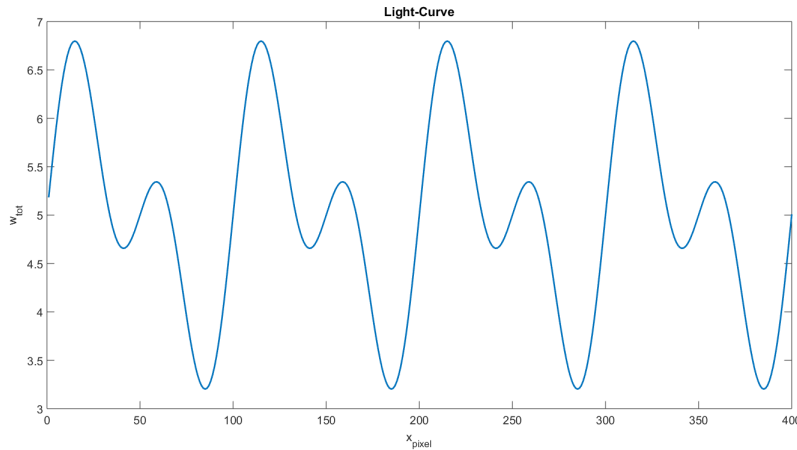
FIGURE 4.17: Sum of the two sine waves.

The simulated light-curve streak is designed to be with defined:

- length (x-direction, along-track): it represents the length evaluated by the TLE and assumed as true.

- width (y-direction, cross-track): it relates to the seeing of the observation. A Gaussian profile is applied in y-direction for the whole length of the streak to represent the Gaussian PSF distribution.

The simulated observation is assumed to be with fixed t_{exp} (typical value for MITO observation of LEO object is $4\,s$) and with a defined plate-scale (assumed for the simulation equals to $4\,arcsecond/pixel$). By considering these values, it is possible to determine the original period of global sine function is equal to $1\,s$ (main frequency $1\,Hz$) and a secondary frequency of $2\,Hz$. This sine wave has been selected because it can replicate real case that can occur when the satellites is spinning fast and its composed by different faces with different reflective properties. Therefore, it is possible to distinguish a front and a back on the orbiting object. Therefore, the streak is generated as:

$$streak_s = bias_{sky} \cdot w_{tot} \tag{4.29}$$

The, it is summed to the obtained sky. The streak end analysis on the generated image is performed as previously described. Then the obtained length is competed to the one assumed from the TLE and considered as true. The difference is used for the shift position. If the values are always higher than the background sky (as presented in Figure 4.18), then the streak end procedure routine and the original length data are according. Therefore, no shifting position are true.
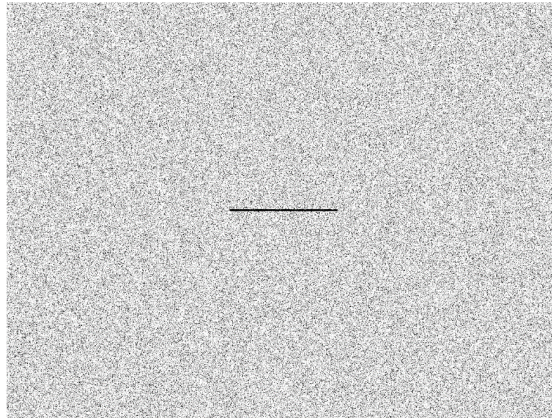
FIGURE 4.18: Median sky with the simulated streak overimposed.

The light is extracted and processed by using Savitzky-Golay filtering [Savitzky et al. (1964)] and Magnitude estimation process. It is possible to notice that ad expected, the light-curve is always above the sky level (Figure 4.19).
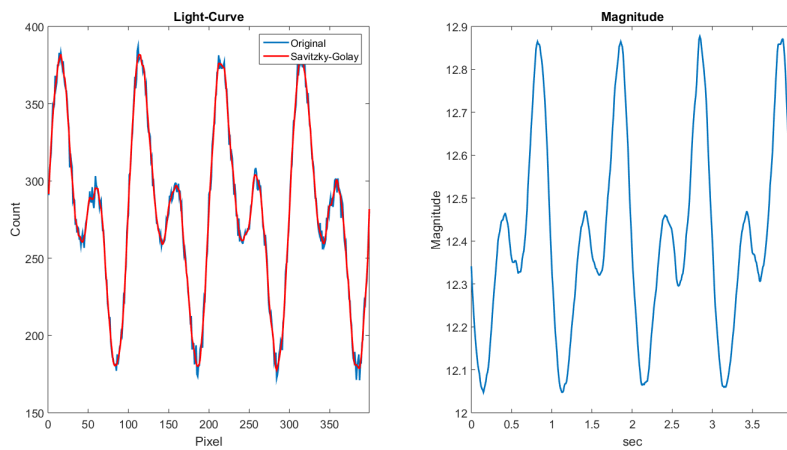
FIGURE 4.19: Savitzky-Golay filtering and Magnitude estimation.

Then the curve is processed and the three-different frequencies extraction method are applied. The results are compliant with the real starting data as shown in (Figure 4.20). The main frequencies of $1\,Hz$ has been detected from all methods, and both the periodogram and Lomb-Scargle method have identified also the frequencies of $2\,Hz$ caused by the second wave period.
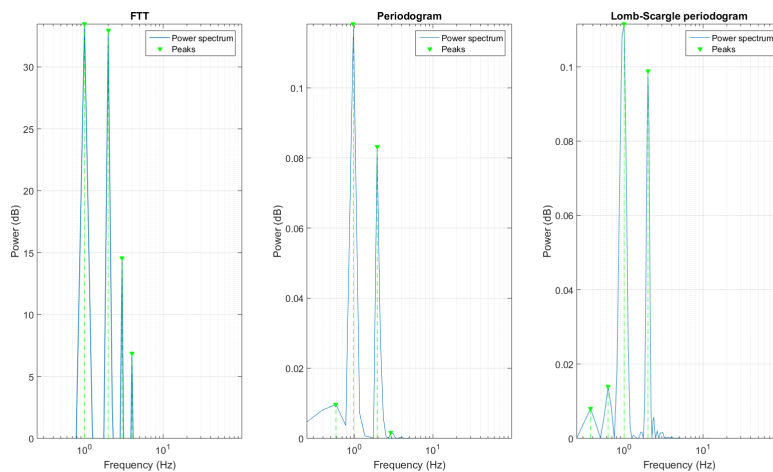
FIGURE 4.20: FFT, Periodogram and Lomb-Scargle periodogram analysis for the simulated streak.

Worst case

More interesting case is when the simulated streak represents a faint satellite which endpoints location is obscure. The generation of the wave is like the one presented in Section 4.2.3, where the gain value G is set to zero. Therefore, the streak is not represented as a continuous trail on the sky frame but some it appears as a series of disconnected streaks (Figure 4.21 and Figure 4.22) caused by the area in which the light curve w_{tot} is below zero. For the parts dimmer than the sky lever, the count value is equal to just the sky values.
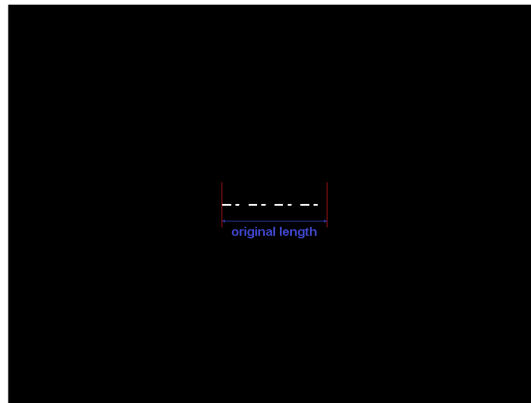
FIGURE 4.21: Simulated disconnected series of streaks.
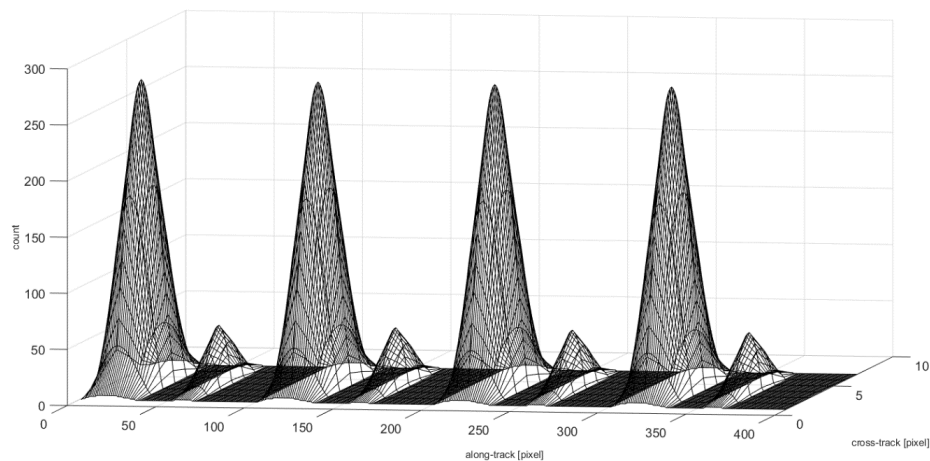
FIGURE 4.22: $3D$ simulated streak profile.

Then the obtained streak is over-impressed on the sky frame to obtain the simulated disconnected streak (Figure 4.23).

FIGURE 4.23: Median sky plus the simulated disconnetced series of streaks.

The theoretical streak length assumed as true is the one given by the sine wave (= 400 pixels), while the obtained length estimated from the image is calculated by the light-curve data process and it is smaller than the real value. Therefore, the shift procedure is applied (Figure 4.24).
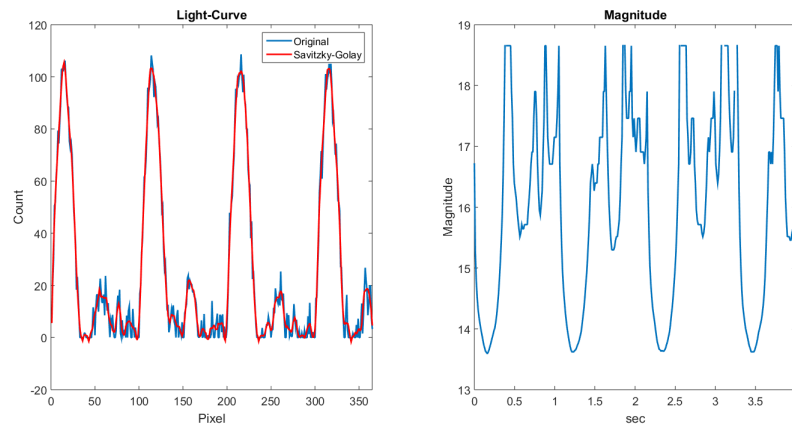
FIGURE 4.24: Results for one of the shifted reconstructed streak. Savitzky-Golay filtering and Magnitude estimation on the disconnected series of streaks.

The results have been processed statistically by identifying the frequencies with the highest occurrences. Each method applied has been able to identify the main frequencies of $1\,Hz$ as the frequency with the highest number of occurrences and the $2\,Hz$ frequency as the second one (Figure 4.25).
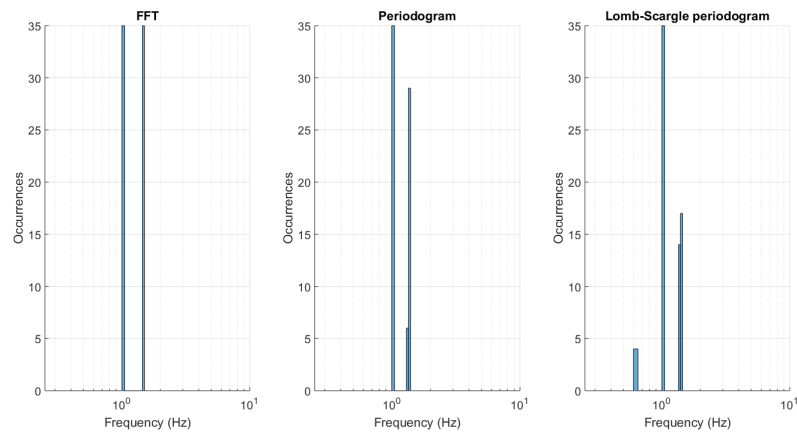
FIGURE 4.25: Occurrences for the three analysis methods.

4.3 Image processing tool applied to real data

Observations have been carried out suing the observatories of the S5Lab Network. MITO observatory has been used for LEO target for the analysis of the collected light-curves for the IADC-AI31.2 as presented in Section 3. Loiano and Curtis-Scmidth observatory have been used for GEO target. Object in GEO are typically sensitive to changes in brightness on timescales of 30 s or longer [Cardona et al. (2016a)] primarily because of the long readout time (25 s) of the CCD. To investigate brightness changes faster object trails across the FOV while the telescope tracked at the sidereal rate and R filter was used. Exposure times were 20 s or longer, such that both ends of the trail were in the FOV. By considering $2\,arcsecond$ FWHM, and the object moving at an average rate of $15.041\,arcsecond/s$ along track, the analysis performed is sensitive to brightness variations as fast as $0.13\,s$.

4.3.1 MITO LEO data

Analysis on the collected light-curves of LEO objects for the IADC AI-31.2 campaign observed from MITO observatory on March, 2017 are presented in Table 4.1 and Table 4.3.1.

TABLE 4.1: Number of trailed images taken at MITO on March, 2017.

SSN	Launch Year	Number of trailed objects
00727	1964	7
00733	1964	12
04589	1970	6
07477	1974	27
11804	1980	1
20491	1990	61
21938	1992	4
22040	1992	88
23088	1994	20
23405	1994	5
24298	1996	3
25893	1999	6
27386	2002	38

TABLE 4.2: Main five frequencies [Hz] detected from MITO data with the highest power [db]. The symbol – represents that the specific frequency has not been identified by the methods among the first five frequencies with the highest power.

SSN	FFT	Periodogram	Lomb-Scargle
	–	0.233	0.250
	0.750	0.800	0.750
00727	1.200	1.165	1.187
	1.600	1.665	1.6525
	3.750	–	–
	0.250	0.300	0.250
	0.075	0.832	0.750
00733	1.250	1.215	1.280

	–	1.665	1.625
	2.000	1.988	2.000
	0.375	0.400	0.411
	0.750	–	0.750
04589	1.625	1.642	1.625
	1.875	1.902	1.9065
	2.600	2.764	–
	0.375	0.318	0.312
	0.750	0.701	0.719
07477	1.000	1.019	1.030
	1.875	1.529	1.562
	2.000	2.100	–
	–	0.087	–
	0.120	0.136	0.125
11804	0.449	0.452	0.500
	1.200	1.114	1.200
	2.00	1.980	1.890
	0.750	0.779	0.756
	0.875	0.857	0.844
20491	1.250	1.474	1.312
	2.125	2.180	2.125
	2.750	–	–
	–	0.170	–
	0.500	0.510	0.500
21938	1.000	1.104	1.125
	1.500	1.525	1.500
	2.000	2.067	2.050
	0.375	0.366	0.375
22040			

	0.625	0.512	0.500
	1.125	–	–
	1.500	1.456	1.510
	–	2.100	2.032
	0.525	0.592	0.625
	0.759	–	–
23088	1.375	1.250	1.210
	2.125	2.125	2.200
	3.500	3.433	3.400
	0.250	0.251	0.281
	0.500	0.527	0.500
23405	1.750	–	1.780
	2.626	2.636	2.655
	3.375	3.355	3.375
	–	–	0.1875
	0.750	0.769	0.750
24298	1.750	1.731	1.750
	2.222	2.308	2.250
	3.250	–	–
	0.250	0.239	0.250
	0.620	0.598	0.625
25893	1.500	1.514	1.500
	1.875	–	1.906
	–	2.322	–
	0.750	0.779	0.750
	1.125	1.072	1.062
27386	1.500	1.461	1.500
	1.750	1.753	1.781

2.500	2.432	2.455

4.3.2 Loiano GEO data

Analysis on the collected light-curves of GEO target observed from Loiano observatory on February 10, 2016 are presented in Table 4.3 and Table 4.3.2.

TABLE 4.3: Number of trailed images taken at the Loiano Observatory on February 10, 2016.

SSN	Launch Year	Number of trailed objects
17873	1979	1
18718	1987	3
27509	2002	2
27780	2003	3

TABLE 4.4: Main five frequencies [Hz] detected from Loiano data with the highest power [db]. The symbol – represents that the specific frequency has not been identified by the methods among the first five frequencies with the highest power.

SSN	FFT	Periodogram	Lomb-Scargle
	–	0.052	0.050
	0.200	0.193	0.195
17873	0.354	0.363	0.3858
	0.505	–	–
	0.646	0.642	0.658
	0.101	0.107	0.104
	0.202	0.200	0.200
18718	0.303	–	–
	0.505	0.560	0.550

		1.014	1.013
	0.101	0.109	0.108
	0.151	0.158	0.154
27509	0.253	–	–
	0.354	0.351	0.355
	–	0.799	0.750
	0.151	0.154	0.162
	–	0.231	0.237
27780	0.303	0.308	0.300
	0.505	–	–
	0.569	0.590	0.600

4.3.3   MODEST GEO data

Analysis on the collected light-curves of GEO target observed from Curtis-Schmidt observatory on November 3, 2015 are presented in Table 4.5 and Table 4.3.3.

TABLE 4.5: Number of trailed images taken at Curtis-Schmidt on November 3, 2015.

SSN	Launch Year	Number of trailed objects
13056	1982	9
19217	1988	8
23536	1995	6
23846	1996	8
25152	1998	7

TABLE 4.6: Main five frequencies [Hz] detected from Curtis-Schmidt data with the highest power [db]. The symbol – represents that the specific frequency has not been identified by the methods among the first five frequencies with the highest power.

SSN	FFT	Periodogram	Lomb-Scargle
	–	0.020	0.023
	0.067	0.060	0.067
13056	–	0.100	0.108
	0.202	0.201	0.200
	0.263	–	–
	0.071	0.070	0.077
	0.131	0.120	0.133
19217	0.263	0.259	0.258
	0.403	0.405	0.404
	0.679	–	–
	–	0.020	0.025
	0.131	0.131	0.135
23536	0.202	–	–
	0.300	0.302	0.300
	0.465	0.463	0.462
	–	–	0.029
	0.071	0.071	0.067
23846	0.101	0.104	0.108
	0.303	0.305	0.306
	0.737	0.739	–
	–	0.070	0.075
	0.202	0.221	0.221
25152	0.303	0.301	0.308
	0.364	0.441	–

0.505   –   –

4.4   LEDSAT a CubeSat with LEDs for optical track-
ing

As presented in Section 3 , ground-based optical tracking of satellites in LEO
requires the satellite to be in sunlight, while the ground-based telescope must
be in darkness. This imposes a constraints on the visibility time for track-
ing to typically 90 minutes in evening and morning twilight ([Seitzer et al.
(2016)], [Seitzer et al. (2017)]).

To work around these limitations, Japanese 1U CubeSat *FITSAT-1* which car-
ried high-powered green and red LEDs, and it was observed with small
ground-based telescopes [Tanaka et al. (2015)].

S5Lab research team and Astronomy Department of University of Michigan
proposes the innovative concept of optical tracking and the strategy is based
on active illumination of the observed target. The proposed mission, called
LEDSAT (LED-based SATellite), is based on a CubeSat equipped with colored
Light Emitting Diodes (LEDs) controlled to flash the light with specific pat-
terns to be visible also when the satellites is in the Earth shadow to demon-
strate that a LEDbased active illumination system may be used to achieve
orbit and attitude determination [Pellegrino et al. (2017)]. In fact, active illu-
mination will improve:

- Astrometry of the light signal against a reference star field, which should
  improve the orbital accuracy and precision ([Masillo et al. (2017)], [Cut-
  ler et al. (2017)]). Critical here is that the timing of the light signal is

generated on the spacecraft itself, so that simple ground-based systems can return useful astrometric information.

- If each CubeSat has different and unique light signals of the same wavelength, then it would be possible to distinguish them shortly after deployment even if they appear in the same image separated by a few arcseconds. This is important when there are large numbers of satellites deployed at the same time. It satisfies the request of JSpOC for markers on CubeSats in the case of such large numbers being deployed in a very short time [JSpOC (2015)].

As outlined in Section 4.2.1, in case of objects without active illumination, the observed quantity is the luminous flux reflected by the surface. For astrometry analysis, triangulation methods are used to assign the coordinates of points of the streak which are usually the midpoint and the endpoints comparing the position to the background star field. Nevertheless, LEO objects might have a non-uniform velocity along the track therefore, previous consideration may not be valid. Only the streak endpoints might be assigned unequivocally with a precise time-tag that are respectively the initial and final time of exposure. However, as mentioned in Section 4.2.1, the magnitude in the along-track dimension might not be constant due to possible tumbling motion of the satellite and different reflective properties of the material of the different faces of the satellites. If this variation occurs near the streak ends, even the time-tag of the endpoints is uncertain. Active illumination and a system for on-board timing precision presented with the LEDSAT aim to solve the problems related to the temporal and positional uncertainty of endpoints generation. By using an ultra-stable oscillator to trigger the LEDs according to a defined pattern, a sequence of dots and lines can be generated. The generated points must have the same relative size of the stars in the background to assign their coordinates with high precision. Therefore, by

comparing the temporal time of generation and image acquired of the dots, it will be possible to improve the orbit determination analysis. An simulation of a LEDSAT streak with different pattern is shown in Figure 4.26.
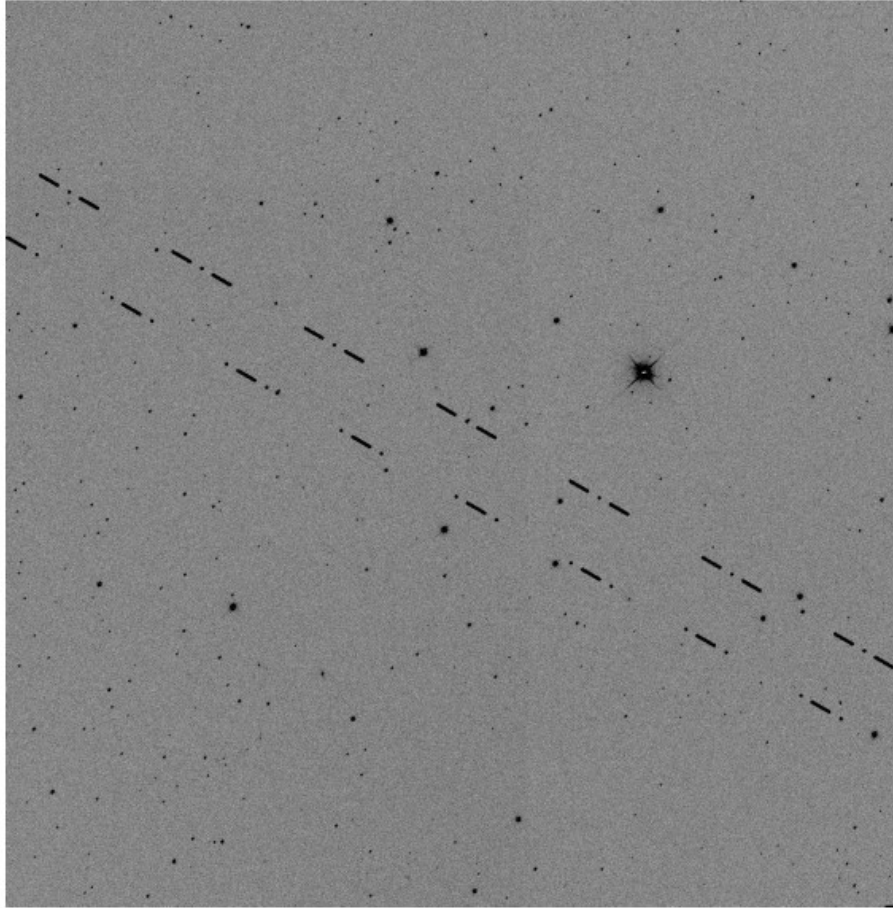

FIGURE 4.26: Simulation of a LEDSAT pattern over-impressed on a real photometric field taken at the Curtis-Schmidt observatory.

In May 2017, the CubeSat was selected for the first phase of the second edition of the Fly Your Satellite! (FYS) Programme, organized by the European Space Agency (ESA), giving LEDSAT the opportunity to be launched from the ISS within two years.

4.5 Streak length controlled analysis

S5Lab research team and astronomy Department of University of Michigan cooperates for photometric analysis of space debris since 2012. Analysis has been conducted for spectrometric measurements of GEO debris in 2012 ([Seitzer et al. (2012b)], [Seitzer et al. (2013a)]) using Magellan Observatory in Chile. The Magellan Observatory is composed by two twin telescopes: Walter Baade Telescope and Landon Clay Telescope. The two telescopes are located 60 meters apart on an isolated peak (Cerro Las Campanas). The telescopes have a diameter of 6.5 m each and have an alt-azimuth design.

The Magellan spectra of observed space debris ([Seitzer et al. (2012b)], [Seitzer et al. (2013a)]) show a wide range of spectral slopes from blue to red. Laboratory measurements of materials used in spacecraft construction have been conducted ([Cowardin et al. (2009)], [Cowardin et al. (2010a)], [Cowardin et al. (2010b)]) and the results were used for comparison. Except for the black paint and the solar panel, it has been demonstrated that there is no good agreement between any of the laboratory curves and the observed spectra. One of the main reason might be that the observed spectra are of a complex surface with multiple materials contributing to the flux measured at the telescope. Moreover, the spectra are time averaged over the length of the exposure, that typically is five minutes. If an irregularly shaped object does not have a constant attitude during the exposure, then a model requiring a mix of materials and sizes related to its and tumbling rate may be required as well. Therefore, for full interpretation of the space debris spectra more complex methods must be implemented in both the acquisition and analysis methods.

The presented solution is to acquire spectra data of GEO debris where the object image is trailed inside the slit in a controlled way by performing rates

changes using *Blind Non-Sidereal Tracking* (BNST) rate code. The main advantage of the presented technique is that in this way, if the object is rapidly tumbling and presenting multiple surfaces towards the observer or the object structure is complex and not a simple surface, it should be possible to identify more spacecraft materials by a comparison with laboratory spectra. This technique has been developed and tested using Angell Hall observatory by performing controlled streak length data collection of GEO and MEO object.

The developed code is an evolution of the BNST developed in ([Seitzer et al. (2012b)], [Seitzer et al. (2013a)]) that allows the operator to select the total length of the streak by selecting an additional tracking rate that is added as a constant bias to the NST rate used to keep the observed object as a dot during long exposures. An example of a controlled streak is presented in Figure 4.27 where the observed is let trail across the FOV with a defined trail rate of $20\,arcsecond/s$ with a total exposition time of $20\,s$. Therefore, the total defined length is $400\,arcsecond$. The developed technique will be applied to Loiano and Magellan spectrometric acquisition date and the results will be compared with standard spectrometric acquisition and laboratory measurements to evaluate the improvements in the physical characterization of GEO debris.
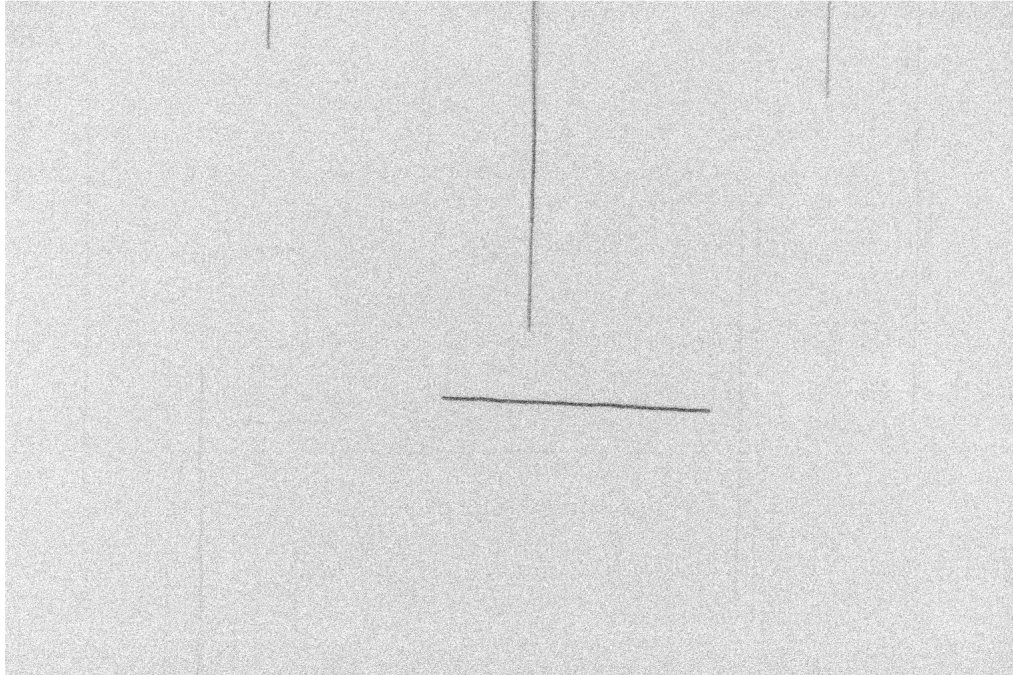
FIGURE 4.27: Collected streak of SSN 41019 observed at Angell Hall with a defined controlled length of $400\ arcosecond$.

Chapter 5

Conclusions

The presented thesis, outlines the activities carried out in the framework of the observation of space debris. The design and the development of the Italian network of optical observatories has been presented in Section 2. This include the refurbishment of MITO observatories and the design and manufacturing of the EQUO-OG observatory in Kenya. The installation campaign has been presented with special focus on the remote operative phase. The development of the off-shore observatories EQUO-OS has been presented. These activities have been supported by the Italian Space Agency, in the framework of the Agreement between Italian Space Agency (ASI) and Sapienza - University of Rome for the Broglio Space Center in Malindi (Accordo Attuativo della Convenzione Quadro N.2013-079-C.0).

The development of the network coordinator fully dedicated for space debris purpose has been presented in Section 3. The design and the implementation of scheduler called NICO has been presented. The main characteristic of the presented network coordinator is the modularity of the designed project by taking care of different observing scenarios (i.e. survey, attitude analysis, orbit improvement) at different orbital regimes. The input phase and main phase of NICO has been presented with special focus on the implemented

observing strategies and the genetic algorithms implemented for the harmonization of the different requests by taking care also of external limitations such as astronomical constraints and weather conditions. NICO has been developed in the framework of the agreement between ASI and National Institute for Astrophysics (INAF) in support to IADC (Inter-Agency Space Debris Coordination Committee) activities (Accordo Attuativo della Convenzione Quadro N.2013-079-C.0)

An automatic pipeline for light-curve extraction for frequencies analysis of orbiting objects has been presented in Section 4. Light-curves analysis proved to be an effective method to determine the attitude of orbiting objects including space debris. The presented thesis focuses on the implemented techniques for the automatic the streak extraction process, with a special focus on how to solve the problem on determination of streaks ends that occurs when the object is faint.

A validation analysis has been carried out by developing a light-curves simulator to verify the implemented methods for the main frequencies determination. The developed automatic pipeline has been tested on real images collected from different observatories at different orbital regimes. The presented thesis reports the results from observing campaign data analysis taken with MITO observatory, the 1.5m Loiano observatory located near Bologna operated by INAF and the University of Michigan's 0.6-m aperture Curtis-Schmidt telescope located in Chile. The observations have been collected with the object trailed across the field of view while the telescope tracked at the sidereal rate. The importance of light-curve analysis relies on the possibility to determine the attitude of the orbiting object using optical measurements. These data are valuable for future mission fro active debris removal mission. More observations of space debris as streaked images are necessary

to improve the knowledge of the main frequencies of the objects, and to determine how the evolution of the dynamic state of the orbiting object with time.

The work developed in this thesis will be the basis for the automatic operation of the S5Lab observatories network. Operational experience was gained during the development of the thesis, showing the satisfactory performance of the proposed algorithms for automatic scheduling. An added value of the proposed algorithm and implementation is the fast evaluation time to obtain the schedule, which makes the algorithm and the related software package potentially very well suited for real time, daily operation of the network.

Bibliography

[Abercromby et al. (2013)] Abercromby, K., Rapp, J., Bedard, D., Seitzer, P., Cardona, T., Cowardin, H., Barker, E. & Lederer, S., Comparisons of a Constrained Least Squares Model versus Human-in-the-loop for Spectral Unmixing to Determine Material Type of GEO Debris, Proceedings of the 6th European Conference on Space Debris, ESA/ESOC, Darmstadt, Germania , 2013

[Adams et al. (1980)] Adams, M., Christian, C., Mould, J., Stryker, L. & Tody, D., Stellar magnitudes from Digital Pictures, Kin Peak National Observatory publication, 1980

[Alby et al. (1997)] Alby, F., Lansard, E. & Michal, T, Collision of Cerise with Space Debris, Proceedings of the Second European Conference on Space Debris. Proceedings ESA SP-393, pp. 589–594. Noordwijk, Netherlands, 1997

[ASCOM (2017)] `ascom-standards.org` Retrieved on October 16th, 2017

[Barbulescu et al. (2004)] Barbulescu, L., Watson, J.P., Whitley, L. D. & Howe, A. E. Scheduling space–ground communications for the air force satellite control network. Journal of Scheduling, 7(1), 7-34, 2004

[Barbulescu et al. (2006)] Barbulescu, L., Howe, A.E., Whitley, L.D. & Roberts, M., Understanding algorithm performance on an oversubscribed scheduling application. J. Artif. Intell. Res. 27, 577–615, AI Access Foundation, 2006

[Bastida Virgili et al. (2016)] Bastida Virgili, B., Dolado, JC., Lewis, HG., Radtke, J., Krag, H., Revelin, B., Cazaux, C., Colombo, C., Crowther, R. & Metz, M., Risk to space sustainability from large constellations of satellites, Acta Astronautica, Vol 126, 154-162, 2016

[Bobrinsky and Del Monte (2009)] Bobrinsky, N. and Del Monte, L., ESA's space situational awareness programme, Proceedings of the 2nd CEAS, Manchester UK, Oct. 26-29, 2009, ISBN 1 85768 2130, 2009

[Boer et al. (2017)] Boer, M., Klotz, A., Laugier, R., Richard, P., Perez, J. C. D., Lapasset, L. & Kennewell, J. A. TAROT: a network for space surveillance and tracking operations. In 7th European Conference on Space Debris ESA/ESOC, Darmstadt/Germany, 2017

[Broumba (1981)] Bromba, M. U. A., and Ziegler, H., Application Hints for Savitzky-Golay Digital Filters, Analytical Chemistry, Vol. 53, pp. 1583−1586, 1981

[Brown et al. (2013)] Brown, T. M., Baliber, N., Bianco, F. B., Bowman, M., Burleson, B., Conway, P. & Dragomir, D. Las cumbres observatory global telescope network. Publications of the Astronomical Society of the Pacific, 125(931), 1031, 2013

[Burrowbridge (1999)] Burrowbridge, S. E. Optimal allocation of satellite network resources, 1999

[Buxey (1979)] Buxey, G.M., The Vehicle Scheduling Problem and Monte Carlo Simulation, The Journal of the Operational Research Society, Vol. 30, No. 6, 563-573, 1979

[Canny et al. (1986)] Canny, J., A Computational Approach to Edge Detection, IEEE Trans. Pattern Analysis and Machine Intelligence, 8(6):679–698, 1986

[Cardona et al. (2015a)] Cardona, T., Diprima, F., Santoni, F., Piergentili, F., Canu, C. & Curiano, F., The automation of the EQUO On-Ground Observatory at Broglio Space Center for Space Surveillance. 67th International Astronautical Congress, Guadalajara, Israel, IAC-16,A6,IP,19,x33440, 2015

[Cardona et al. (2015b)] Cardona, T., Seitzer, P., Rossi, A., Piergentili, F. & Santoni, F., Photometric characterization of geo objects from the Loiano Telescope, Proceedings of the 66 IAC International Astronautical Congress, IAC-15,A6,1,3,x29238, 2015

[Cardona et al. (2016a)] T. Cardona, P. Seitzer, A. Rossi, Piergentili, F. & Santoni, F., BVRI photometric observations and light-curve analysis of GEO objects. Advances In Space Research, vol. 58, 514-527, ISSN: 0273-1177, doi: 10.1016/j.asr.2016.05.025, 2016

[Cardona et al. (2016b)] Cardona, T., Seitzer, P. & Rossi, A., Analysis of the Brightness Variability of GEO Objects,Proceedings of the 67 IAC International Astronautical Congress , IAC-16,A6,1,3,x33439, 2016

[Cardona et al. (2016c)] Cardona, T. and Diprima, F., The automation of the EQUO On-Ground Observatory at Broglio Space Center for Space Surveillance, Proceedings of the 67 IAC International Astronautical Congress IAC-16,A6,IP,19,x33440, 2016

[Cardona et al. (2017a)] Cardona, T., Seitzer, P., Piergentili, F. & Santoni. F., Automatic pipeline for light-curves variability analysis of GEO objects, Proceedings of the 7th European Conference on Space Debris, ESA/ESOC, Darmstadt, Germania , 2017

[Cardona et al. (2017b)] Cardona, T., Curiano, F., Santoni. F. & Castronuovo, M., Optimal Planning of Space Surveillance Network For Orbital Debris, Proceedings of the 68 IAC – International Astronautical Congress IAC-17,A6,IP,15,x38273, 2017

[Cardona et al. (2017c)] Cardona, T., Seitzer, P., Rossi. A. & Castronuovo, M., Automatic analysis of light-curves variability of orbital objects, Proceedings of the 68 IAC – International Astronautical Congress IAC-17,A6,IP,9,x38771, 2017

[Clement et al. (2005)] Clement, B.J. and Johnston, M.D., The Deep Space Network scheduling problem, IAAI'05 Proceedings of the 17th Conference in Innovative Applications of Articial Intelligence, 3 (AAAI, Palo Alto, CA, 1514–1520, 2005

[Cowardin et al. (2009)] Cowardin, H., et al, An Assessment of GEO Orbital Debris Photometric Properties Derived from LaboratoryBased Measurements, 2009 AMOS Technical Conference Proceedings, Kihei, Maui, HI, 2009

[Cowardin et al. (2010a)] Cowardin, H., Characterization of Orbital Debris Objects over Optical Wavelengths via Laboratory Measurements, PhD thesis, Houston, TX, 2010

[Cowardin et al. (2010b)] Cowardin, H., Seitzer, P., Abercromby, K., et al., Characterization of orbital debris photometric properties derived from laboratory-based measurements. Proceedings of AMOS Technical Conference, Maui, Hawaii, USA, 2010

[Cutler et al. (2017)] Cutler, J., Seitzer, P., Lee., C., et al., Improved Orbit Determination of LEO CubeSats: Project LEDsat, 2017 AMOS Technologies Conference, Maui, Hawaii, 2017

[Damiani et al. (2006)] Damiani, S., Dreihahn, H., Noll, J., Niezette, M. & Calzolari, G.P., Automated allocation of ESA ground station network services, in International Workshop on Planning and Scheduling for Space (American Association for Articial Intelligence, Palo Alto, CA), 2006

[Damiani et al. (2007)] Damiani, S., Dreihahn, H., Noll, J., Niezette, M. & Calzolari, A planning and scheduling system to allocate ESA ground station network services, in The International Conference on Automated Planning and Scheduling, ICAPS 2007 (AAAI, Palo Alto, CA), 2007

[Diprima et al. (2016)] Diprima, F. and Cardona, C., Lessons learned in automatic operation of observatories for space debris observation, Proceedings of the 67 IAC – International Astronautical Congress IAC-16,D1,5,7,x33419, 2016

[Dreihahn et al. (2007)] Dreihahn, H., Niezette, M. & Gotzelmann, M., Centralized schedule and SLE service conguration file generation with the ES-TRACK scheduling system. European Ground System Architecture Workshop (ESA, Paris), 2007

[Earl et al. (2014)] Earl, M. A., Observation and Analysis of the Apparent Spin Period Variations of Inactive Box-wing Geosynchronous Resident Space Objects, iAC-14-A6.9.1, 2014

[ESA SSA Programme (2017)] `www.esa.int/Our_Activities/ Operations/Space_Situational_Awareness/SSA_Programme_ overview`, Retrieved on October 16th, 2017

[ESA SST Programme (2017)] `www.esa.int/Our_Activities/ Operations/Space_Situational_Awareness/Space_ Surveillance_and_Tracking_-_SST_Segment`, Retrieved on October 16th, 2017

[Fielding (2000)] Fielding, T., Architectural Styles and the Design of Network-based Software Architectures, Ph.D. Thesis in Information and Computer Science, University of California, 2000

[Frank et al. (2001)] Frank, J., Jonsson, A., Morris, R., Smith, D. E. & Norvig, P. Planning and scheduling for fleets of earth observing satellites, 2001

[Fruh et al. (2010)] Fruh, C. and T. Schildknecht, Analysis of Observed and Simulated Light Curves of Space Debris, Proceedings of the 61st International Astronautical Congress, IAC-10-A6.1.9, 2010

[Garey et al. (1979)] Garey, M.R. and Johnson, D.S., Computers and Intractability: A Guide to the Theory of NP-Completeness. A Series of Books in the Mathematical Sciences. San Francisco, Calif.: W. H. Freeman and Co. ISBN 0-7167-1045-5. MR 519066, 1979

[Globus et al. (2004)] Globus, A., Crawford, J., Lohn, J. & Pryor, A., A comparison of techniques for scheduling Earth observing satellites, Proceedings of the Sixteenth Innovative Applications of Articial Intelligence Conference. IAAI, 2004

[Gonzalez et al. (1992)] Gonzalez, R., Woods, R. Digital Image Processing, Addison-Wesley Publishing Company, 524-552, 1992

[Gooley (1993)] Gooley, T. D. Automating the satellite range scheduling process (No. AFIT/GOR/ENS/93M-06). Air Force Inst Of Tech Wright-Patterson AFB-OH School Of Engineering, 1993

[Gooley et al. (1996)] Gooley, T. D., Borsi, J.J. & Moore, J. T. Automating air force satellite control network (AFSCN) scheduling. Mathematical and computer modelling, 24(2), 91-101, 1996

[Gottlieb et al. (2001)] Gottlieb, R. G., Sponaugle, S. J. & Gaylor, D. E. Orbit determination accuracy requirements for collision avoidance. Spaceflight Mechanics (Advances in the Astronautical Sciences), vol. 108, San Diego, CA: American Astronautical Society, AAS 01-181, 2001

[Gottwald (2012)] Gottwald M., The Impact of the ENVISAT Loss, Polar Space Task Group, Geneva, 12-14 June 2012

[Gualandi et al. (2001)] Gualandi, R. and Merighi, R., BFOSC – Bologna Faint Object Spectrograph & Camera - User Manual Technical Report, 2001

[Gullixson (1992)] Gullixson, C., Astronomical CCD Observing and Reduction Techniques, ASP Conference Series Vol. 23. ed. S. Howen, 1992

[Hays et al. (2006)] Hays, B.R., Carlile, A.M. & Mitchel, T.S., Visualizing and integrating AFSCN utilization into a common operational picture. Advanced Maui Optical and Space Surveillance Technologies Conference, AMOS 2006 (Maui Economic Development Board, Kihei, HI), 2006

[Heinen et al. (2010)] Heinen, W. and Unal, M., Scheduling tool for ES-TRACK ground station management, SpaceOps 2010 American Institute of Aeronautics and Astronautics, Reston, VA, 2010

[Herzog et al. (2013)] Herzog, J., Schildknecht, T., Hinze, A., Ploner, M. & Vananti, A., Space Surveillance Observations at the AIUB Zimmerwald Observatory. Proceedings of 6th European Conference on Space Debris, Darmstadt, Germany, 2013

[IADC (2002)] IADC Space Debris Mitigation Guidelines, 2002

[INDI (2017)] `indilib.org`, Retrieved on October 16th, 2017

[Ito (2017)] Ito, M., Maximizing Post Mission Disposal Of Mega Constellations Satellites Reaching End Of Operational Lifetime, Proceedings of the 7th European Conference on Space Debris, ESA/ESOC, Darmstadt, Germania , 2017

[Johnson et al. (1953)] Johnson, H.L. and Morgan, W.W., Fundamental stellar photometry for standards of spectral type on the revised system of the Yerkes spectral atlas. The Astrophysical Journal. 117 (3), 313–352 doi:10.1086/145697, 1953

[Johnston et al. (2006)] Johnston, M.D. and Clement, B.J., Automating Deep Space Network scheduling and conict resolution, in Autonomous Agent and Multiagent Systems, AAMAS'06, ACM, 2006

[Johnston et al. (2011)] Johnston, M.D. and Tran, D., Automated scheduling for NASA's Deep Space Network, 6th International Workshop on Planning and Scheduling in Space (Space Telescope Science Institute, Baltimore, MD), 2011

[Johnston et al. (2012)] Johnston, M.D., Tran, D., Arroyo, B., Sorensen, S., Tay, P., Carruth, B, Coffman, A. & Wallace, M., Automating mid- and long-range scheduling for NASA's Deep Space Network, SpaceOps 2012 (American Institute of Aeronautics and Astronautics, Reston, VA) 2012

[Johnston et Miller (1994)] Johnston, M. D. and Miller, G. Spike: Intelligent scheduling of hubble space telescope observations. Intelligent Scheduling, 391-422, 1994

[JSpOC (2015)] JSpOC Recommendations for Optimal CubeSat Operations V2, published August 4, 2015, available at `https://file.space-track.org/documents/Recommendations_Optimal_Cubesat_Operations_V2.pdf`

[Kaasalainen et al. (2001)] Kaasalainen, M.; Torppa, J. & Muinonen, K., Optimization Methods for Asteroid Lightcurve Inversion. II. The Complete Inverse Problem Icarus, Volume 153, Issue 1, pp. 37-51, 2001.

[Kawase et al. (1979)] Kawase, S. and Tanaka, T. A simple method for evaluating the system observability in satellite orbit determination. IEEE Transactions on Aerospace and Electronic Systems, AES-15, 1, 152–156, DOI: 10.1109 / TAES .1979 .308807, 1979

[Kelso (2007)] Kelso, T.S., Analysis of the 2007 Chinese ASAT Test and the Impact of Its Debris on the Space Environment, 2007 AMOS Conference,

Maui, Hawaii, 2007

[Kelso (2009)] Kelso, T.S, Analysis of the Iridium 33 and Cosmos 2251 Collision, 2009 AMOS Conference, Maui, Hawaii, 2009

[Kessler (1991)] Kessler, D., Collisional Cascading: The Limits of Population Growth in Low Earth Orbit. Advances in Space Research 11 (12): 63-66, 1991

[Kirchner et al (2012)] Kirchner, G., Koidl, F., Friederich, F., Buske, I., Volker, U. & Riede, W., Laser measurements to space debris from Graz SLR station, Advances in Space Research, Volume 51, Issue 1, 21-24, 2013

[Kucharki et al. (2014)] Kucharki D. et al., Attitude and Spin Period of Space Debris Envisat Measured by Satellite Laser Ranging, IEEE Transactions On Geoscience And Remote Sensing, Vol. 52, N. 12. 2014

[Kucharski et al (2017)] Kucharski, D., Kirchner, G., et al, Photon pressure force on space debris TOPEX/Poseidon measured by Satellite Laser Ranging, Earth and Space Science, 2017

[Kurosaki et al. (2012)] Kurosaki, H., Yanagisawa, T. & Nakajima, A., Observation of Light Curve of GEO Debris Transactions of the Japanese Society for Artificial Intelligence, Aerospace Technology Japan, Volume 8, 2012.

[Larsson et al. (1996)] Larsson, S., Parameter estimation in epoch folding analysis, Astronomy Astrophysics, Supplement Series 117, 197-201, 1996

[Liou (2011)] Liou, J.C., An active debris removal parametric study for LEO environment remediation. Advances in Space Research, 47(11), 1865-1876, 2011

[Marinelli et al. (2005)] Marinelli, F., Rossi, F., Nocella, S. & Smriglio, S., A Lagrangian heuristic for satellite range scheduling with resource constraints. Comput. Oper. Res. 38(11), 1572–1583, 2005

[Masillo et al. (2017] Masillo, S., et al., A LED-based Technology to improve the orbit determination of LEO satellite, Proceedings of the 68 IAC – International Astronautical Congress IAC-17,A6,9,5,x41229, 2017

[Massey et al. (1992)] Massey, P. and Jacoby G., Astronomical CCD Observing and Reduction Techniques, ASP Conference Series Vol. 23. ed. S. Howell, 1992.

[Mehrholz et al. (2002)] Mehrholz, D., Leushacke, Flury W., Jehn, R., Klinkrad, H. & Landgraf, M. Detecting, Tracking and Imaging Space Debris, ESA bulletin, 109, S.128-134, 2002

[Molotov (2011)] Molotov, I., Optical Tracking of Space Debris Overview of ISON's Capabilities and Future Plans, 2011 Beijing Space Sustainability Conference, 2011

[NASA Orbital Debris Quarterly News (2017)] NASA Orbital Debris Quarterly News, Volume 21 - Issue 1, 2017

[Papushev et al. (2009)] Papushev P. et al., Investigations of the evolution of optical characteristics and dynamics of proper rotation of uncontrolled geostationary articial satellites, Advances in Space Research, volume 43, Issue 9, 2009

[Parish (1994)] Parish, D. A. A genetic algorithm approach to automating satellite range scheduling (No. AFIT/GOR/ENS/94M-10). Air Force Inst Of Tech Wright-Patterson AFB-OH School Of Engineering, 1994

[Payne et al.(2002)] Payne, T., Gregory, S., Burdullis, T. & Houtkooper, N., Classification of Geosynchronous Satellites Using Color Photometric Techniques, 2002 Core Technologies for Space Systems Conference, Colorado Springs, 2002

[Pellegrino et al. (2017)] Pellegrino, A., Seitzer, P., Piergentili, F., Santoni, F.,

Cutler, J., Cardona, T., et al., LEDSAT: in-orbit demonstration mission for LED-based cluster launch early identification and improved LEO surveillance, Proceedings of the 68 IAC – International Astronautical Congress IAC-17,A6,10-B4.10,8,x41050, 2017

[Pemberton (2000)] Pemberton, J. C. Towards scheduling over-constrained remote sensing satellites. In Proceedings of the 2d International Workshop on Planning and Scheduling for Space, 2000

[Piattoni et al. (2014)] Piattoni, J., Ceruti, A. & Piergentili, F., Automated image analysis for space debris identification and astrometric measurements. Acta Astronautica, vol. 103, 176-184, ISSN: 0094-5765, doi: 10.1016/j.actaastro.2014.05.025, 2014

[Piergentili et al. (2009)] Piergentili, F. et al. Italian activity in space debris measurements. Fifth European Conference on Space Debris, ESOC, Darmstadt, Germany, Mar. 30-Apr. 2, 2009

[Piergentili et al. (2014)] Piergentili, F., Ceruti, A., Rizzitelli, F., Cardona, T., Battagliere, M.L. & Santoni, F., Space Debris Measurement Using Joint Mid-Latitude and Equatorial Optical Observations. IEEE Transactions On Aerospace And Electronic Systems, vol. 50, 664-675, ISSN: 0018-9251, doi: 10.1109/taes.2013.120272, 2014

[Piergentili et al. (2015a)] Piergentili, F., Arena, L., Cardona, T., Diprima, F., Scire, G., Spinetti, A., Canu, C., Portelli, C. & Santoni, F., EQUO: an equatorial observatory to improve the Italian space surveillance capability. 66th International Astronautical Congress, Jerusalem, Israel, IAC-15,A6,IP,28,x30770, 2015

[Piergentili et al. (2015b)] Piergentili, F., Arena, L., Cardona, T., Scire, G., Spinetti, A., Canu, C., Portelli, C., Santoni, F. & Diprima, F., EQUO: an

EQUatorial Observatory to improve the Italian space surveillance capability, Proceedings of the 66 IAC International Astronautical Congress, IAC-15,A6,IP,28,x30770, 2015

[Piergentili et al. (2017)] Piergentili, F., Santoni, F. & Seitzer, P., Attitude Determination of Orbiting Objects from Lightcurve Measurements. IEEE Transactions On Aerospace And Electronic Systems 53.1: 81-90. doi: 10.1109/TAES.2017.2649240, 2017

[Porfilio et al. (2003)] Porfilio, M., Piergentili, F. & Graziani, F. The 2002 Italian optical observations of the geosynchronous region. Spaceflight Mechanics (Advances In the Astronautical Sciences), vol. 114. San Diego, CA: American Astronautical Society, AAS 03-186, ISBN:0-87703-504-0, 2003

[Porfilio et al. (2004)] Porfilio, M., Piergentili, F. & Graziani, F., First optical space debris detection campaign in Italy. Advances In Space Research, 34, 5, 921–926, ISSN: 0273-1177, 2004

[Rossi et al. (2011)] Rossi, A., Cardona, T., Dotto, E., Perna, E., Santoni, F. & Piergentili, F., Physical Characterization of Space Debris in the Geosynchronous Region, . Proceedings of the 62 IAC International Astronautical Congress, IAC-11,A6,1,7,x10320, 2011

[Rossi et al. (2012)] Rossi, A., Marinoni, S., Cardona, T., Dotto, E., Santoni, F. & Piergentili, F., The Loiano campaigns for photometry and spectroscopy of geosynchronous objects, Proceedings of the 63 IAC International Astronautical Congress, IAC-12,A6,1,3,x13587, 2012

[Rossi et al. (2013)] Rossi, A., Marinoni, S., Cardona, T., Dotto, E., Santoni, F. & Piergentili, F., Physical characterization of objects in the GEO region with the Loiano 1.5m telescope, Proceedings of the 6th European Conference on Space Debris, ESA/ESOC, Darmstadt, Germania , 2013

[RTS2 (2017)] `rts2.org`, Retrieved on October 16th, 2017

[Santoni et al. (2013a)] Santoni, F., Piergentili, F. & R. Ravaglia. Nanosatellite Cluster Launch Collision Analysis. Journal of Aerospace Engineering, vol. 26, 618-627, doi: 10.1061/(asce)as.1943-5525.0000175, 2013

[Santoni et al. (2013b)] Santoni, F., Cordelli, E. & Piergentili, F., Determination of disposed-upper-stage attitude motion by ground-based optical observations, Journal of Spacecraft and Rockets, Vo. 50, Issue 3, 701-708; doi: 10.2514/1.A32372, 2013

[Santoni et al. (2014)] Santoni, F., Ravaglia, R. & Piergentili, F., Close Approach Analysis in the Geosynchronous Region Using Optical Measurements. Journal Of Guidance Control And Dynamics, vol. 37, 705-710, ISSN: 0731-5090, doi: 10.2514/1.59821, 2014

[Santoni et al. (2015)] Santoni, F., Piergentili, P., Arena, L., Cardona, T., Diprima, F., Scire, G., Spinetti, A., Grossi, A., Curiano, F., Pellegrino, A., Canu, C. & Portelli, C., Equatorial Italian Observatory for Space Debris Monitoring at the Broglio Space Center, Proceedings of the 23 Conferenza AIDAA Associazione Italiana di Aeronautica e Astronautica, 2015

[Santoni et al. (2017)] Santoni, F., Piergentili, P., Cardona, T., Curiano, F., Diprima, F., Hossein, S.H., Canu, C. & Mariani, L., EQUO - Equatorial Italian Observatory At The Broglio Space Center For Space Debris Monitoring, Proceedings of the 68 IAC – International Astronautical Congress IAC-17,A6,IP,15,x38273, 2017

[Saunders (2016)] Saunders, C., Service Oriented Active Debris Removal, CleanSpace Event ESTEC, 2016

[Saunders et al. (2006)] Saunders, E. S., Naylor, T. & Allan, A. Optimal placement of a limited number of observations for period searches. Astronomy Astrophysics, 455(2), 757-763, 2006

[Savitzky et al. (1964)] Savitzky, A. and Golay, M., Smoothing and differentiation of data by simplified least squares procedures, Anal. Chem. 1964

[Scargle et al. (1982)] Scargle, J. D., Studies in Astronomical Time Series Analysis. II. Statistical Aspects of Spectral Analysis of Unevenly Spaced Data, The Astrophysical Journal, 1982, 263:835-853, December 15, 1982

[Schalck (1993)] Schalck, S. M. (1993). Automating satellite range scheduling (No. AFIT/GSO/ENS/93D-14). Air Force Inst Of Tech Wright-Patterson AFB-OH School Of Engineering, 1993

[Schildknecht et al. (2004)] Schildknecht, T., Musci, R. Ploner, M. Beutler, G. Kuusela, J. de Leon Cruz, J. & de Fatima Domınguez Palmero, Optical Observations of Space Debris in GEO and in Highly-Eccentric Orbits. Advances in Space Research, 34(5), 901–911, 2004

[Schildknecht et al. (2005)] Schildknecht, T., et al, Properties of High Area-to-Mass Ratio Space Debris Population in GEO, 2005 AMOS Technical Conference Proceedings, Kihei, Maui, HI, 2005

[Schildknecht et al.(2007)] Schildknecht, T., Optical surveys for space debris. Astronomy Astrophys. Rev. 14 (1), 41–111, 2007

[Schildknecht et al. (2008a)] Schildknecht, T., Musci, R., Fruh, C., Ploner & M., Color Photometry and Light Curve Observations of Space Debris in GEO. Proceedings of AMOS Conference, Maui, Hawaii, 2008

[Schildknecht et al. (2008b)] Schildknecht, T., Musci, R. & Flohrer, T., Properties of the high area-to-mass ratio space debris population at high altitudes. Adv. Space Res. 41, 1039–1045, 2008

[Schildknecht et al. (2013)] Schildknecht, T., Hinze, A., Schlatter, P., Silha, J., Peltonen, J., Santti, T. & Flohrer, T., Improved Space Object Observation

Techniques using CMOS Detectors, Proceedings of 6th European Conference on Space Debris, Darmstadt, Germany, 2013

[Schildknecht et al. (2015)] Schildknecht, T., Linder, E., Silha, J., Hager, M., Koshkin, N., Korobeinikova, E., Melikiants, S., Shakun, L. & Strakhov, S., Photometric Monitoring of Non-Resolved Space Debris and Databases of Optical Light Curves, AMOS - Advanced Maui Optical and Space Surveillance Technologies Conference, 2015

[Schmidt (2011)] Schmidt, M., Ground station networks for efcient operation of distributed small satellite systems. Ph.D. Thesis, University of Wurzburg, 2011

[Scire et al. (2015)] Scire G., Santoni, F. & Piergentili F. Analysis of orbit determination for space based optical space surveillance system. Advances In Space Research, vol. 56, 421-428, ISSN: 0273-1177, doi:10.1016/j.asr.2015.02.03, 2015

[Scire et al. (2016)] Scire, G. and Cardona, T., Development of the Italian observatory network for Space Surveillance, Proceedings of the 67 IAC – International Astronautical Congress IAC-16,A6,IP,20,x34416, 2016

[Seitzer et al. (2004)] Seitzer, P., Jorgensen, K.J., Africano, J., Parr-Thumm, T., Matney, M., Jarvis, K. & Stansbery, E., Results from the geo debris survey with modes, Science and Technology SeriesVolume 110, 2005, 19-24, International Academy of Astronautics Space Debris and Space Traffic Management Symposium 2004; Vancouver, Canada, 2004

[Seitzer et al. (2012a)] Seitzer, P., Lederer, S.M., Abercromby, K.J., Barker, E.S., Burkhardt, A., Cowardin, H., Krisko, P. & Silha, J., Searching for optically faint geo debris, Proceedings of the International Astronautical Congress, IACVolume 3, 2012, 2209-2211, 63rd International Astronautical Congress 2012, IAC 2012, Naples, Italy, 2012

[Seitzer et al. (2012b)] Seitzer, P., Lederer, S., Cowardin, H., Cardona, T., Barker, E. & Abercromby, K., Visible Light Spectroscopy of GEO Debris, Proceedings of the AMOS Conference, 2012

[Seitzer et al. (2013a)] Seitzer, P., Cardona, T., Lederer, S.M., Cowardin, H., Abercromby, K.J., Barker, E.S. & Bedard, D., Optical reflection spectroscopy of GEO objects, Proceedings of the International Astronautical Congress, IACVolume 3, 2013, 2000-2004, 64th International Astronautical Congress 2013, IAC 2013, Beijing, China, 2013

[Seitzer et al. (2013b)] Seitzer, P., Cardona, T., Lederer, S., Abercromby, K., Barker, E. & Bedard, D., Optical Reflection Spectroscopy of GEO Objects, Proceedings of the 64 IAC International Astronautical Conference, IAC-13,A6,1,4,x18377, 2013

[Seitzer et al. (2016)] Seitzer, P., Piergentili, F., Santoni, F., Cutler, J., Cowardin, H., Cardona, T., Curiano, F., Pellegrino, A., Gianfermo, A., Lee, C. & Sharma, S., LEDsats: LEO Cubesats with LEDs for Optical Tracking, Proceedings of the AMOS Technical Conference, 2016

[Seitzer et al. (2017)] Seitzer, P., Piergentili, F., Santoni, F., Cutler, J., Cowardin, H., Cardona, T., Curiano, F., Pellegrino, A., Gianfermo, A., Lee, C. & Sharma, S., LEDSat: Design of a CubeSat equipped with LEDs as calibration target,Proceedings of the 7th European Conference on Space Debris, ESA/ESOC, Darmstadt, Germania, 2017

[Soille (1999)] Soille, P., Morphological Image Analysis: Principles and Applications, Springer-Verlag, 173-174, 1999

[Soma et al. (2004)] Soma, P., Venkateswarlu, S., Santhalakshmi, S., Bagchi, T. & Kumar, S. Multi-satellite scheduling using genetic algorithms. IS-TRAC/ISRO, SpaceOps, 2004

[Somers (2011)] Somers, P., Cylindrical RSO Signatures, Spin Axis Orientation and Rotation Period Determination, AMOS - Advanced Maui Optical and Space Surveillance Technologies Conference, 2011

[Space Track (2017)] Space Track Public catalogue, `www.space-track.org`, Retrieved on October 16th, 2017

[Spangelo (2013)] Spangelo, S., Modeling and optimizing space networks for improved communication capacity. Ph.D. Thesis. University of Michigan, 2013

[Tanaka et al. (2015)] Tanaka, K., Kawamura, Y. & Tanaka, T., Development and operations of nano-satellite FITSAT-1 (NIWAKA), Acta Astronautica, Vol. 107, 112-129, 2015

[Tsapras et al. (2009)] Tsapras, Y., Street, R., Horne, K., Snodgrass, C., Dominik, M., Allan, A. & Mottram, C., RoboNetII: Follow-up observations of microlensing events with a robotic network of telescopes. Astronomische Nachrichten, 330(1), 4-11, 2009

[Vallado (2001)] Vallado, D., Fundamentals of Astrodynamics and Applications, Space Technology Library, Microcosm Press, Portland, OR, 2001

[Vazquez et al. (2014)] Vazquez, A.J. and Erwin, R.S., Optimal xed interval satellite range scheduling, Proceedings of the 3rd International Conference on Operations Research and Enterprise Systems (Scitepress, Angers), 401–408, 2014

[Vazquez et al. (2015a)] Vazquez, A.J. and Erwin, R.S., On the tractability of satellite range scheduling. Optim. Lett. 9(2), 311–327, 2015

[Vazquez et al. (2015b)] Vazquez, A.J. and Erwin, R.S., Noncooperative satellite range scheduling with perfect information, 2015 IEEE Aerospace Conference (IEEE, Big Sky) 2015

[Vazquez et al. (2015c)] Vazquez, A.J. and Erwin, R.S., Robust xed interval satellite range scheduling, 2015 IEEE Aerospace Conference (IEEE, Big Sky) 2015

[Wang et al. (2014a)] Wang, J., Demeulemeester, E. & Qiu, D., A pure proactive scheduling algorithm for multiple Earth observation satellites under uncertainty of clouds. SSRN. doi:10.2139/ssrn.2495339, 2014

[Wang et al. (2014b)] Wang, J., Zhu, X., Qiu, D. & Yang, L.T., Dynamic scheduling for emergency tasks on distributed imaging satellites with task merging. IEEE Trans. Parallel Distrib. Syst. 25(9), 2275–2285, 2014

[Warwick (1959)] Warwick, J. W., Decay of spin in Sputnik 1, Planet. Space Sci., 1, 43-49, 1959

[Welch (1967)] Welch, P.D., The Use of Fast Fourier Transform for the Estimation of Power Spectra: A Method Based on Time Averaging Over Short, Modied Periodograms, IEEE Transactions on Audio and Electroacoustics, Vol. AU-15, No.2, 1967

[Wolfe et al. (2000)] Wolfe, W.J. and Sorensen, S.E., Three scheduling algorithms applied to the Earth observing systems domain. Manag. Sci. 46(1), 148–168, 2000

[Yanagisawa et al. (2009)] Yanagisawa, T., Kurosaki, H. & Nakajima, A., Activities of JAXA's innovative technology center on space debris observation. In Advanced Maui Optical and Space Surveillance Technologies Conference, Poster presentations, 2009

[Yanagisawa et al. (2012)] Yanagisawa, T. and Kurosaki, H., Shape and motion estimate of LEO debris using light curves. Adv. Space Res. 50, 136–145, 2012

[Zhao et al. (2016)] Zhao, X.F., Zhang, H.Y., Yu, Y. & Mao, Y.D., Multicolor

photometry of geosynchronous satellites and application on feature recognition. Adv. Space Res. 58, 2269–2279, 2016

[Zufferey et al. (2008)] Zufferey, N., Amstutz, P. & Giaccari, P. Graph colouring approaches for a satellite range scheduling problem. Journal of Scheduling, 11(4), 263-277, 2008